UNIVERSITEIT VAN PRETORIA
UNIVERSITY OF PRETORIA
YUNIBESITHI YA PRETORIA

# DESIGN CONSIDERATIONS AND ANALYSIS OF A BIOREACTOR FOR APPLICATION IN A BIO-ARTIFICIAL LIVER SUPPORT SYSTEM.

By

L.J.T Ronné

A project submitted in partial
fulfilment of the requirements for the
degree of

MEng: (Mechanical Engineering)

University of Pretoria

2006

University of Pretoria

Abstract

# DESIGN CONSIDERATIONS AND ANALYSIS OF A BIOREACTOR FOR APPLICATION IN A BIO-ARTIFICIAL LIVER SUPPORT SYSTEM.

By L.J.T Ronné

Study leader: AJ van wyk
Department of Mechanical and Aeronautical Engineering
University of Pretoria

Acute Liver Failure (ALF) is a devastating ailment with a high mortality rate and limited treatment alternatives. This study presents a methodology for the design and development of a bio-artificial bioreactor to be used in a Bio-Artificial Liver Support System. The system will ultimately be used either to bridge a patient to orthotopic liver transplant (OLT), the only current cure for end stage ALF, or spontaneous recovery. Methods to optimize and visualize the flow and related mass transfer in the BR are presented. The use of magnetic resonance imaging (MRI), scanning electron microscopy (SEM) and simple testing methodology is applied with emphasis on modeling the flow conditions in the BR. The bioreactor (BR) used in the Bio-Artificial Liver Support System (BALSS), currently undergoing animal trials at the University of Pretoria, was modeled and simulated for the flow conditions in the device. Two different perfusion steps were modeled including the seeding of hepatocyte cells and later the clinical perfusion step. It was found that the BR geometry was not optimal with "dead spots" and regions of retarded flow. This would restrict the effective transport of nutrients and oxygen to the cells. The different perfusion rates for the seeding and clinical perfusion steps allowed for different velocity contours with cells seeing inconsistent flow patterns and mass transfer gradients. An optimized BR design is suggested and simulated, that effectively reduces the areas of retarded flow (dead spots) and increases the flow speed uniformly through the BR to an order of magnitude similar to that found in the sinusoidal range. The scaffolding volume was also decreased to allow a larger local cell density promoting cell-cell interaction. Finally a summarized design table for the design of a hepatic BR is presented.

# TABLE OF CONTENTS

# LIST OF FIGURES

# LIST OF TABLES

# ACKNOWLEDGMENTS

The author wishes to thank the following people and organizations for their valuable contributions to the completion of this study:

- Mr. AJ van Wyk for his patience, guidance and advice.
- Mr. Jan Brand for the machining and advice on a number of the experimental setups.
- Mr. A N Hall for the advise and preparation of the SEM samples.
- The ladies at UNITAS hospital, MRI division, for their time and effort in making the MRI study a reality.
- Mr. Tony W. H. Sheu for permission to reproduce certain figures published in one of the group's publications.
- Mrs. DM Tripp from the United Network of Organ Sharing for her invaluable statistics of liver failure.

# GLOSSARY

**Acinus** A functional unit of the liver, smaller than a portal lobule, being a diamond shaped mass of liver parenchyma that is supplied by a terminal branch of the portal vein and of the hepatic artery and drained by a terminal branch of the bile duct [1].

**Acute** Having a short and relatively severe course [1].

**Aggregate** For the purpose of this investigation an aggregate is a number of cells were a biological skin has given the structure a smooth spherical appearance.

**Boundary conditions** The necessary upstream and downstream conditions used by a numerical solver to calculate the interior points of a discrete meshed domain.

**Biocompatible material** A substance that has no detrimental effect to the differentiation and viability of the cells in question and promotes cell to cell interaction as well as cell growth.

**Cell viability** A description of the structural integrity of the cell, measured by trypan blue exclusion test. If the cell membrane is damaged then the dye penetrates the cell and it is no longer regarded as a viable cell.

**Chronic** Persisting over a long period of time [1].

**Cluster** For the purpose of this investigation a cell cluster was defined as a group of cells with more than one layer relative to the scaffolding without a biological skin visible.

**Creep** The progressive plastic deformation over a period of time [2].

**Cold welding** The welding of materials without the input of heat.

**Dead spots** Regions in the scaffolding were the flow is either stationary or were gas has become trapped resulting in zero flow velocity.

**Differentiation** The act or process of acquiring completely individual characters, as occurs in the progressive diversification of cells [1].

**Encephalopathy** Any degenerative disease of the brain [1].

**Fixation** To stabilize cellular organization such that the ultra structural relations are preserved during dehydration, embedding and exposure to the electron beam [3].

**Hepatocyte cells** The polyhedral epithelial cells that constitute the substance of an acinus of the liver [1].

**Hepatic functional unit** Defined as the minimal amount of tissue in a liver required to perform the functions of the liver.

**Hepatic lobule** The building blocks of the liver, according to the hepatic lobule model (*see:* 2.1.1: The hepatic lobular model).

**Hepatic microvascular system** Comprises of all the intra-hepatic vessels having internal diameters of smaller that 300μm [4].

**Hydrodynamic dispersion** The spreading phenomenon of a tracer, typically found in porous flow [5].

**Hydrophilic** The name given to a material that has the affinity to attract water.

**Hilus/ Hilim** Anatomic nomenclature for a depression of a pit at the part of the organ where vessels and nerves enter [1].

***In vitro*** Within the glass, observable in a test tube in an artificial environment [1].

***In vivo*** Within the living body [1].

**Internal resistance factor** A factor used in the modeling of porous scaffoldings where the pressure drop over the scaffolding needs to be characterized. The factor is calculated from Equation 6**.**

**Kupffer cells** Large star shaped cells with a large oval nucleus and a small prominent nuclleolus. These intensely phagocytic cells line the walls of the sinusoids of the liver [1].

**Leukocytes** The white blood cells that, amongst other things, contribute to the oxygen transfer mechanisms of blood.

**Metastasis** A growth of pathogenic microorganisms or of abnormal cells distant from the site primary involved by the morbid process [1].

**Monolayer** For the purpose of this investigation a monolayer is defined as a single layer of cells that are in contact with each other either by direct cell-to-cell contact or via a protein like web or strand.

**Narcosis** A nonspecific and reversible depression of function.

**Phagocytic** Cells that take up material by means of membrane-bound vesicles. The engulfed material is killed and digested [1].

**Parenchimal cells** The functional elements as distinguished from its framework, the stoma.

**Pericentral region** Surrounding a center [1].

**Perfusion** For the purpose of this investigation, the flow of a medium including blood, plasma etc. through a loop in contact with a biological component i.e. a BR.

**Permeability** The property of state of being permeable [1].

**Proliferation** The reproduction or multiplication of similar forms [1].

**Scaffolding** A matrix to which the cells can adhere, without jeopardizing the cells differentiation and viability.

**Seeding** The deposit, attachment and differentiation of cells in a scaffolding ultimately allowing the cells to become viable.

**Tolerance** The gap or clearance between two surfaces.

**Turbulent inertia tensor** A term added by the averaging of the Navier Stokes equations, given by Equation 4**.**

# ACRONOMES

| | |
|---|---|
| BAL | Bioartificial liver |
| ALF | Acute liver failure |
| BALSS | Bio-artificial Liver Support System |
| BC | Boundary conditions |
| BR | Bioreactor |
| CAT | Computerised axial tomography |
| CFD | Computational fluid dynamics |
| FDA | Federal Drug Administration |
| LED | Light emitting diode |
| LES | Large eddie simulation |
| LF | Liver failure |
| NMRI | Nuclear magnetic resonance imaging |
| MRI | Magnetic resonance imaging |
| NM | Nuclear medicine |
| OLF | Orthotropic liver failure |
| PFC | Perfluorochemical |
| PFOB | Perfluorooctyl bromide |
| PUF | Polyurethane foam |

RANSE Reynolds Averaged Navier-Stokes Equations

SEM Scanning electron microscope

TEM Transmition electron microscope

# NOMENCLATURE LIST

| SYMBOL | DEFINITION | UNITS |
|---|---|---|
| $A$ | Area | $m^2$ |
| $A_s$ | Surface area (Equation 13) | $m^2$ |
| $C_2$ | Internal resistance factor (Equation 6) | $m^2/kg$ |
| $D$ | Diffusion coefficient | $m^2/s$ |
| $Di$ | Internal diameter (Appendix C) | m |
| $D_h$ | Hydraulic diameter (Equation 12) | m |
| $d$ | Diameter | m |
| $h$ | Height (Equation 16) | m |
| $g$ | Gravitational acceleration | $m/s^2$ |
| $k$ | Turbulence generation (Appendix B) | |
| $L$ | Length (Equation 16) | m |
| $m$ | Mass | kg |
| $\dot{M}$ | Mass flow | kg/s |
| $NC$ | Number of cells (Chapter 7.3) | |
| $NS$ | Number of spheroids (Chapter 7.3) | |
| $p$ | Porosity (Equation 24) | |
| $P$ | Wetted perimeter (Equation 12) | m |
| $P$ | Pressure | Pa |
| $\overline{P}$ | Average pressure (Equation 3) | Pa |
| $P_{atm}$ | Atmospheric pressure | Pa |
| $\dot{Q}$ | Volumetric flow rate | $m^3/s$ |
| $Q_{EAS}$ | Equiangle Skewness (EAS) (Equation 1) | |
| $Re$ | Reynolds number (Equation 18) | |
| $S_i$ | Momentum sink term (Equation 5) | |
| $t$ | Time | s |
| $T$ | Temperature | K |
| $u$ | Vector velocity | m/s |
| $V$ | Average velocity | m/s |
| $V_{BR}$ | Bioreactor volume | $m^3$ |
| $V_c$ | Volume of a cell (Chapter 7.3) | $m^3$ |
| $V_s$ | Volume of a spheroid (Chapter 7.3) | $m^3$ |
| $V_{total}$ | Total volume (Equation 24) | $m^3$ |

| | | |
|---|---|---|
| $V_{void}$ | Volume of a void (Equation 24) | $m^3$ |
| $v$ | Kinematic viscosity (Equation 21) | $m^2/s$ |
| $x$ | Spatial vector | m |
| $w$ | Specific turbulent dissipation rate (Appendix B) | |

*Greek symbols*

| | | |
|---|---|---|
| $\Delta$ | Change/ difference | |
| $\theta$ | Angle | rad |
| $\theta_{EQ}$ | Angle of equivalent element in equilateral form (Equation 1) | rad |
| $\pi$ | Pi | |
| $\phi$ | Undisclosed dependant variable | |
| $\nabla$ | Gradient operator | |
| $\delta_{ij}$ | Chronica delta (Equation 4) | |
| $\mu$ | Viscosity | kg/ms |
| $\mu_t$ | Turbulent viscosity (Appendix B) | kg/ms |
| $\rho$ | Density | $kg/m^3$ |
| $\alpha$ | Permeability (Equation 5) | kg/s |
| $\tau_w$ | Shear stress at the wall (Equation 22) | Pa or $kg/ms^2$ |

*General subscripts*

| | |
|---|---|
| *abs* | Absolute |
| *ave* | Average |
| *cf* | Cell footprint |
| *i,j* | Directional term used in Einstein notation |
| *max* | Maximum |
| *min* | Minimum |
| *op* | Operating |
| *r* | Radial |

# 1 INTRODUCTION AND BACKGROUND

*"The significant problems we face cannot be solved at the same level of thinking we were at when we created them." - Albert Einstein (1879-1955)*

The liver is one of the world's biological marvels, vexing medical practitioners and researchers alike with respect to its functionality and treatment. It is the largest organ in the human body and to date a complete list of the liver's functions is unavailable [6,7]. The mortality for acute liver failure (ALF) is as high as 80% and at the time of this study the only known cure for end stage ALF was orthotopic liver transplantation (OLT) [6,8,9]. Dr Thomas Starzl performed the first successful liver transplant in 1963 [10] and since then it remains the only successful cure for ALF. Unfortunately due to shortage of donor organs and an exponential increase in the organ waiting list (*see* Appendix A) the mortality rate for ALF is high. In other organ transplants, support systems are commonly used to bridge the patient to transplant. An example includes the dialysis machine (kidney). From Figure 1 it can be seen that the procedure for liver transplants has a relatively high rate of success, with the last 14 years seeing an improvement of about 10.2%. This gives a good indication of the viability of the transplant technique. At the time of this study there was no approved system available that could **successfully** support a patient while waiting for a donor liver.

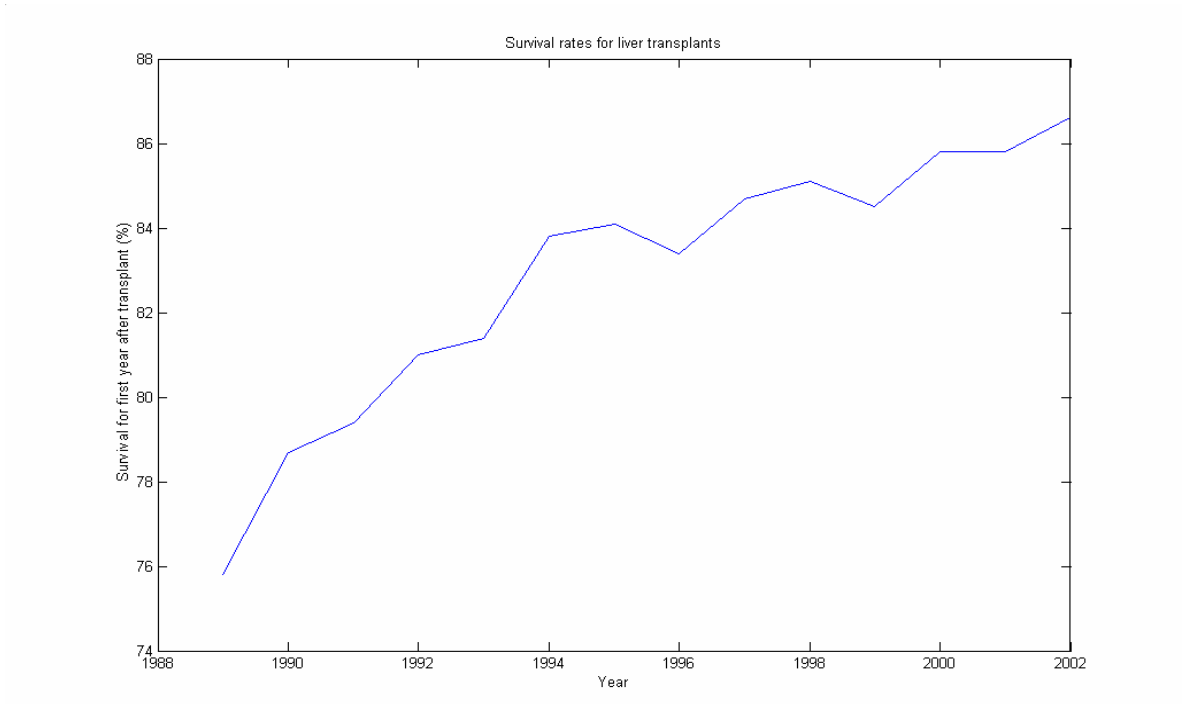


Figure 1: Survival rates for liver transplants

Causes of liver failure include non-cholestatic cirrhosis, cholietatic liver diseases/cirrhosis, billary artesia, acute hepatic necrosis, metabolic diseases and certain cancers[1]. This study deals with the development of technology and techniques that contributes to a solution to the ever-growing problem of liver failure (LF) with the emphasis on the flow in a bio-artificial liver bioreactor.

As mentioned a complete list of the liver's functions are unavailable but an incomplete list is presented below [6,7];

- The liver helps with processing of digested food,
- fat, lipid and protein metabolism,
- glucose regulation (glyconeogenesis and glycogenolysis),
- combating infections,
- clearing the blood of particles like bacteria,
- detoxification,
- manufacturing bile, which is important for digestion of fats,
- storing iron, vitamins and other essential chemicals,
- carbohydrate metabolism,
- synthesis of lipoproteins and cholesterol,
- manufacturing and regulation of numerous hormones, including sex hormones,
- manufacturing enzymes and proteins that are responsible for most chemical reactions in the body, such as those involved in blood clotting and repair of damaged tissue.

From the above list it is clear that a filtration/detoxification device like that used in renal dialysis on its own is inefficient to successfully treat a patient suffering from ALF.

With the liver functions in mind an effective BAL needs to accomplish the following:

[1] A more comprehensive list is available from www.optn.org.

- It must sufficiently support the patient untill OLT or recovery by replication the livers functions.
- Immune reactions must be properly managed [6,7].
- The system must be clinical applicable, taking into consideration the ICU environment and staff competency levels.

When setting out to design a device that would satisfy the above-mentioned points, lessons can be learnt from normal design-for-system procedures. The natural evolution of any system follows a circular loop of testing and redesigning of subsystems. A BAL should be no different. The design loop starts off with a need; the system is designed with metabolic or similar trials to determine the efficiency of the design. At later stages of the system design, more complex levels of testing are incorporated with animal and clinical trials used to determine the efficiency of the system.

Each step in the design phase needs to go through certain approval steps, for example the approval for animal studies by the ethics comities, or the clinical trials by the FDA (Federal Drug Administration). The FDA recognizes extra corporeal use of hepatocytes to treat liver failure as a drug and not a device, as a result clinical trials must be performed in accordance with an active investigational new drug application reviewed by the Center for Biological Evaluation and Research at the FDA [11].

Each test phase can be expanded further; for example the metabolic and animal trials could be expanded into complex design loops including testing of different sources of cell cultures i.e. rat, primary porcine etc. Figure 2 shows a simplified design loop for a BAL. Included as an outcome of this study is a comprehensive design methodology for the design of a hepatocyte BR.

Technology is to a large extent need driven, with most technological systems following a biological s-curve evolution. This s-curve comprises of an infancy, growth and maturity stage. According to the *Prevailing Trends of Technological Systems Evolution* set out by Genrikh Altshuller [12] a technology will evolve towards an increase degree of ideality, the subsystems will evolve non-uniformly, it will transform to a higher level system, increase in flexibility, the energy flow path will shorten and the system will transform from a macro to a micro system. In the following paragraphs it will be shown were the current 'state of the art' technology is and in what aspects the technology can evolve to a viable profitable means to contribute to a solution towards LF.

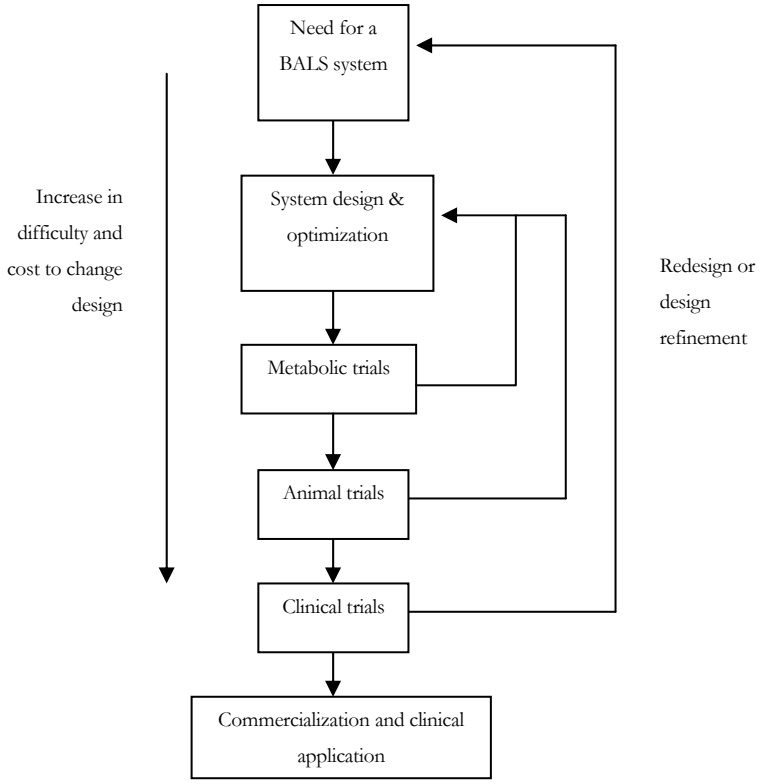


Figure 2: Design loop for a BAL system

# 2 THEORY OF LITERATURE SURVEY

*"Education is a progressive discovery of our own ignorance."* - *Will Durant*

## 2.1 Flow *in vitro* of a healthy liver

Unlike most designs where the design specifications are outlined in the problem statement and an optimal solution to the presented problem is designed for, in the case of the BAL the optimal design is readily available in most healthy mammals. The design specifications, however, is a study on its own but in describing the basic functions of a healthy liver, a better understanding can be developed for the optimal conditions required for hepatocyte cell survival in a BR.

Flow to the liver is well documented [4,7] with the blood draining from the intestines into the portal vein then to the liver. In the liver the blood is cleaned of toxins before returning to the heart and lungs. The blood from the intestines is not very oxygen rich with the hepatic artery supplying the necessary oxygen.

The liver itself consists of parenchymal cells, hepatocyte cells, stellate cells, Kupher cells, ito cells and non-parechymal cells. Hepatocyte cells constitute 80-90% of the liver mass [6], and can be assumed that they are the predominant cells responsible for liver function. From this the designer needs to understand the necessity for mass transfer and especially oxygen supply to the hepatocyte cells.

Understanding the microcirculation of the liver is important for refining designs of hepatic BR's [13]. The factors that influence flow in the microvascular system of a healthy mammal are poorly understood [4]. There is however models that attempt to describe hepatic microcirculation including the hepatic lobular model and the acinar model [13]. A short discussion of the abovementioned models follows.

### 2.1.1 The hepatic lobular model

The schematic of the hepatic lobular model, Figure 3a&b, shows the circulating blood entering the hexagonal lobule via portal tracts and draining thought the central venules. These central venules are tributaries of the hepatic vein. The portal tract branches to the hepatic artery, lymph ducts and bile ducts. This hexagonal structure is replicated throughout the liver tissue.

Figure 3b shows a segment of the hepatic lobule. The blood flows in the sinusoidal space, the lymph in the space of disse with the bile in the bile caniculli. Hepatocytes have essentially two surfaces, the sinusoidal side absorbing oxygenated blood and nutrients from the portal vein, and the bile side delivering bile and other products of conjugation and metabolism to the canalicular network which joins up the bile ductules [14].

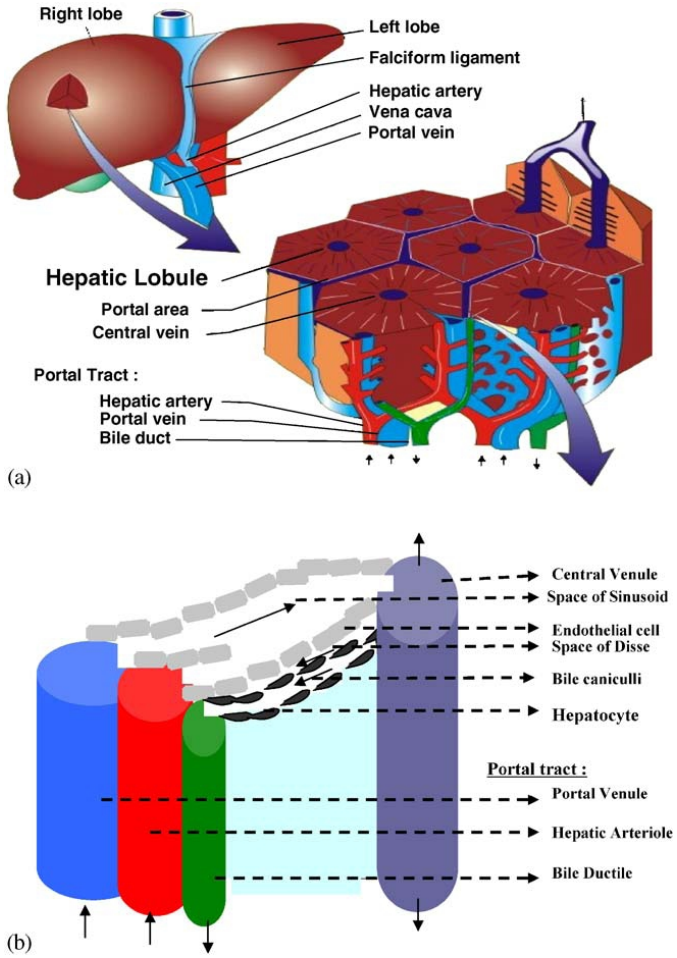


Figure 3: Schematic of (a) hexagonal hepatic lobule and portal tract (b) segment of hepatic lobule. *Reproduced with permission from*: Rani, H.P. *et al [13]*

The short falls of the lobular model lie in the construction of an actual hepatic micro vascular system. In most of the mammals studied the peripheral boundaries that circumscribes the lobule are poorly defined with pigs and seals being the exception [13]. Another discrepancy lies with the fraction of blood that flows to the sinusoids by the hepatic artery, differ between the hilus and perifery of hepatic lobes [4]. For these reasons the acinar model was developed.

### 2.1.2 The hepatic acinar model

The acinar model has the portal tract at the centre with the outer boundary defined by a line segment surrounding the terminal hepatic venule. The hepatic acinus unit has no distinct morphological boundaries. This is presented schematically in Figure 4. The area called the acinus has three metabolic zones, which due to their relative spatial distance from the supply blood have been given different metabolic models. Several of these simple acini would be the building blocks for the classical lobular model. Wolfe *et al* [15] designed and tested a novel hollow fibre bioreactor simulating the acinar model.

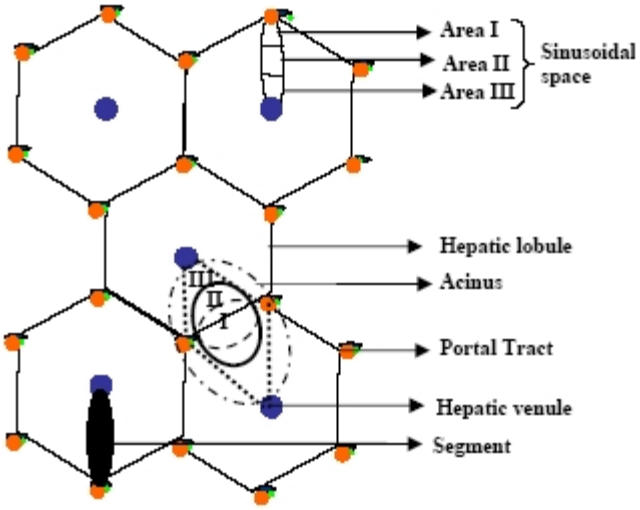


Figure 4: Schematic of hepatic acinar model. *Reproduced with permission from*: Rani, H.P. *et al [13]*

From the two-presented models a number of aspects of BR design for BALSS systems can be highlighted. The importance of the cell placement relative to the oxygen and nutrient supply is critical. The use of hepatocyte cells in the BR is adequate for liver support. And importantly the volumes of flow through the BR must be adequate to support mass transfer and cell viability.

## 2.2 Shear and pressure drop in the liver

The principle site for the regulation of blood flow is in the sinusoids. The sinusoids are also where the major pressure drop occurs in the liver. The sinusoids are the principal site for exchange between blood and hepatocytes [4]. Typically the blood flow velocity in the sinusoid ranges from 0.003-0.03cm/s, with the average hydrostatic pressure ranging from 0.9-1.3kPa [15]. The wide variations reported are due to the structural features of the sinusoids as well as the intermittent inflow from the arterial venule, not to mention the difficulty in measuring accurately. These ranges can be used for comparison of flow in optimised BR's or flow devices.

The complexity of determining the shear stress on the liver cells is difficult due to the non-Newtonian like characteristic of blood. This makes comparison of devices and the liver difficult, necessitating another approach to determine the maximum shear on hepatocyte cells. A method is investigated in Chapter 6.

## 2.3 Mass transfer in the liver

The mass transfer in the liver is what makes the organ function, clearing toxins and harmful elements in the biological system. The mass transfer in the liver is predominantly diffusion driven. The positioning of the cells

with respect to the blood supply is the basis for this assumption. The hepatocytes cells are typically 100µm from the nutrient rich blood supply[2], with the sinusoidal networks enabling oxygen etc. to diffuse to the cells.

Apart from the metabolism of certain toxins, the liver also requires nutrients for cell metabolism. For this, the cells require large amounts of oxygen. The reported value of oxygen tension at the periportal region is 70 mm Hg and 20 mm Hg in the pericentral region [15]. From this the designer can see the importance of mass transfer and oxygen supply in BR designs for this specific application. Again the relative positioning of the cells to the oxygen supply is critical with large gradients and small distances between cells and oxygen source highlighted.

## 2.4 Current trends in liver treatment research

There are a number of groups currently investigating various means to bridge a patient successfully to liver transplant or support the liver long enough to regenerate. The groups are briefly summarized in Table 1[3].

In general the research groups involved in BAL system research can be divided into biological and artificial systems. The biological systems support cells[4], in a BR, and the artificial systems do not have cells in the system. The biological systems are further subdivided into direct or indirect perfusion systems. If there is a membrane separating the cells and the perfusion medium the method is classified as indirect perfusion. For direct perfusion there is no membrane and the perfusion media comes into direct contact with the cells. Unfortunately the lower mass transfer of the indirect perfusion methods counters the added benefit of imminogoblin retention. Most of the existing biological systems are hollow fiber cartridge type bioreactors, where the membranes act as cell anchorage scaffolding and immuno isolation barrier.

The use of encapsulation systems, where the cells are suspended in a collagen matrix, try to place the cell in a suspension conducive to cell growth and differentiation. Unfortunately the poor mass transfer makes these systems less than optimal. There are groups (*see section 2.4.2.2*) pursuing an alternative to the above-mentioned methods whereby cells are seeded on scaffoldings and medium is perfused directly over the cells. Immino isolation is achieved by means of a membrane upstream of the bioreactor, with an additional oxygenation system. This is the configuration chosen for the BALSS system.

The artificial systems have no biological component. They are similar to the dialysis machine used for renal dialysis. The systems are discussed below as well as the relative success of the groups with their chosen configuration.

[2] See 4.3.2: Cell clusters (spheroids).

[3] Only groups that have conducted clinical trials are included in Table 1 (pg 10).

[4] Hepatocyte cells or co-cultures of hepatocyte and stelate cells.

### 2.4.1 Artificial systems

At the time of this study the only commercially available system, with FDA approval[5], was the MARS® (Molecular Absorbent Recirculation System) system by Teraklin. Unfortunately due to the complex biological nature of the liver this device is incapable of producing the enzymes and hormones that are commonly excreted by a healthy liver [16]. The MARS® system has the advantage that it can move free and albumin bound low and middleweight toxins with high selectivity due to the polysulphone membrane, as well as the human serum albumin as a selective absorbent for the removal of the toxins [17]. Gerlach *et al* has shown that the clearance capabilities of the MARS® system compares to that of a single pass albumin dialysis system [18]. Although there is research showing positive results in the clinical application of the MARS® system including improvement of intrarcranial pressure, encephalopathy and metabolic indicators, improvement in terms of patient survival has only been shown in two small randomized controlled trials, with larger clinical trials to determine patient outcome in terms of survival currently being conducted [17].

The Promethius system by Fresenius Medical care AG, which is a fractionated plasma separation and absorption system combined with high flux haemodialysis of the patient's blood as apposed to the MARS® system where the Albumin dialysate is haemodialized, is currently undergoing clinical trials.

### 2.4.2 Biological (or bio-artificial) systems

#### 2.4.2.1 Hollow fiber systems

The hollow fiber BR design methodology has received much attention in the BAL research field. They have different configurations and perfusion loops, but are consistent in that they use a hollow fiber cartridge. The flexibility of the hollow fiber cartridges allows for a number of BR configurations including the hepatocytes on the shell side of the lumen, examples include the Arbios systems INC (HepatAssist-2TM) [19,20], or the cells could be on the inner lumen with the blood/plasma on the shell side, for example the Algenix/ University of Minnesota, (LIVERx 2000 system) [21], other systems including the Excorp Medical (BLSS), infuse the hepatocytes into the extraluminal space with the patients blood inside the fibers and a nutrient rich media perfused over the cells on the shell side [22], and finally with even more complex designs containing interwoven, independent, capillary membrane system with each serving a different function. In the Charite Virchow Clinic-Berlin (MELS) system hepatocyte cells are seeded on the outer surface of the fibers with the plasma, oxygen supply and CO2 removal in independent fiber loops respectively [16,23].

#### 2.4.2.2 Direct perfusion systems with scaffold cell attachment

Other 3D scaffolding types include a porous type scaffolding were the cells are seeded into the scaffolding. Kaneko *et al* tested multi-capillary polyurethane foam packed bed bioreactors in animal trials. The group showed good metabolic results and reported an increase in the survival times of ALF induced pigs. The functional use of the capillaries in their BR was unclear [24,25]. The AMC-BAL system, adopts an oxygenator tubing wrapped in

[5] MARS® system obtained FDA approval on **16 June 2005.**

a polyester fabric [26,27,28]. The BALS system developed at the University of Pretoria in collaboration with the CSIR uses polyurethane foam scaffolding in a radial flow BR and is currently undergoing animal trials[6][6].

Table 1: Summery of groups with commercial support investigating means of liver support at the time of this study

| Company/group | Perfusion type | Last known Development phase | Notes | BR type | Ref |
|---|---|---|---|---|---|
| **Artificial systems** | | | | | |
| Teraklin (MARS®) | Blood | Commercially available | Received U.S. FDA 510(k) clearance **16 June 2005** | Albumin impregnated polysulfone membrane | [29] |
| Hemocleanse technologies.LLC (BioLogic-DT) | Blood | FDA-approved multicenter/ NO DEVELOPMENT | Recieved FDA 510(k) Approval. The licensee subsequently suffered financial failure in 2001, and all of the technology was returned to HemoCleanse, Inc. as of the end of 2003. | NA | [30,31] |
| Fresenius Medical care AG (Promethius system) | Plasma | Phase I clinical trials | Fractionated Plasma Separation and Absorption system (FPSA) | | [32,33] |
| **Bio-artificial - membrane-based systems** | | | | | |
| Arbios systems INC (HepatAssist-2TM) | Plasma | Phase II/III multicenter | Hepatocyte bioector | hollow fiber indirect perfusion | [19,20] |
| Algenix/ University of Minnesota (LIVERx 2000) | Blood | Phase I | Hepatocyte bioector | Hollow fiber indirect perfusion | [21] |
| Excorp Medical (BLSS) | Blood | Phase I/II | Hepatocyte bioector | Hollow fiber indirect perfusion | [22,34] |
| Charite Virchow Clinic-Berlin (MELS) | Plasma | Phase I/II | Primary human liver cell biorector | Hollow fiber | [16,35] |
| Chinese PLA General Hospital (TECA) | Plasma | Phase I | Hepatocyte bioector | Hollow fiber | [36] |
| **Bio-artificial – direct perfusion systems** | | | | | |
| Univ. of Pretoria & CSIR (BALSS) | Plasma | Pre clinical trials | Hepatocyte bioector | | [6] |
| Vital Therapies, Inc. (VTI) (ELAD®) | Plasma | Phase I/II clinical trials | Originally Hepatix, then Vitagen now Vital therapies | | [37,38] |
| Academic medical center-BAL (AMC-BAL) Amsterdam | Plasma | Phase 1 clinical trials / TRIALS STOPPED | Hepatocyte bioector | Immobilized on a non-woven polyester tissue, spirally wound in a polysulfon cartridge with an integral hollow fiber oxygenator | [26,27, 28,39] |
| **Bio-artificial- Unknown** | | | | | |
| MultiCell's Xenogenics Subsidiary (Sybiol® Synthetic BioArtificial Liver Assist Device.) | Unknown | Pre clinical trials | Immortalized human liver cells lines | | [40] |
| Cell Biotech limited (Bioliv A3) | Unknown | Clinical trials | Porcine | Hollow fiber | [41,42] |

[6] A description of the system is presented in 2.5: The BALSS system.

### 2.4.3 The cell encapsulated systems

The cell-encapsulated systems have to a large extent been combined with the hollow fiber BR's with the cells encapsulated in the BR. The most recent is the packed collagen bed with hepatocytes at the inner core and an outer shell of methyl methacrylate [43]. The advantage of these systems is that the cells are protected from the potential shear and pressure drops of high perfusion rates. The cells have a good area to volume ratio and cell-cell interaction is encouraged [44]. Unfortunately the disadvantages are poor mass transfer and non-optimal cell topography.

Desille *et al* has shown neurological improvement in pigs with acute liver failure using a BR containing alginate gel beads [9].

The encapsulation systems encountered by the author are still under development with no groups' research included in Table 1 because they have not reached clinical trials.

### 2.4.4 New technologies

Each system mentioned above has its own advantages and disadvantages. The future of systems used to support patients with ALF will need to be flexible, thus a system with a built in measurement and control system will be advantageous. The system should be small and compact, easy to use in a clinical setting by clinical personell. Non-uniform subsystem improvement in cell cultures and bioreactors etc. will contribute to the success of the system as a whole.

A system that could support patients until they receive a transplant or until the liver repairs itself would drastically increase the survival rate for ALF patients.

## 2.5 The BALSS system

The design optimization presented in this dissertation deals with a Bio-artificial Liver Support System (BALSS) currently under development by the University of Pretoria and the Council for Scientific and Industrial Research (UP-CSIR). The BALS system is currently undergoing animal trials (pig model) at University of Pretoria, Biological Research Unit (UPBRC) [45]. The BALS system is designed to support liver function in an ALF patient, supporting the patient on a metabolic level without adversely affecting the hemodynamic status of the patient.

The BALS system is an extra corporeal system where plasma from the patient, obtained by normal plasma separation via a commercially available plasma separator, is perfused through a bioreactor. The bioreactor is a radial flow type bioreactor with a cylindrical open pore polyurethane foam core that acts as scaffold for hepatocyte cell adhesion. The bioreactor is seeded with procine hepatocyte and stellate cell co-cultures prior to testing the BALS system in an ischemic pig model. The polyurethane 3d structure with open celled pores, allows

for a large surface area to volume ratio. The advantage of such scaffolding is the inherent cell-to-cell interaction that has been proved to positively affect cell growth and differentiation [42,46,47]. In order to enhance the oxygenation of the hepatocytes located in the bioreactor, an artificial oxygenator, Perfluorochemical (PFC) is added to the plasma perfusion. Before returning the plasma back to the patient, the PFC is removed by means of a tangential flow filter. A photo of the BALS system is shown in Figure 5.

### 2.5.1 Liver cell isolation, cell seeding and BR cultivation

Liver cells (hepatocytes and stellate cells) are isolated be means of a modified Senglin method as described by Niewoudt *et al* five days prior the ischemic liver failure animal model experiment [48]. After isolation the cells are suspended in Dulbecco's modified Eagle's medium (DMEM) supplied by Bio-Whittaker, Adcock Ingram Scientific (Johannesburg, South Africa), and perfused through the BR at a flow rate of 100ml/min. This process is called seeding. Most of the cells, being anchorage dependent, will adhere to the surface areas of the foam. The remaining cells that don't adhere to the scaffolding drop out of suspension and accumulate at the bottom of the BR. The BR[7] is maintained by means of constant perfusion and oxygenation for five days allowing cell differentiation and optimal metabolic viability.

The current seeding and cell attachment mechanism is poorly understood and the author could find no reported means for the prediction of where the cells will finally seed or drop out. Having the ability to predict this affords the researcher the ability to minimize ineffective areas in similar 3d structures. This will be dealt with later in the text. The seeding as well as performance parameters of the BR is therefore heavily dependant on the flow conditions within the BR for optimal operation. For example if the flow rates are not optimal the possibility for cell narcosis is good due to inadequate mass transfer and convection to the seeded cells. If the flow rates are too extreme then cell breakaway is possible and other related shear phenomena [49,50].

### 2.5.2 BALSS testing on a porcine animal model

The clinical efficacy of the BALS system is tested in a porcine, large animal ischemic liver failure model conducted on pathogen free, female, white Landrace pigs. ALF is induced in the animal by means of an ischemic surgical model described by Niewout *et al* [48]. After surgery the animal is treated in an ICU setting with the BALSS connected 6 hours after surgery. The BALS system removes plasma from the animal's blood by means of a commercially available plasma separator at a blood flow rate of 200ml/min. The plasma is fed to the BALSS system into a central reservoir at a flow rate between 30-60ml/min; see Figure 5. The artificial oxygen carrier (perfluorooctyl bromide (PFOB)) which is a Perfluorochemical (PFC), is located in the reservoir and plasma entering the reservoir is mixed with the PFOB. This emulsion is then oxygenated by means of a new natal oxygenator, Lilliput 1 (D901) by dideco (http://www.dideco.com), where the temperature is regulated at 38°C and perfused through the radial flow BR at 400ml/min. The plasma PFC mixture is then returned to the reservoir. The other perfusion loop removes the PFOB emulsion from the central reservoir and separates the

[7] A more detailed description of the BR is given in section 3.2 Geometric representation of the model.

PFC emulsion from the plasma by means of a tangential flow filter (Microza MF modules PSP-103) supplied by PALL SA. The plasma filtered off is returned to the plasma separator and, with the hemocritic components of the blood, returned to the animal. Figure 5 shows the system.

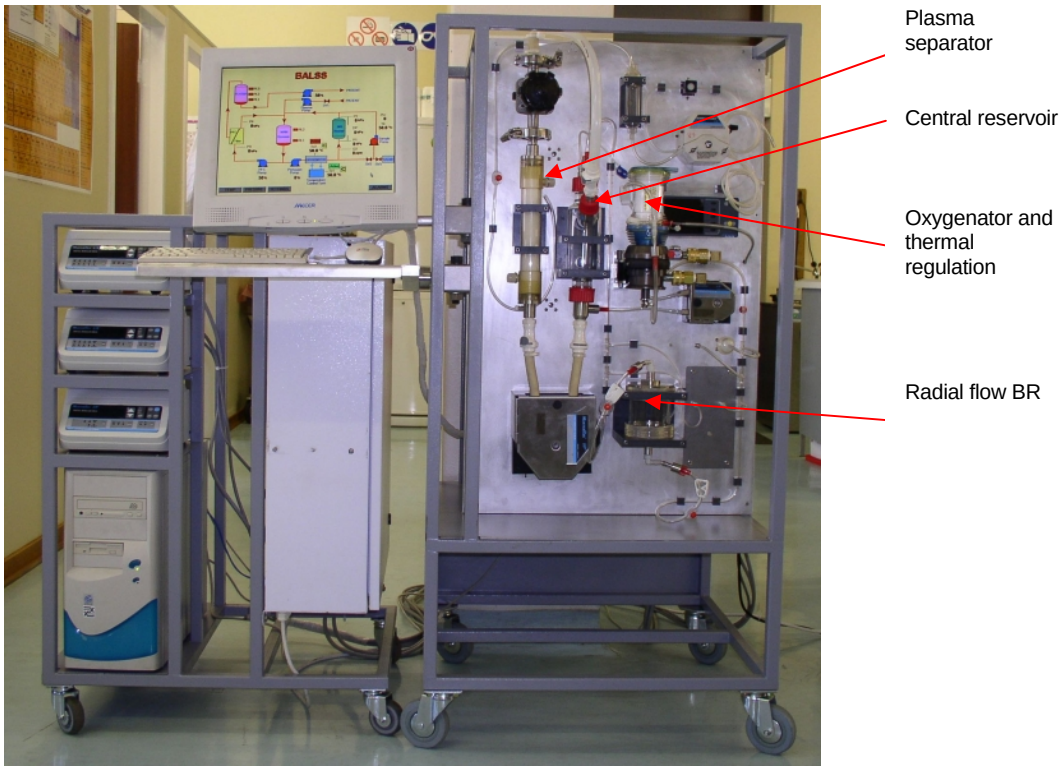


Figure 5: BALSS system as used in the animal trials

### 2.5.3 Autopsy and data analysis

The experiment is a terminal model. An autopsy is performed after the experiment to determine the cause of death, if not due to liver failure. This might seem odd, but due to the complexity of the ALF model, some animals invariably die from secondary effects including: cardiac failure, multi organ failure and surgical complications.

Biological indicators are monitored at four hourly intervals during the experiment to determine changes in the animal's clinical and metabolic activity. Examples are blood glucose levels, ammoniac concentration levels, liver enzymes, blood gas parameters and pH values, etc. These parameters are indicative of the metabolic activity and functioning of the BALS systems as a liver assistance form of therapy.

Having dealt with literature on the general nature of BAL systems and other related topics further in-depth investigations into modeling and testing techniques describing the flow and seeding conditions in the BALSS BR will be investigated, with relevant literature on more specific topics dealt with, as an introductory text were relevant.

# 3 SIMULATION OF FLOW THROUGH THE BIO-ARTIFICIAL LIVER SUPPORT SYSTEM, BIOREACTOR

*"Making the simple complicated is commonplace; making the complicated simple, awesomely simple, that's creativity."* - *Charles Mingus*

## 3.1 Considerations for CFD simulations

Simulations geared at aiding the design optimization of flow systems are common in engineering fields. Computational Fluid Dynamics (CFD) is used to simulate various aspects of flow or flow related phenomena and has the ability to effectively simulate devices dependant on flow. The use of these tools in other fields, like medical research, has been slow due to the complexity of the software and the fact that the user must have a strong mathematical fluid dynamic background to correctly interpret the results and solver limitations. The evaluation of mass transfer for two different collagen systems [51] and modeling of the microcirculation of blood flow in the hepatic lobule [13] are examples of CFD used in the medical research field. With this tool, correctly used, the researcher could visualize the flow through the BR as well as predict cell dropout through the BR. CFD can also be used to optimize the BR geometry for optimal flow conditions.

The importance of modeling biological systems, including bioreactors, stems from the lack of comprehensive understanding of the flow conditions and related mass transfer in these devices. In the following chapter, methods for the simulation and verification of the BR used in the BALSS, developed by the UP-CSIR, are discussed. This methodology can be extended to future designs of essentially any BR. As an outcome, the CFD modeling must predict flow rates, localized flow velocity, related pressure drops and flow paths in the BR. During these simulations areas that show poor performance can be optimized, by changing the BR geometry and flow speeds. It is important to note that flow conditions in the BR are crucial factors for governing mass transfer, as well as seeding in the scaffolding.

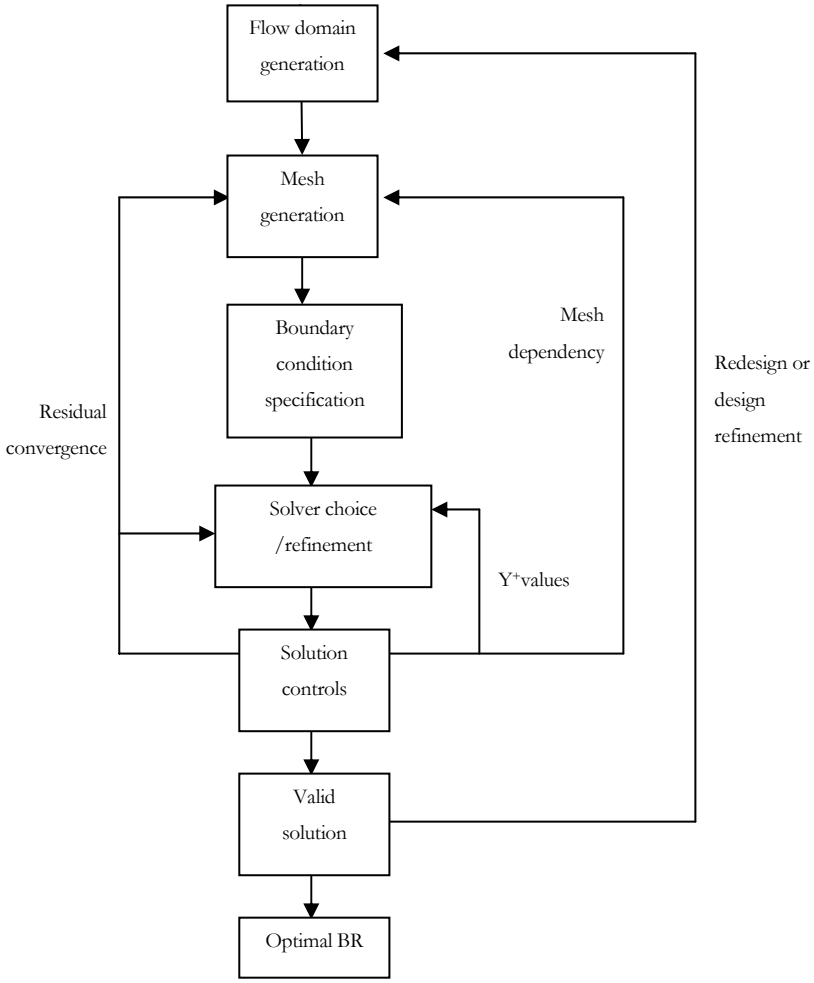


Figure 6: Flow diagram for CFD design methodology

## 3.2 Building the model

The modeling of the flow region in the BALSS BR begins at the design phase were a solid model of the assembled BR is constructed and a lifelike representation of the final BR, is developed. The model is then imported into a preprocessor were the flow region is determined and meshed (i.e. broken up into spatial points). This meshed model is then exported to a numerical processor were the governing flow equations or, more typically, simplified versions thereof are solved in discrete spatial steps through the mesh. Finally in post processing the velocity profiles, pressure drops etc. of the individual spatial points are combined and displayed. This then needs to be interpreted for design refinement. Figure 6 shows the typical simulation flow diagram for CFD modeling, each step is expanded further to give the reader a better understanding of the complexity of modeling a biological system with porous scaffolding.

### 3.2.1 Geometric representation of the model

The geometric modelling of the BR was done using a commercially available parasolid modelling software package namely Solid Edge (Version 14), and was done by Mr AJ van Wyk from the University of Pretoria. The

assembled sectioned model, shown in Figure 7, has the flow entering from the bottom, at 4, and diffusing over the cone insert (3). The BR is drawn in the orientation of service with gravity against the inlet flow. The foam scaffolding (2) is radially situated around the internal cone insert, with the flow flowing radially from the inside diameter to the outer diameter. The flow Accumulates at the outermost radial cavity and is forced upwards where the geometry of the BR converges. The flow exits the BR at the central outlet (1) at the top of the BR.

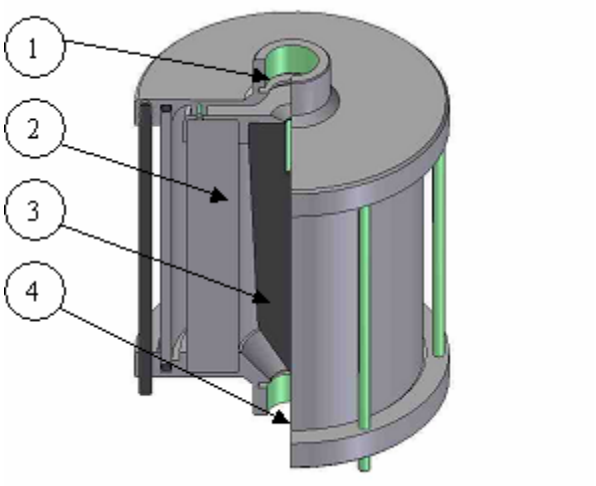


Figure 7: Solid model of the BALSS BR

### 3.2.2 Construction of flow domain and meshing

The solid model, representing the geometry of the BR, was imported into Gambit 2.2.30 with only the assembled model as a start. To model the flow area using the solver (discussed later) the flow area needed to be determined. A Boolean operation was performed on the solid model subtracting a cylindrical volume from the imported geometry. The resulting cavities are the flow domain. Included in this are the fastening holes, seals etc. These volumes increase the computational effort required to solve the system. The remaining geometry was simplified by deleting arbitrary volumes. The resulting volume is the true flow area for the BR. To simplify the solving step, and to minimise the computational effort of the solver, the BR was assumed to be axi-symetric with only a quarter of the volume modelled. This assumption is valid provided the flow just prior to the inlet has no swirl, caused by a bent pipe etc.

The flow volume was further divided into three volumes including the inlet volume, porous volume and the outlet volume[8] shown in Figure 8. The inlet and outlet fluid regions have similar governing constraints with the boundary conditions varying for the inlet and outlet. The porous scaffolding is predefined by Gambit as a fluid region and later redefined in Fluent as a porous region.

[8] The inlet volume comprises of the flow region before the scaffolding, the porous volume is the region occupied by the scaffolding and the outlet flow is the exit volume of the BR.

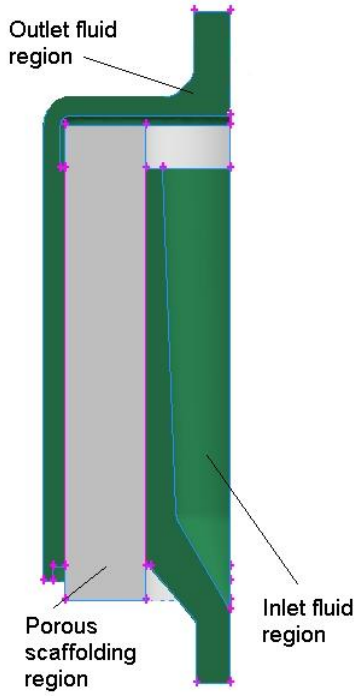


Figure 8: Gambit fluid regions

The porous volume was meshed using a brick-cooper scheme[9], which essentially discretises the volume by means of a 2D mesh on a surface of the volume with quadrilateral elements and builds the bricks using an equal distance along the length of the volume. The other two volumes were meshed using the common tetrahedral scheme. The quality of the meshes was determined using the equiangle skewness (EAS) defined by Equation 1[10].

$$Q_{EAS} = \max\left\{\frac{\theta_{\max} - \theta_{eq}}{2\pi - \theta_{eq}}, \frac{\theta_{eq} - \theta_{\min}}{\theta_{eq}}\right\}$$

Equation 1

Where $\theta_{min,max}$ is the minimum and maximum angle between the edges of an element and $\theta_{eq}$ is the angle of an equivalent element in equilateral form. For example a hexagonal element will have $\theta_{eq}=90°$ and for a tetrahedral element $\theta_{eq}=60°$. The practical measure of the EAS is the quality of the individual elements with perfect hexagonal elements having $Q_{EAS}\approx 0$; this would theoretically be the optimal. Because of the inherent averaging used by the numerical solver, elements with lower EAS values perform better. This is because averaged values are placed closer to the centre of an equilateral element than that of a skew element. Accordingly a mesh with an average EAS <0.4 is a high quality mesh [52].

[9] A description of the brick cooper scheme can be found in any good numerical techniques textbook.

The number of elements for each volume is given in Table 2[11]. Figure 9 gives a histogram plot of the element quality in terms of EAS. From the plot it is clear that the mesh is of a high quality, with an average of approximately 0.25.

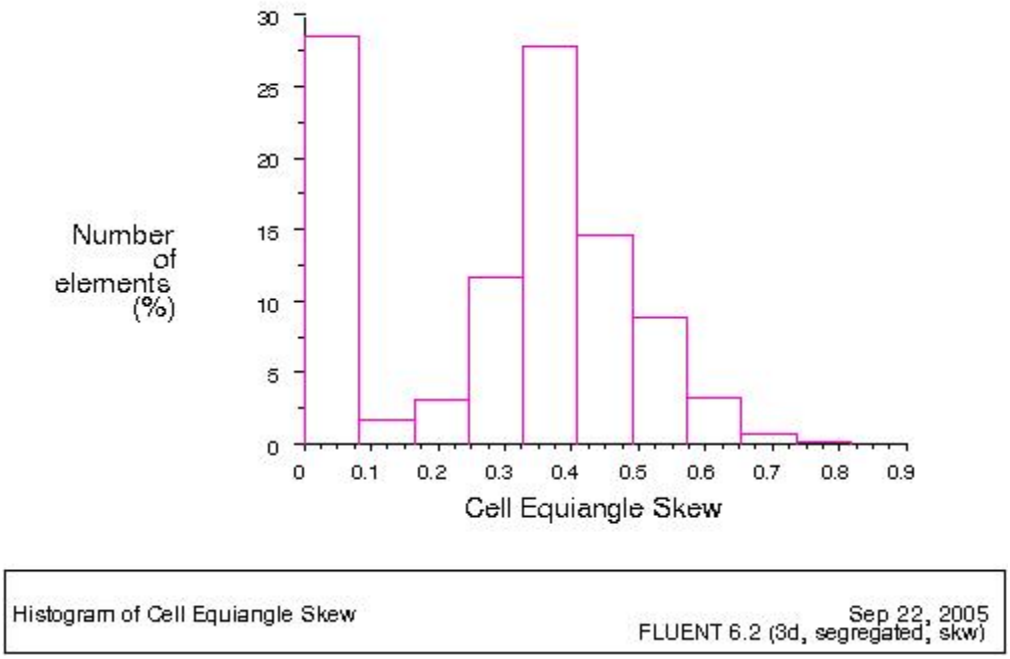


Figure 9: EAS for the final mesh independent solution

The high peak with cells that are excellent i.e. 0<EAS<0.1 is a result of the scaffolding where a brick meshing scheme was used. The brick scheme is well known for showing good numerical results. It would not, however, be economical to mesh difficult geometries using the brick scheme.

## 3.3 Solving the flow domain

### 3.3.1 The solver

The discretisation scheme used by the Fluent solver is a finite volume based method. Essentially, the domain is divided into discrete control volumes, with the governing Navier-Stokes equations integrated around the individual volumes to construct algebraic equations in terms of dependent unknowns, i.e. pressure, velocity etc. These equations are linearized and the resultant is used to update the dependent variables as the iterations progress. The linearization determines the order of accuracy for the specific scheme.

[10] From: // Fluent.Inc/gambit2.2.30/help/html/users_guide/ug0304.htm#spec_quality_type

[11] Table 2 can be found at the end of the chapter on pg 47. Only mesh independent solutions are displayed.

The problem encountered by the discretization of the equations lie in the method for determining the flow conditions of the centre cell in terms of the surrounding cells. When the convective terms needs to be solved for, the assumption that the node of interest depends on both upstream and downstream nodes is incorrect. The remedy for this convective instability is simply to model the convective term using only the upstream contribution to the discretised term [53]. The stabilisation procedure is called up winding and essentially uses only information from upstream cells. This method determines the accuracy of the final numerical result with 1st order being first order accurate and so forth.

A 2nd order discretization scheme was used to minimize diffusion of the numerical error. This would occur because the flow is not aligned to the grid especially because part of the mesh volume is a tetrahedral meshing scheme. There was little difference between the stabilisation methods investigated.

### 3.3.2 The model

#### 3.3.2.1 Turbulence modelling

The Shear Stress Transport k-ω model (SSTk-ω) was used as the turbulence model. The choice of this turbulence model depended on a number of restrictions. Attention to the physics encompassing the flow i.e. fluid density, temperature, geometry etc., the level of accuracy required, the available computational resources and the available time all contributed to the choice of this model. In the current simulation the k-ω SST model was used due to is ability to model near wall phenomena without the addition of wall boundary meshing techniques. Relying on the Reynolds Averaged Navier-Stokes Equations (RANSE), it is an empirical based model, which combines the accurate formulation of near wall regions with the free stream capabilities of the standard k-ε model. The SSTk-ω model is different to the standard k-ω model in the definition of turbulent viscosity, which is modified to account for the turbulent shear stresses. The change in free stream and wall formulation is more gradual than the standard model[12]. This makes the SSTk-ω more accurate for a larger number of flows than the standard k-ω model [54].

The method of calculation and the governing equations used are given in the Fluent help files [54]. The method is summarized in Appendix B for the specific case used in this study. A short summarised discussion of the turbulence modelling is presented below.

Turbulent modelling is based on fluctuation velocity fields. This results in mixing of the momentum, heat transfer, species transport terms etc. found in true flows. These fluctuation velocities at the time of this investigation were impractical to solve directly. The frequencies are high and the magnitude small resulting in substantial computational effort to solve.

[12] The methods used by Fluent for near wall formulations including log law turbulent modelling etc. are described by White [53].

As a result, researches and industry were forced to use an averaging approach minimizing the computation time and memory required to solve the flow domain. The Reynolds equations of turbulent motion effectively model the turbulent flow, i.e. the fluctuations, as an average flow variable in addition to a fluctuating variable. Equation 2 is the Reynolds equation where $\phi$ holds for pressure, temperature, species etc.

$$\phi = \bar{\phi} + \phi'$$

Equation 2

Where $\bar{\phi}$ is the average and $\phi'$ is the fluctuating part of the flow. The above method of modelling turbulent flows result in both the averaging component as well as the fluctuation component, individually, satisfying the continuity equation. The proof of which is given in Viscous Flow by Frank White [53].

With considerable effort and taking the time average of the non-linear Navier Stokes equations, Equation 3 can be obtained. With Einstein notation adopted for simplicity[13].

$$\rho \frac{D\bar{U}}{Dt} + \rho \frac{\partial}{\partial x_j}\left(\overline{u_i' u_j'}\right) = \rho g - \nabla \bar{p} + \mu \nabla^2 \bar{U}$$

Equation 3

[13] Where repeated subscripts imply summation, and individual subscripts, vector orientation [53].

Where $\rho$ is the density, $\frac{D\overline{U}}{Dt}$ is the local derivative and is the first order time differential for the local velocity vector in all three directions, u is the local velocity vector, x is spatial vector, g is the gravitational constant $g = 9.81\,{}^{m}/_{s^2}$, $\nabla$ is the gradient operator and represents the first order differential of average pressure ($\overline{p}$) in each spatial direction, μ is the fluid viscosity, $\nabla^2\overline{U}$ is the 2nd order differential in each spatial direction of the velocity vector u.

The problem with the averaged momentum equation is the second term involving the turbulent inertia tensor $\overline{u_i' u_j'}$, which is never negligible. This new tensor adds another nine unknowns in 3d flows that need to be solved for. These terms are dependent on the fluids physical properties as well as the local flow properties i.e. geometry, flow conditions etc.

The turbulent inertia tensor is solved in Fluent[14] using the Boussinesq hypothesis. The hypothesis relates the tensor to the mean velocity gradients as shown in Equation 4.

$$-\rho\overline{u_i' u_j'} = \mu_t\left(\frac{\partial u_i}{\partial x_j} + \frac{\partial u_j}{\partial x_i}\right) - \frac{2}{3}\left(\rho k + \mu_t \frac{\partial u_i}{\partial x_i}\right)\delta_{ij}$$

Equation 4

[14] The two equation models.

Where $\delta_{ij}$ is the chronica delta used for matrix manipulation in the solver, if i=j then $\delta_{ij}$ =1 if i≠j $\delta_{ij}$ =0. In the two equation models presented by Fluent two additional equations, $k$ and $\omega$ which are turbulence generation and specific dissipation rate respectively, are solved as shown in Appendix B. The turbulent viscosity $\mu_t$ is solved in terms of the $k$ and $\omega$ variables.

Alternative modeling approaches include Large Eddie Simulation (LES), which attempts to solve the larger eddies due to turbulence but filters out the smaller fluctuations in the flow. This filtering results in a number of unknowns with the method not receiving much attention due to the substantial computational cost and time.

The mixture multiphase model was used to model the different phases and the interaction between them. This is more accurate than discrete phase modelling if the volume fraction of the secondary phase exceeds 10%. In the seeding of the BR the cells constitute one phase and the Williams E Media the other and in the clinical perfusion step the plasma and PFOB are the two phases respectively.

#### 3.3.2.2 Porous modelling

In theory, hydrodynamic dispersion through a porous media can be described by the Navier-Stokes equations and can be solved to a reasonable degree numerically. However this would entail formulating correctly boundary conditions for highly irregular boundaries, *see* Figure 34 on pg 51, both in the sense of the chaotic movement of the fluid as well as the porous geometry that needs to be described [5]. This was overcome in Fluent by the addition of a momentum source term in the standard flow equations. The momentum source term adds resistance to the flow and a pressure drop essentially modeling the effects the scaffolding has on the flow. In the model used, homogeneous porous media was simulated, because the scaffolding is uniformly expanded in all directions. Equation 5 [55] gives the momentum source term.

$$S_i = -\left( \frac{\mu}{\alpha} u_i + C_2 \frac{1}{2} \rho u_{mag} u_i \right)$$

Equation 5

Where α is defined as the permeability, $\mu$ is the fluid viscosity, $u_i$ is the local velocity vector, $\rho$ is the fluid density and C2 as the internal resistance factor for the porous section. Equation 5 is the momentum sink, which contributes to the pressure gradient in the porous cells proportional to the fluid velocity. This can be measured experimentally and the coefficients solved for and then incorporated into the model. An important assumption used by the porous model is that the solid scaffolding is not meshed; only the effects of it are interpreted.

An experimental set-up was constructed by expanding polyurethane foam (PUF) in a 27mm diameter PVC pipe section with a length of 100mm. The 100mm section was mounted centrally in a flow conduit with a total length

of 500mm. The 200mm sections upstream and downstream of the porous test section were incorporated to minimise jetting effects. Refer to Figure 10.

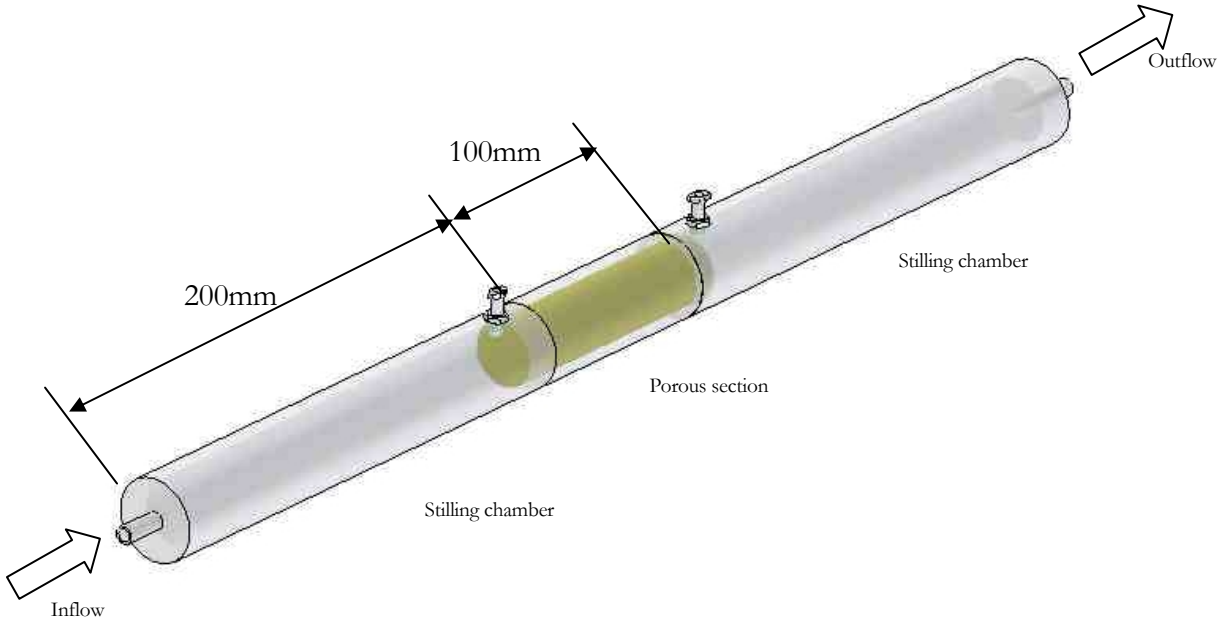


Figure 10: Schematic of the porous pressure drop experiment.

A digitally controlled pump was used to regulate the flow speed, (digital standard drive-\easy load masterflex model 7518-60 supplied by Cole Parmer). The pump was calibrated using demineralised water prior to the experiment. The pressure drop over the porous section was measured by means of a manometer[15]. Different flow rates, 0-500ml/min, were perfused over the foam test section and the pressure drops were noted. Demineralised water was used for testing. The following pressures were measured as a function flow speed, Figure 11.

[15] The working fluid (i.e. demineralised water) was used in the manometer loop so that the density and temperature was consistent. A schematic of the system is given in Figure 61 on pg 78.

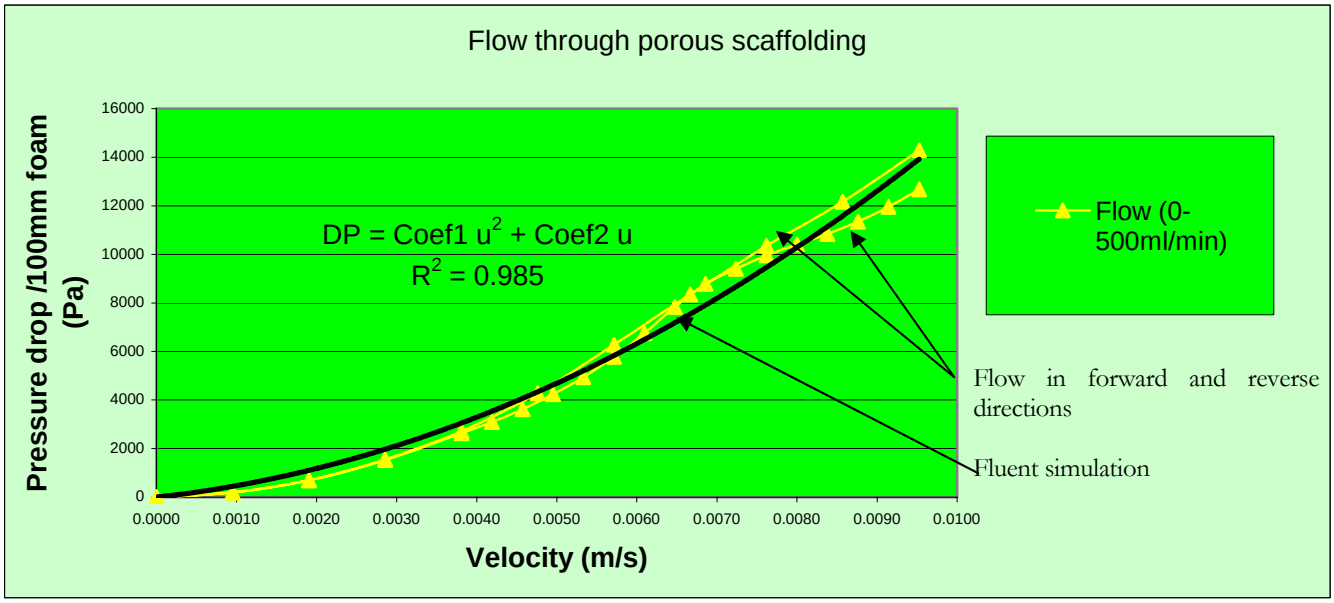


Figure 11: Comparison of the porous modelling in Fluent and the porous pressure drop experiments

The trend line obtained by curve fitting through the data, takes the form of Equation 5 Thus the first coefficient ($Coef1$) produces the internal resistance, Equation 6.

$$Coef1 = C_2 \frac{1}{2} \rho \Delta x$$

Equation 6

Where Δx is indicative of the finite length of the flow path through the porous media, this needs to be incorporated because the test setup has a different length compared to the model. Using the density of the fluid media; $C_2$ can be calculated. The viscous resistance or permeability $1/\alpha$ can be calculated in a similar manner using Equation 7.

$$Coef2 = \frac{\mu}{\alpha} \Delta x$$

Equation 7

Were μ is the viscosity of the fluid media. Simulating, in Fluent, the identical test setup for different flow rates and comparing them to the tested values verified the model. The verification is shown in Figure 11 and shows

very good correlation to the measured pressure drops. The assumption of homogeneous porous scaffolding was verified by testing the flow in both forward and reverse directions, in the porous pressure drop experiments. The data shown in Figure 11 shows good correlation (R=0.985) with the pressure drop essentially the same in both directions.

## 3.4 Operating conditions

Gravity was orientated according to the positioning of the BR in its operating position. The overall pressure drop is small in comparison to absolute static pressure if the flow has a low mach number; this results in round off errors in the numerical approximation [56]. Fluent minimises the round off error by subtracting the operating pressure from the absolute pressure using the resulting gauge pressure for calculations. Equation 8 shows the relationship for gauge pressure etc. The operating pressure was left at the default of standard atmospheric pressure

$$P_{abs} = P_{op} + P_{gauge}$$

Equation 8

## 3.5 Simulated materials

The materials specified for different simulations include Williams-E medium (Fluid), used for metabolic trials and for seeding, PFOB background solution (which is the fluid used as an oxygen carrier) and blood plasma. The particles modelled include the hepatocyte spheroids. The characteristics of the fluids are included in Table 3[16] as well as their sources.

## 3.6 Boundary conditions (BC)

The BR was divided into ¼ sections with only one-quarter modelled. Symmetry was assumed due to the axi-symetric radial nature of the BR. The outlying parameters of the BR were modelled as walls with the energy equation disabled. The symmetry planes of the BR were modelled using symmetry BC's.

The outlet was modelled as outflow (i.e. mass balance was enforced over inlet and outlet boundaries) and the inlet was varied as mass flow inlet and velocity flow inlet to determine possible solution dependence on the flow. No discrepancy was observed between the respective inlet BC's. The BC between the porous flow region and the remaining flow regions was modelled as interior faces, where the solved flow conditions are carried between the regions with no constraints.

[16] Table 3 can be found at the end of the chapter on pg 48.

The inlet flow boundary conditions were calculated as follows; for the mass flow BC, the mass flow is related to the inlet volumetric flow rate $\dot{Q}$ by means of Equation 9:

$$\dot{M}_{in,1/4} = \frac{\dot{Q}\rho}{4}$$

Equation 9

The velocity inlet can be calculated from the flow rate in a similar manner, with the total inlet area calculated from Equation 10

$$A_{in} = \frac{\pi}{4} d^2$$

Equation 10

The velocity is simply the total flow rate divided by the total cross sectional area perpendicular to the flow, Equation 11:

$$V_{in} = \frac{\dot{Q}}{A}$$

Equation 11

Equation 12 gives the hydraulic diameter [53]

$$D_h = \frac{4A}{P}$$

Equation 12

Where A is the cross sectional area perpendicular to the flow and P is the wetted parameter. The hydraulic diameter was used by the solver to calculate the geometry of the inlet face.

## 3.7 Outcomes of CFD simulations

In the design of a BR a number of important design aspects[17] need to be verified and optimized. Ultimately, modeling is a tool to achieve this. In the post processing the following results must be highlighted:

1. The pressure drop over the scaffolding.

2. The flow speed over the scaffolding.

3. The maximum shear stress over the scaffolding.

4. Adequate species transport, related to flow speed.

5. Minimizing dead spots (i.e. areas of non-circulation and species diffusion dead spots).

### 3.7.1 Post processing of CFD and results

During the normal operational procedure of the BR, two distinct modes of operation can be distinguished namely;

1. The seeding of the BR with hepatocyte cells (20% hepatocyte phase, volumetric) in suspension at a flow rate of 100ml/min,

2. and operational utilization of the BR in the BALSS system during which time the BR is perfused with a plasma PFOB (10% PFOB phase, volumetric) mixture at a flow rate of 400ml/min.

Both these perfusion conditions will be addressed and the CFD results discussed subsequently.

## 3.8 Modelling seeding and hepatocyte dropout

The first step in preparing the BR for incorporation in the BALSS entails the seeding of the hepatocyte cells into the BR. After isolation from the liver, the cells are in single and cell aggregate suspension. This cell suspension is perfused through the BR, where the hepatocytes will adhere to the porous scaffolding due to the anchorage dependent nature of the cells. The positioning of the cells in the porous scaffolding is a flow related function, with the seeding process currently done by perfusing the cells through the scaffolding at a lower flow speed than that of the clinical perfusion rate. Currently the cells are seeded at 100ml/min and the clinical perfusion rate is 400ml/min.

In modeling the seeding step a better understanding of the flow characteristics, with regards to the specific bioreactor geometries, as well as how they differ with the later increase in flow speeds can be developed. With this information the researcher could postulate what effects this would have on the successful operation of the BR.

[17] *See* 7.1 Concluding hepatocyte BR design considerations

## 3.9 Velocity and pressure contours for cell seeding

The cell seeding procedure results are shown in Figure 12 to Figure 14. The hepatocyte cells were modeled as a separate phase with the interaction of Williums-E medium taken into account. The two phases were modeled separately due to the differences in their respective densities and concentrations in the global flow. The flow rates for the various phases were determined using similar techniques discussed in section 3.6. The global flow shown in Figure 12 move's from the bottom of the BR to the outlet at the top. The white areas, typically at the inlet and outlet, are outside the reported values and are omitted for clarity. Localized regions of higher flow rates were evident at the inlet and outlet due to the path restriction in these areas. The flow over the conical diffuser is uniform with little flow separation. The flow through the scaffolding is not uniform with localized areas of retarded flow.

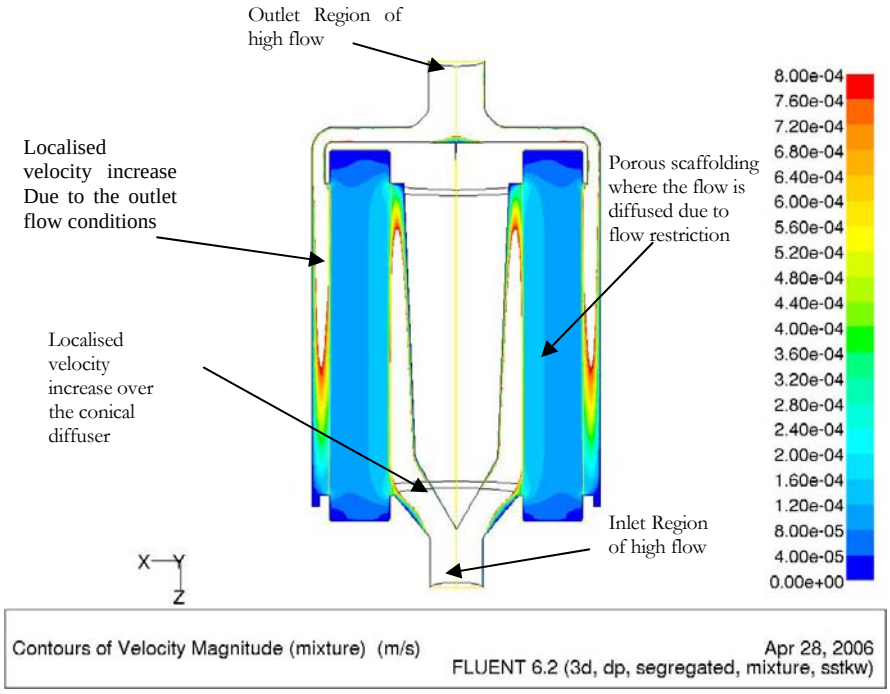


Figure 12: Velocity contours for global flow, including the cells and Williams-E media

The pressure drop, shown in Figure 13, shows more or less uniform pressure at the inlet and outlet flow areas with the dynamic pressure head neglected due to the small local velocities. There is a pressure drop over the scaffolding as what would be expected due to the momentum sink, Equation 5, imposed by porous modeling.

The areas of retarded flow, shown in Figure 14, increase the chances of cell dropout especially when the effects of gravity are taken into account. These areas are detrimental for cell function due to the lack of convective mass transfer. With these two negative factors taken into account the net result is a large area of ineffective and possible detrimental BR volume. Detrimental because of the negative impact these narcotic cells might have on the rest of the BR, and more importantly on the remaining healthy cells.

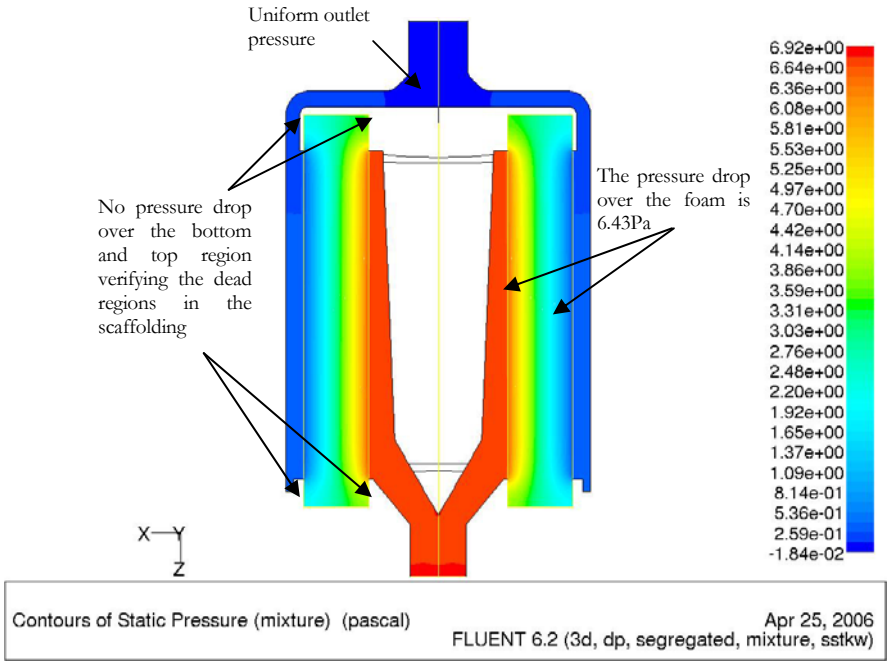


Figure 13: Pressure contours over the BR during cell seeding

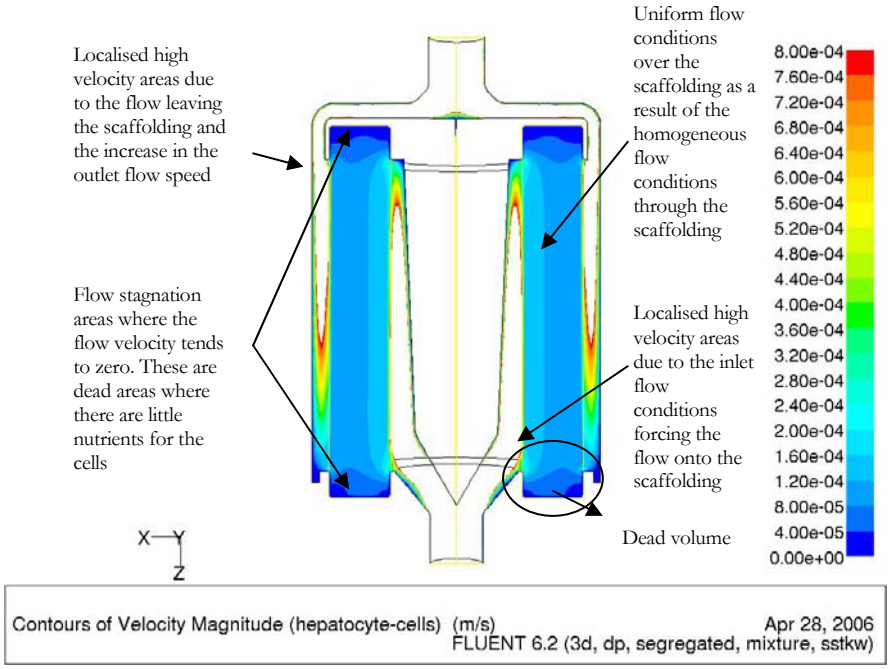


Figure 14: Velocity contours over the scaffolding during cell seeding

The pressure drop over the foam scaffolding is a mere 6.43Pa, and the velocity in the foam calculated using the mass weighted average[18] at the inlet of the foam, is in the region of 0.0004454m/s (0.04454cm/s) and at the outlet 0.00028m/s (0.028cm/s). In comparison to the flow rates typically found in sinusoid ranging from 0.003cm/s-0.03cm/s and a hydrostatic pressure ranging from 0.9-1.3kPa [15] the flow in the scaffolding is faster. The slow flow rate in terms of convective forces needed to drive mass transfer are inadequate and may result in cell narcosis thus a more uniform flow distribution is required in the BR's scaffolding allowing adequate mass transfer to all regions of the foam. Another inconsistency with the sinusoid region is the diffusion path length. Because of the small distances for diffusion in a healthy liver the mass transfer doesn't have to be flow driven, with the cells receiving adequate nutrients for survival purely by diffusion gradients. This is not the case in a BR with large diffusion paths, were there are relatively large distances between seeded cells and the oxygen source.

The dead spots during the seeding perfusion can be found at the lower and uppermost parts of the scaffolding and this is due to the method the foam is held in place in the BR. These regions are necessary for the correct placement of the foam but the dead volume created is approximately 17% of the scaffolding volume.

## 3.10 Modelling cell seeding using particle tracking

The cell drop out during the seeding procedure is an important consideration for the design flow speed. Because the cells are denser than the surrounding Williams-E media the forces on the cells, including buoyancy, drag and weight need to balance for the cells to stay suspended in the flow. As this is too complex to solve analytically in a moving fluid, particle tracking was used by means of discrete phase modeling.

The density of the hepatocyte cells was based on the density gradient method used for cell isolation [48]. The value was derived from the density of percoll medium which is used to separate parenchymal cells and debris from cell aggregates [57]. The density used in the iso-density percoll centrifugation method is 1.06g/ml. Thus it is reasonable to assume the hepatocyte density is 1.065g/ml. With this the model can balance the forces and the particles can be tracked. The drag and buoyancy forces are calculated in the model in terms of the particles size and density. The values used are presented in Table 3[19].

Figure 15 and Figure 16 shows the results of the particle tracking. An important consideration in the interpretation of the results is the scaffolding is not modelled as a true porous region but the effects of which are modelled. Thus if the cells slow down to a point where they drop out of the flow they will not be obstructed by the scaffolding but would drop to the bottom of the BR, in reality this would not occur. The simulation does

[18] The mass weighted average is an indication of the localised velocity of the bulk of the flow. For example if 90% of the mass flow is fast the average mass flow rate would be faster than the area average flow rate. This gives a better description of what the bulk of the flow is doing.

[19] Table 3 can be found at the end of the chapter on pg 48.

give an insight to where the cells would end up in the scaffolding. Clearly the cells would only seed the bottom third of the scaffolding predominantly the lower areas around the inner circumference.

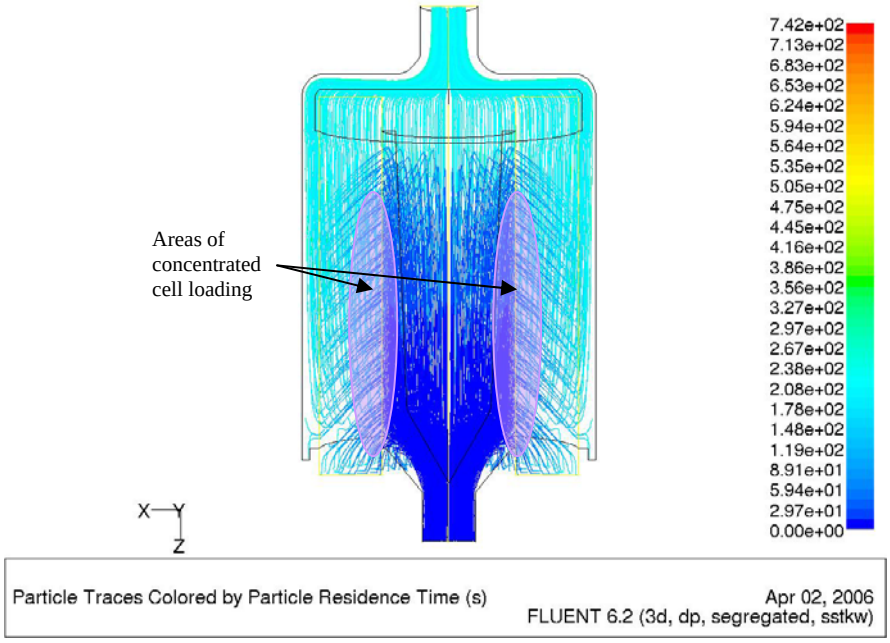


Figure 15: Particle tracking of hepatocyte cells through the BR during seeding

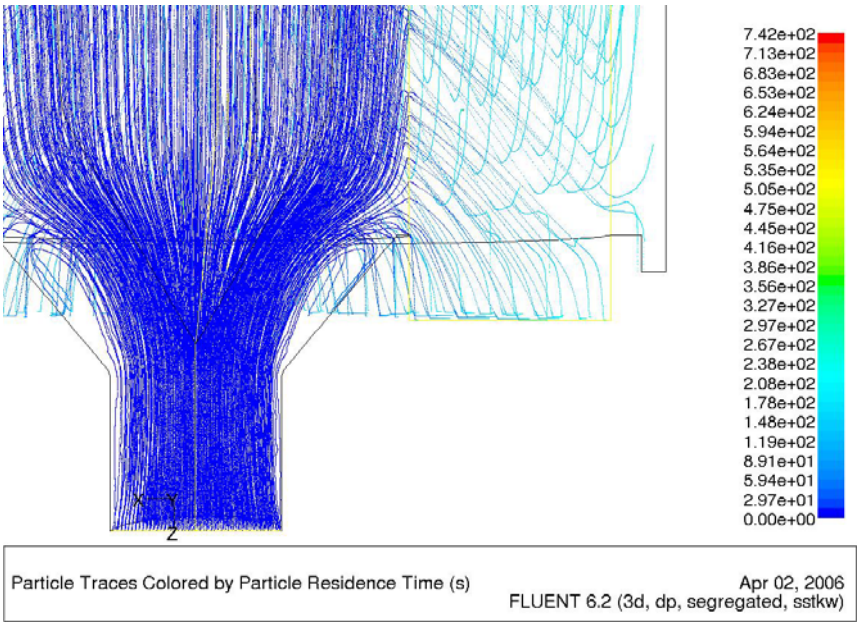


Figure 16: Hepatocyte cells dropping out of the flow during cell seeding

This is not ideal because large areas of the porous medium in the BR are resulting in unused reactor volume. The unused volume can be found at the top of the porous scaffolding with a densely seeded region lying at the inlet-perfused region of the BR. The bottom section of the BR was also not optimally perfused, resulting in inadequate mass transfer to the cells, (during seeding) which would lead to cell narcosis.

## 3.11 Modelling of flow during clinical perfusion using PFOB in solution with hepatocytes seeded in the scaffolding

The modeling of the BR when used on a patient in a clinical setup differs from the seeding step dealt with in *section* 3.8. The hepatocytes are in the scaffolding and the perfusion medium changes from Williams-E medium to the patient's plasma. An oxygen carrier namely PFOB is incorporated into the perfusion loop to facilitate oxygen transfer to the cells. The PFOB constitute a large portion of the total volume and was consequently modeled as a separate phase. The modeling parameters are given in Table 2[20]. The perfusion rate differs from seeding and is 400ml/min.

### 3.11.1 Velocity and pressure contours for animal trial perfusion

From Figure 17 a similar pattern can be seen as in the seeding step with dead spots at the upper and lower most areas of the foam scaffolding.

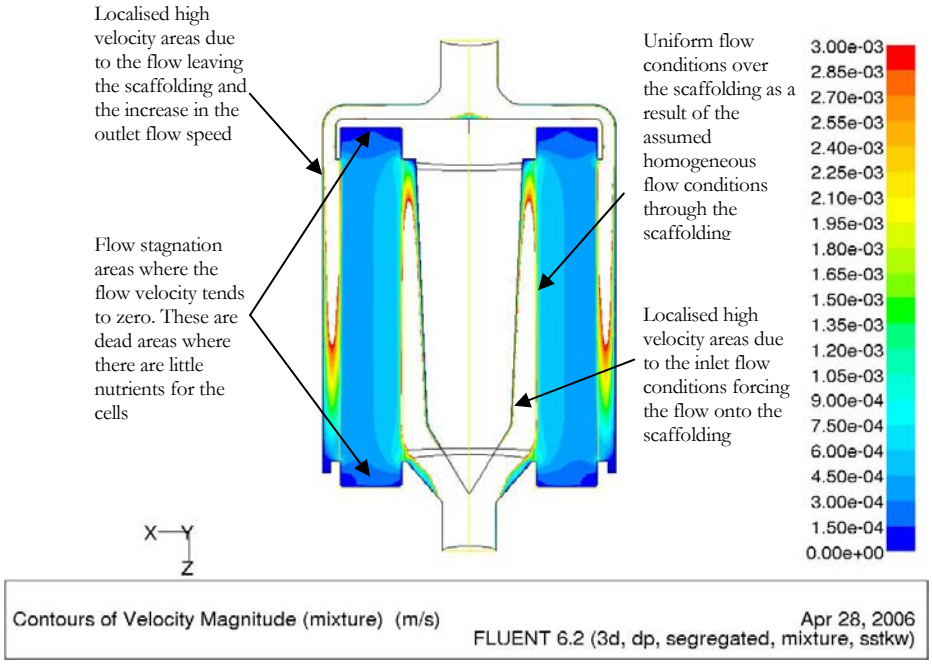


Figure 17: Velocity contours for the mixture over the scaffolding for clinical perfusion

[20] Table 2can be found at the end of the chapter on pg 47.

From Figure 17 & Figure 18 the contours at the diverging part of the inlet diffuser shows flow separation, resulting in lower velocities at the bottom part of the BR.

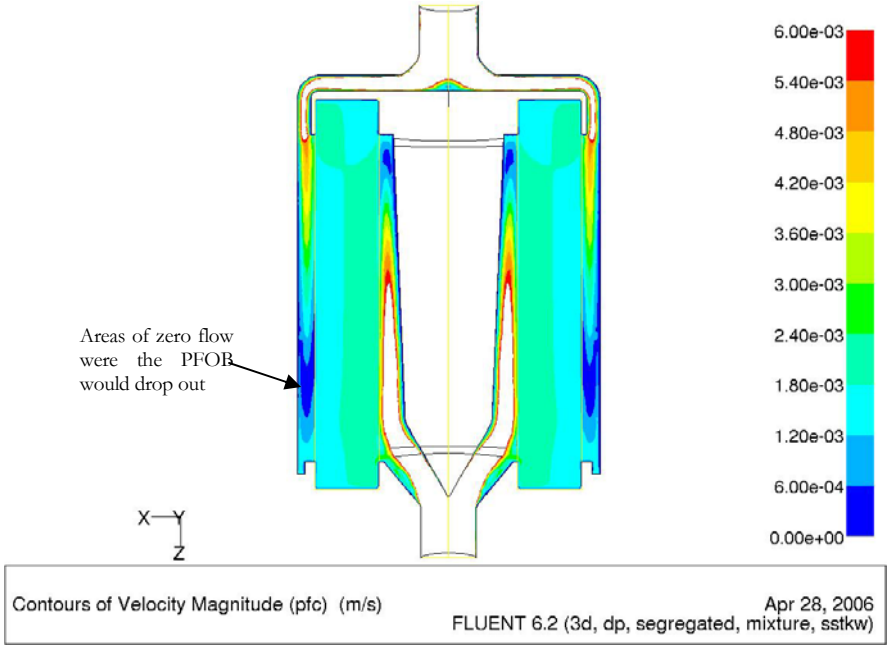


Figure 18: Velocity of the PFOB over the BR for clinical perfusion

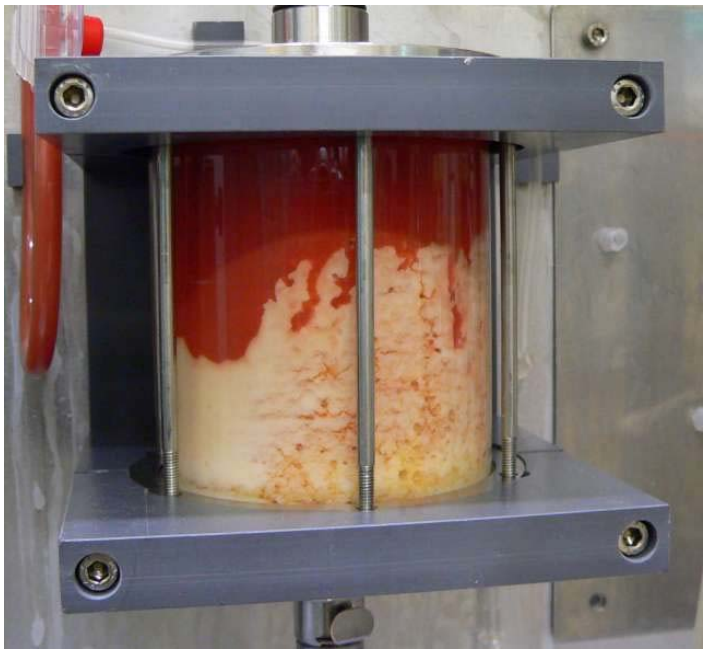

Figure 19: PFOB dropout during an animal trail at UPBRC

From Figure 18, considerable drop out would be expected were the PFOB saturates and drops to the bottom of the BR because the flow can no longer be keep in suspension. This was observed experimentally during the animal trials at UPBRC. From Figure 19 the reader can see the two phases and the PFOB phase dropout at the bottom of the BR.

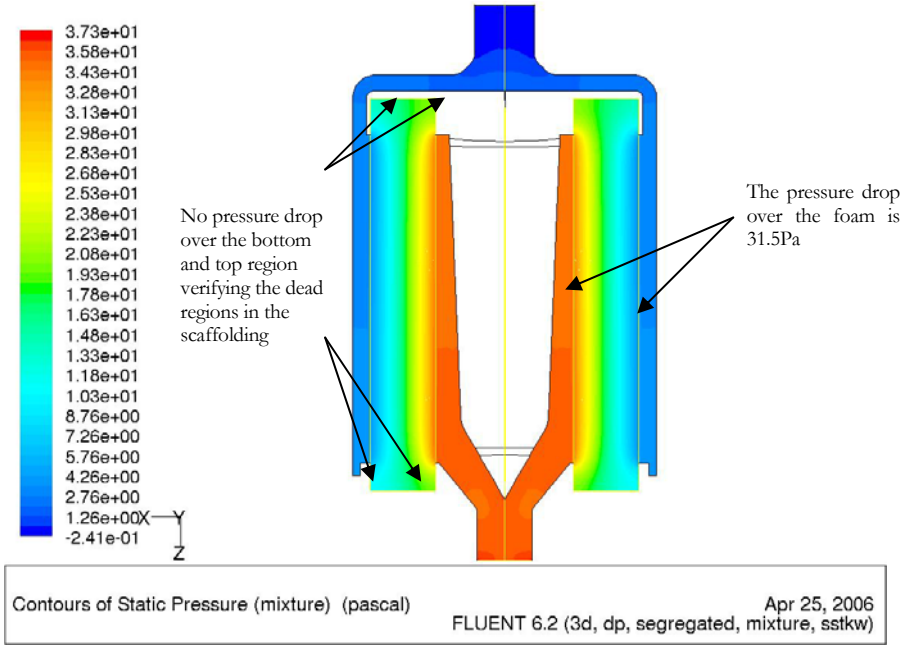


Figure 20: Pressure over scaffolding for clinical perfusion

From Figure 20 the pressure drop over the foam scaffolding is a mere 31.50Pa. This is much lower than is commonly found in the sinusoids and should have no detrimental mechanical effects on the cells, due the related shear etc.

Taking into account the previous investigation of the cell dropout during seeding the reader can see that the cells that have dropped out at the lower part of the scaffolding would be in an ineffective perfusion areas. These cells would be starved of nutrients, and added to this, the PFC that drops out will smother the cells resulting in large areas of cell narcosis. Again the major concern in the design and development of any bioreactor is the minimisation of dead spots and regions of re-circulation.

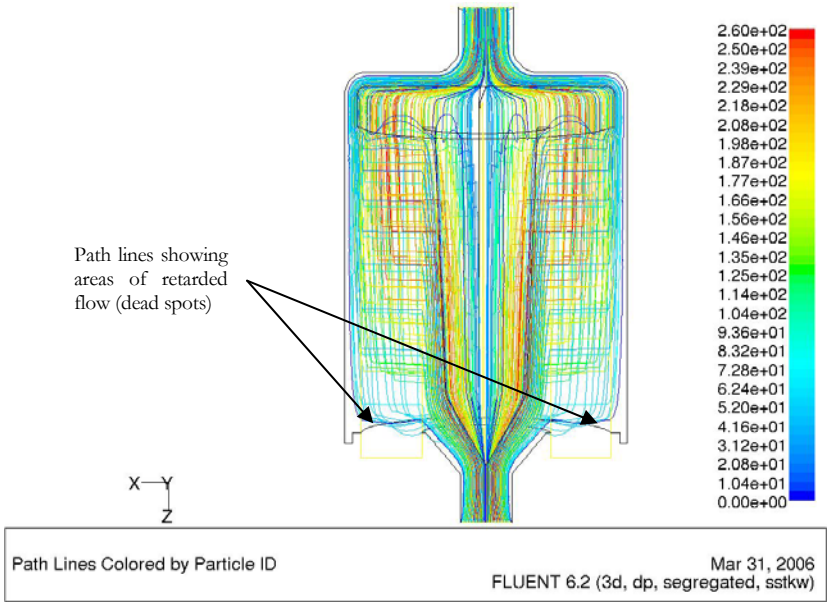


Figure 21: Flow path lines through the BR for clinical perfusion

A number of flow simulations were done with the most important parameters presented in Figure 22 and Figure 23. Each flow simulation had identical initial parameters with only the inlet boundary condition changing, i.e. different flow rates. From the simulations the pressure drop over the scaffolding follows a polynomial curve. This is as a result of the method Fluent uses to calculate the pressure/velocity relation, which was based on experimental observations described previously[21].

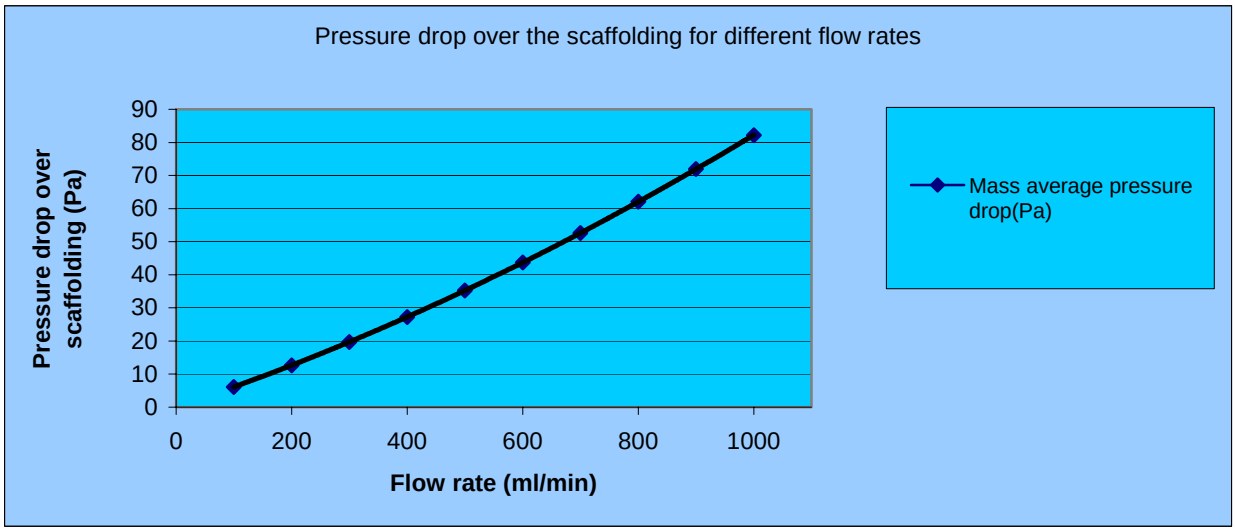


Figure 22: Simulated pressure drop over the scaffolding, for different flow rates

[21] The 2nd order curve used to calculate the momentum sink in Equation 5 is based on experimental observations described by 3.3.2.2: Porous modelling. The solver uses the coefficients to calculate the pressure drop over the scaffolding based on this curve fit. The result would be a simulation congruent to the experimental observations.

Because the porous source term is dependent on the media viscosity and density a number of variables can be changed and the results interpreted accordingly with only a limited number of different fluids being tested. If the scaffolding is changed new experiments need to be set up to define those specific scaffoldings. The designer could use the pressure drop, Figure 22, and the velocity curves, Figure 23, to determine the best perfusion settings for the specific BR. Unfortunately the dead spots and cell dropout is dependant on the geometry of the BR forcing the flow to follow certain flow paths. The dead spots and cell drop out could not be optimized by changing the perfusion rate for this specific BR due to this geometric flow dependency.

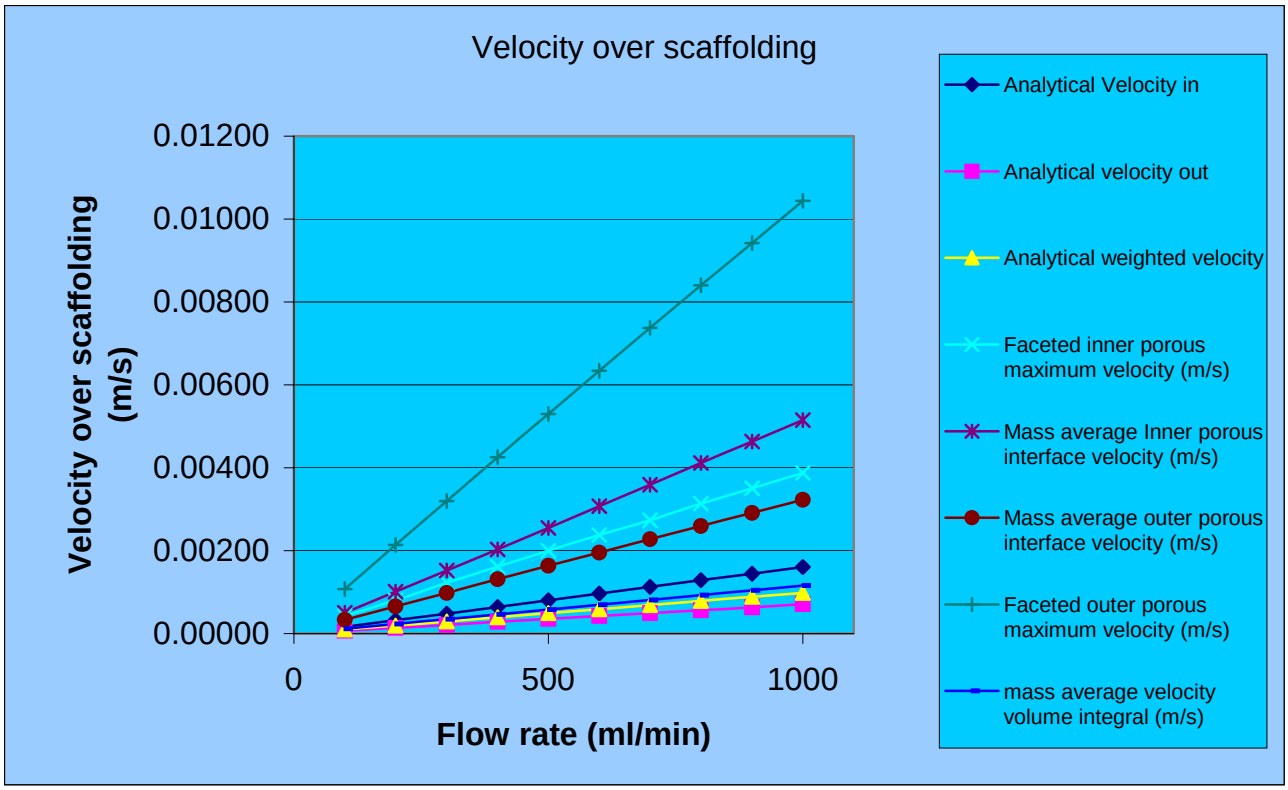


Figure 23: Local velocities at different points in the BR for different pump speeds

Figure 23 also compares different methods for calculating the flow at specific regions in the BR. The area's of interest are the inlet and outlet interface of the scaffolding volume. The analytical velocity is the average velocity calculated by dividing the flow rate by the cross sectional area, this is a simple hand calculation[22]. The faceted maximum velocity is the largest velocity at the specified porous interface. This is calculated by the solver and is a specific nodal value. The mass weighted average is simply the average velocity calculated at the bulk of the flow. I.e. if 80% of the flow is perfused through a small cross sectional area then the mass weighted average would be large but the area average would be smaller.

[22] The derivation of which is presented in Appendix C.

From the Figure 22 & Figure 23, the following is highlighted:

1. The flow velocity is not uniform with areas of high local velocities at the outlet and low local velocities through the foam. This is highlighted by the difference in mass average and area average flow rate.

2. The flow rates are small with a double precision solver implemented to minimize the round off errors in the simulation.

This is unavoidable with a radial flow design and is not necessarily bad. The problem is the nutrient transfer in the areas of low local velocity. With the different perfusion rates for seeding and clinical perfusion the flow lines aver the cells are different. This results in areas of cells that were seeded that do not receive consistent nutrients.

3. The maximum local velocity is at the outlet region of the foam with the maximum local velocity at the inner porous interface not as high, this indicates the conical diffuser allows effective diffusion of the flow over the inlet of the scaffolding.

Added to this is the outlet cross sectional area, which is considerably smaller than the inlet, and the flow is forced to increase in speed to conserve mass balance.

4. The analytical flow calculation based on elementary division of the volumetric flow rate by the cross-sectional area differs from the mass weighted average calculated by the solver, the mass weighted average being more accurate and reflective of the real life scenario.

## 3.12 Mass transfer as a flow driven phenomena

Mass transfer is synonymous with heat transfer, with a number of mechanisms used to describe observed behaviour. The first and most common is diffusion where a species would move from a higher concentration to a lower concentration. This relies on diffusion gradients and is similar to the end of a copper rod in a fire. Where the opposing end is initially cool but would become warm after a certain length of time. Another mechanism is convective mass transfer and mixing, where the species are forced to mix because of the flow conditions. An analogy would be tapping warm water into a bath. You could rely on diffusion for uniform temperature but if you stir the bath the mixing and convective flow forces the temperature to become uniform. With these analogies in mind it is clear that having a BR based on convective mixing is better than BR's based on purely diffusion, if the diffusion gradients are small and the diffusion lengths are large.

A major concern in the design of optimal BR's is the adequate transfer of nutrients, oxygen, toxins and metabolic products to the cells as well as the removal of carbon dioxide and metabolites from the cells. In direct perfusion BR's the convective transfer of these nutrients is important, with bulk diffusion lesser so because it is

assumed the mass transfer products are mixed in the reservoir. Convective mass transfer is flow driven, with insufficient flow speeds, the chances of sub optimal BR performance and cell narcosis is a concern.

The different flow speeds used for the seeding and clinical trial perfusion show different velocity contours and velocity magnitudes, this allowing different flow channels for these respective flow steps. Essentially the final position where the cells become attached during seeding is fixed (they do not migrate) and if they are starved of nutrients, they die. The flow conditions are then changed at the clinical operation step. The cells don't see the same conditions that they saw at seeding with different flow paths and flow rates. Observed dead spots during simulations are sub-optimal with the added problems of PFOB dropout contributing to the need for an optimisation of the BR. The seeding step being a nutrient dependent step needs to be optimised for successful cell seeding and differentiation. Later in the clinical operation of the BR care must be taken to ensure the same path lines are followed by the flow allowing areas that were seeded to have the same conditions seen during seeding.

## 3.13 Design refinement and optimisation

From the previous results it is clear that the design of the BR is sub-optimal in terms of flow conditions resulting in cell dropout during the seeding process and subsequent under-perfusion of critical regions in the scaffolding. This will lead to cell narcosis and non-optimal usage of available volume in the BR.

Several important design parameters used for design optimisation of the BR include; the total volume of the BR, the flow conditions in the bioreactor for optimal perfusion and the scaffolding surface area available for cell adhesion. Due to the porous nature of the scaffolding the surface area is directly proportional to the polyurethane foam volume.

An optimal BR design is one with the smallest total internal volume[23], and large scaffolding surface area for the cells to attach to. The surface area in the scaffolding presented is extensively large with the current seeding techniques unable to fully utilise the surface area. An optimised redesign of the presented radial flow BR was completed based on the above-mentioned design constraints.

For adequate liver support approximately[24] 20% of a liver mass is required for survival, this relates to approximately $20\times10^{10}$cells in an average human [11,17,58,59,60]. These cells require a surface area, assuming:

- hepatocyte cell has a footprint diameter[25] of approximately 20μm,

[23] The smaller the internal volume the less perfusion medium is required, reducing the hemodynamic effects on the patient.

[24] Derived from partial hepatectomy studies where 10-30% of a healthy liver mass is needed for survival [11,17].

[25] See 4.3: SEM results and discussion.

- for the most conservative required surface area the cells populate the scaffolding as a monolayer only,

- the minimum required surface area would be if all the cells were in spheroids.

Equation 13 was used to calculate the required surface area

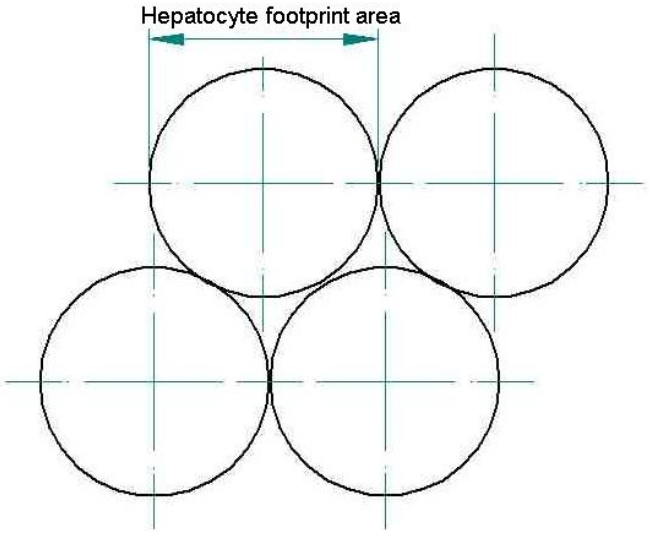


Figure 24: Schematic of hepatocyte layout and footprint area

$$A_s = \frac{\pi}{4} d_{cf}^2 NC$$

Equation 13

Were $A_s$ is the required surface area, $d_{cf}$ is the diameter of the cell footprint and NC is the number of cells. With NC=$20\times10^{10}$, $d_{cf}$=$20\times10^{-6}$m (*see* section 4.3) then the required surface area is $A_s$ =62.831m². For the minimum required surface area all cells would have to be in spheroids. With the maximum-accepted "theoretical" spheroid diameter of 100µm [15,44,58], the sphere volume can be calculated from Equation 14.

$$V_s = \frac{\pi}{6} d_s^3$$

Equation 14

With $d_s=100\times10^{-6}$m the volume is $V_s=5.24\times10^{-13}m^3$. The volume of a single cell (assuming $d_c$ =20μm) can be calculated using the same method, and is $V_c=4.19\times10^{15}m^3$. The optimal number of cells in a spheroid is $\frac{V_s}{V_c}$ =125cells. Thus the effective number of spheroids needed based on the minimum number of cells required is NS=NC/125=$1.6\times10^9$ spheroids. Substituting NS for NC and $d_{cf}=100\mu m$ in Equation 13, the minimum allowable surface area is $A_s=12.56m^2$.

The required BR volume can be calculated using the above surface areas (62.83m² for monolayer vs. 12.56 m² for spheroids). With the reported surface area of polyurethane foam equal to 669m²/L [61], the required BR volume is the maximum area divided by the foam surface area. For monolayers this equates to 0.019L and spheroids 0.094L. For the design of the optimized BR shown in Figure 25 a safety factor was incorporated and a design volume of 0.1L was based on the number of spheroids commonly found in the BALSS research group reported by Dr Moolman [6]. A summery of these design values is presented in Table 5[26]. This is well within the theoretical values and one and a half times smaller than the previous BR.

To minimise the changes required to the BALSS system the different scaffolding volume was achieved by decreasing the height of the BR to a value that achieved the 0.1L. The scaffolding support was also substantially reduced to minimise the upper and lower dead spots. The decreased BR height has the added advantage of decreasing the flow area that increases the flow speed through the BR.

The decrease in scaffolding volume minimizes dead spots, increases flow speed, increases packing density of cells (which is positive for cell-cell interaction), decreases chances of homodynamic effects to the patient and increases mass transfer gradients. The design of the optimised BR is included in the accompanying results and data DVD.

[26] Table 5 can be found at the end of the chapter on pg 101.

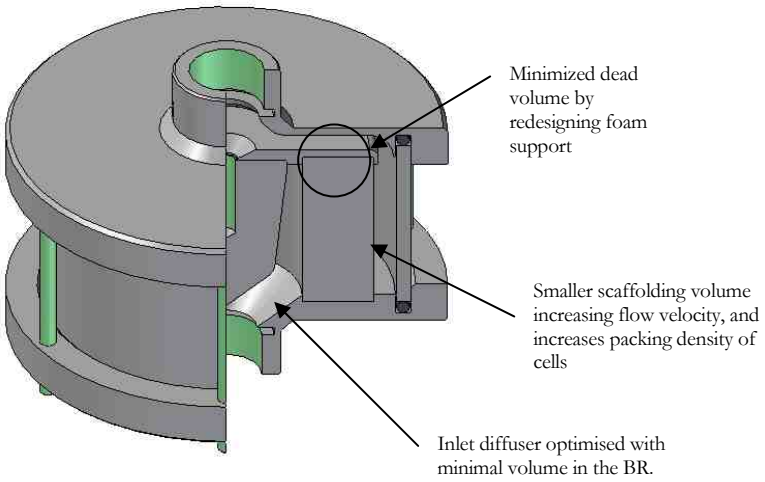


Figure 25: Optimised BR

## 3.14 Modelling of the optimized BR

### 3.14.1 Cell seeding for the optimized BR

The flow rate for both seeding and perfusion was kept at 100ml/min to ensure similar path lines for both cases. The seeding step for the optimised BR has a mass weighted average at in inlet of the scaffolding of 0.0004m/s (0.04cm/s) which is slightly more than that reported in the sinusoid range. The mass weighted outlet velocity is 0.000759m/s (0.076cm/s), which is higher than the inlet and is due to the outlet flow conditions. This is a similar effect found in the previous design. This high outlet flow speed can be seen at the upper areas of the BR, see Figure 26, with the velocity radially closer to the centre much lower. The areas affected by these flow conditions are small in comparison to the available volume.

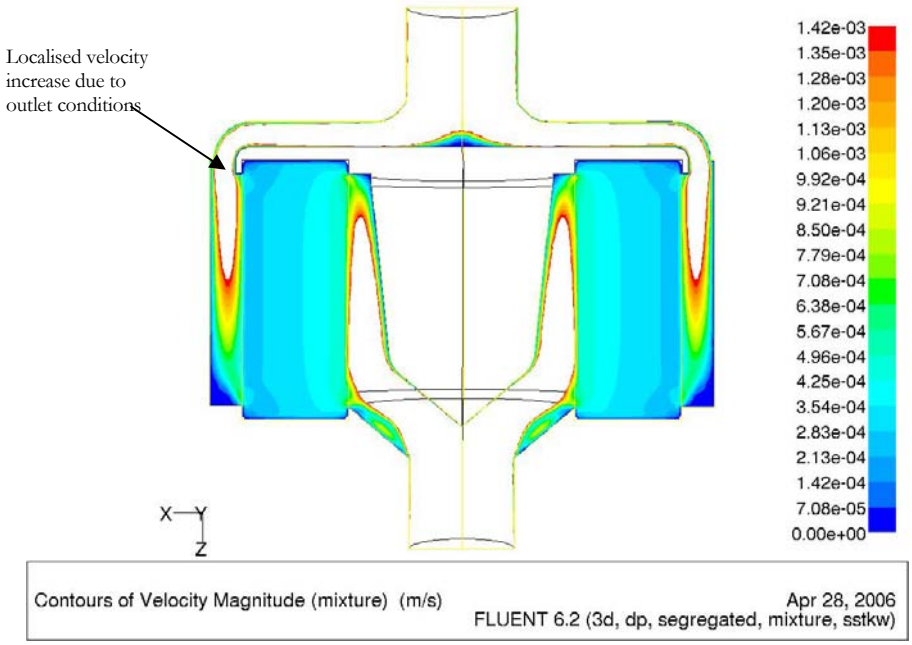


Figure 26: Velocity magnitude during cell seeding, including hepatocyte cells and Williams-E media for the optimised BR

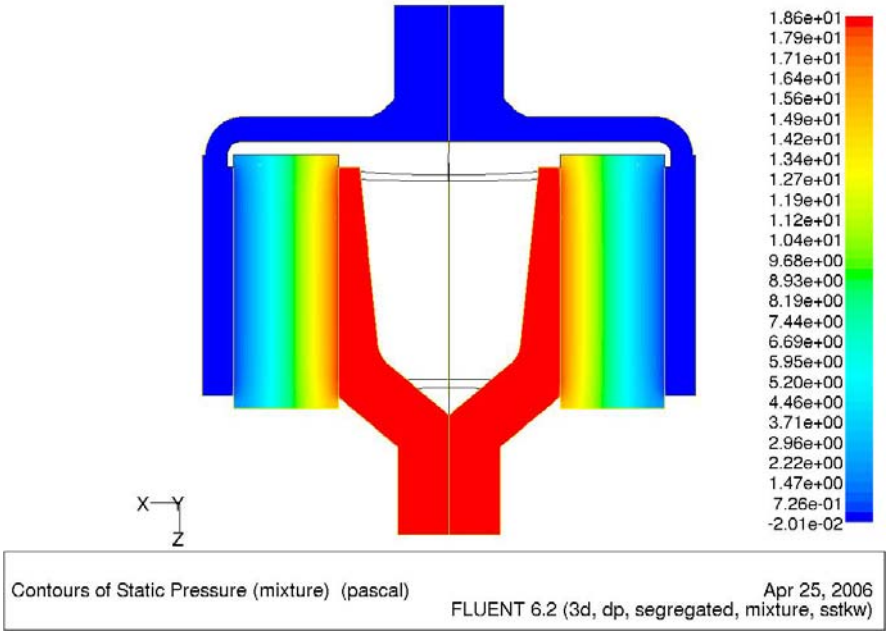


Figure 27: Pressure contours during cell seeding, including hepatocyte cells and Williams-E media for the optimised BR

The pressure drop over the scaffolding during seeding is 18.23Pa, which is smaller than that reported in the sinusoidal and should not be detrimental to the cells. This is because the related shear and flow speeds will not disrupt the normal metabolic and structural elements of the cells and adhesive mechanisms[27].

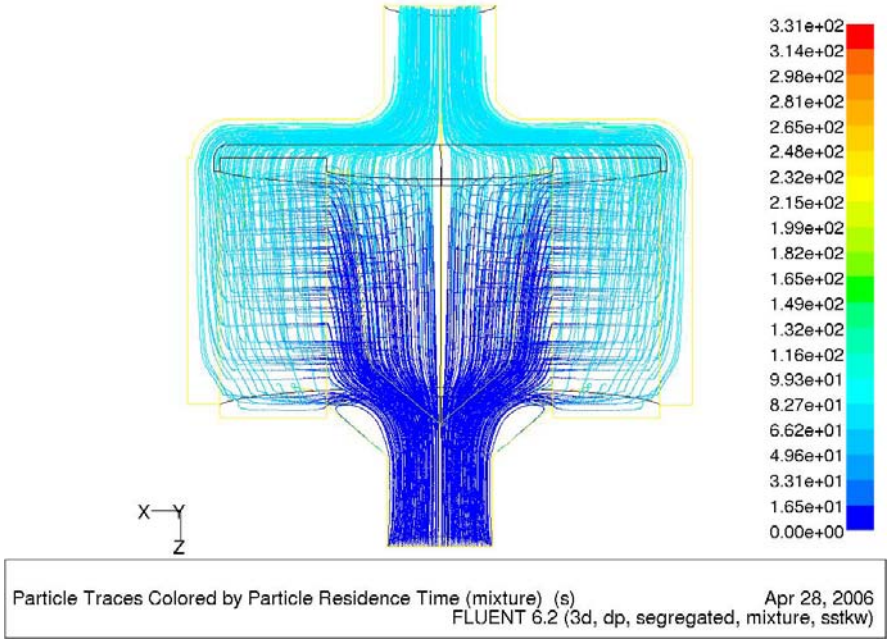


Figure 28: Particle tracks for hepatocyte cells during cell seeding

Modelling the hepatocyte cells during seeding, Figure 28, shows more uniform cell dispersion in comparison to Figure 15, with very little drop out at the bottom of the BR. The dead spots are essentially eradicated and the flow conditions for the cells are uniform through the scaffolding. This uniformity will ensure the full volume being utilised by the cells. Cell-to-cell interaction will also have a beneficial effect for cell metabolism and toxin clearance.

### 3.14.2 Perfusion during clinical operation for the optimized BR

From the previous BR it was found that different seeding and clinical perfusion rates are detrimental for the optimal operation of the BR because of the different flow paths through the BR. Thus it was decided to perfuse during seeding and operation of the BR at 100ml/min. From Figure 29, similar characteristics as seeding with negligible dead areas of flow are shown. The similarity between seeding and perfusion is advantageous for the cells allowing similar perfusion of nutrients for both cases. The Local average velocities are in the same order as given for cell seeding.

[27] This was experimentally verified with the results discussed in 6.6: Hepatocyte breakaway: experimental results and discussion

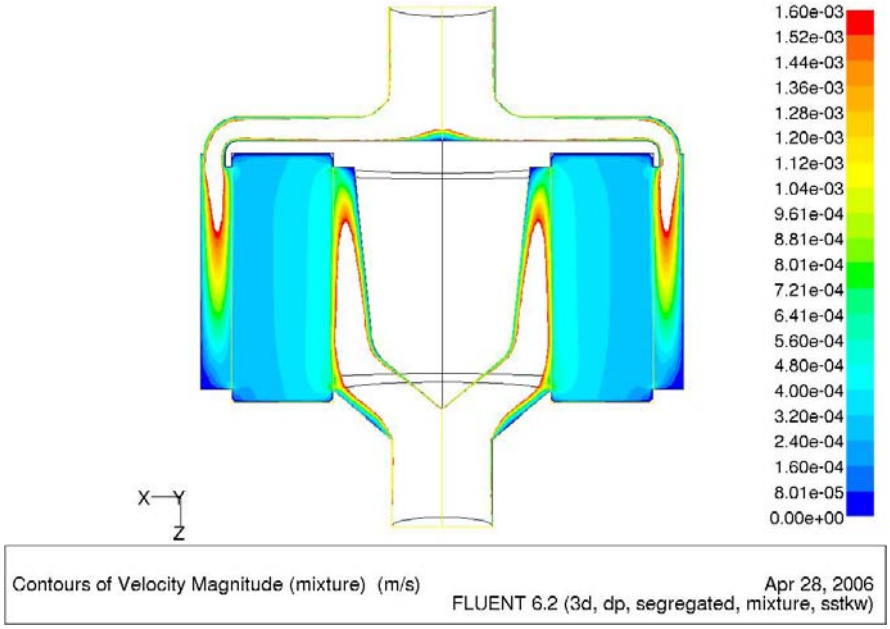


Figure 29: Velocity contours for the PFOB-plasma mixture over the scaffolding during clinical perfusion

The PFOB velocity contours, Figure 30, are uniform in comparison to the larger BR discussed above. The dead spots have been eliminated, allowing the PFOB to remain in suspension and efficiently carry the oxygen to the cells, with no PFOB settling over the cells.

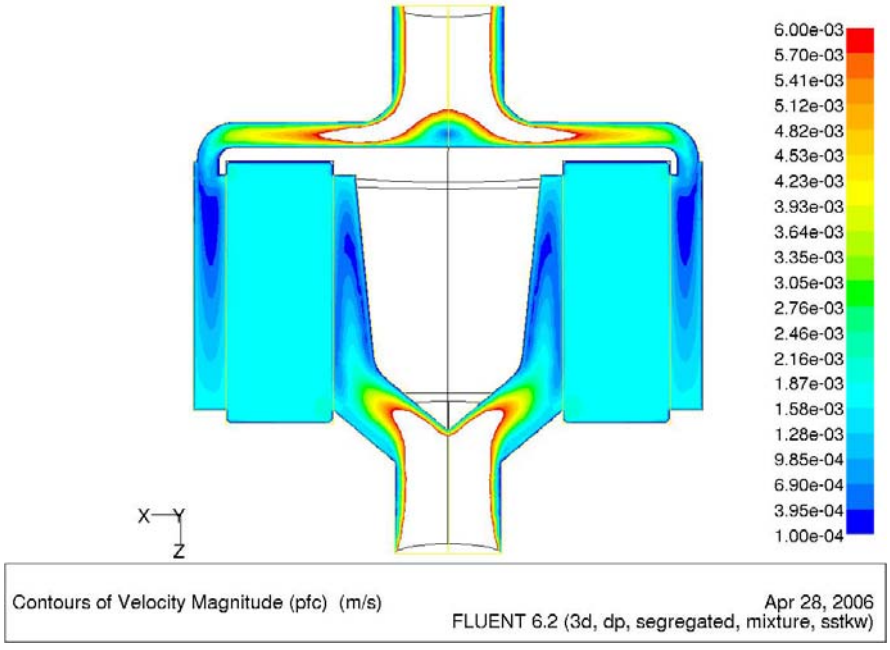


Figure 30: Velocity contours for the PFOB phase during clinical perfusion

## 3.15 Computational solution controls and results verification

The $y^+$ value is a parameter used to give an indication of whether the grid has been correctly refined in the boundary layer (BL). Due to the model assumption of near wall and free stream flows the solver will misinterpret grids that are too fine in this region enforcing the free stream conditions prematurely, if the BL was to coarse the wall effects would be incorrectly carried to the free stream flow. For the k-ω model the $y^+$ values are the same for near wall functions. The $y^+$ values were adapted in the models presented to fall within the model constraints[28].

The residuals in all the simulations presented, converged smoothly with no oscillating convergence.

The mesh dependent solution presented was refined from previous meshes. In doubling the number of elements the difference in pressure between the final two meshes over the inner and outer porous regions was less than 3%. This verifies that the final solution is mesh-independent.

## 3.16 Discussion of CFD modelling

The simulation of the BR used in a BALS system currently undergoing animal trials at the University of Pretoria was considered. The presentation of CFD as a tool to model the flow through the device is presented with the limitations and advantages highlighted. The success of the tool as a visual means for the flow through the BR is challenged only by the computational effort and the expertise required to performing the simulation as well as the model assumptions and limitations.

In the specific case dealt with, the designer developed insight into dead spots in the BR as well as highlighted possible problems with mass transfer due to slow perfusion speeds.

From the initial model results the BR was refined and optimized addressing the shortfalls observed in the animal trials and in the simulations. The optimized BR showed negligible dead spots; uniform flow conditions over large areas of the scaffolding and uniform cell seeding. The perfusion speed for clinical operation was adjusted to that of seeding to take advantage of uniform and consistent flow paths, which would be advantageous to successful cell survival and function.

The practical operation of the BALSS BR differs from that of the simulation. The modelling cannot take into account the localised effects of the foam on the flow itself. If the foam used is not exactly homogeneous on a micro scale the flow through the foam will channel choosing the path of least resistance. This is highlighted in section 5.4.1, Figure 31, showing flow conditions in the scaffolding during the MRI investigation, (Done at Unitas hospital, Pretoria, South Africa, MRI division). Air pockets would also restrict the flow thus care must be taken in removing all air pockets from the foam prior to clinical operation. With this in mind the consistency of

[28] Described in section 11.10.1 Near-Wall Mesh Guidelines for Wall Functions ($30<y^+$ values$<300$) from Fluent help files.

the flow speeds used for cell seeding and animal trial perfusion is highlighted. If the flow speed is changed the channels through the scaffolding might be changed starving cells that were seeded in these regions.

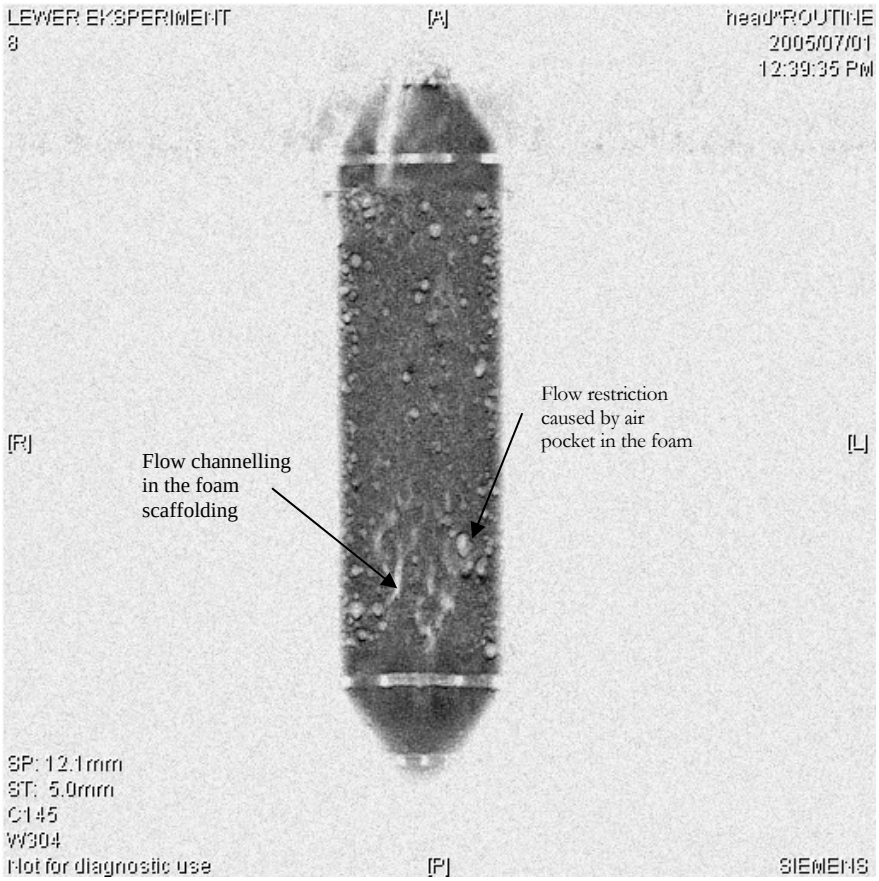


Figure 31: MRI imagining, flow channelling in the scaffolding

## 3.17 Summery of modelling parameters

Table 2: Summery of modelling parameters used in Fluent

| *Specified conditions for Radial flow BALSS BR in Fluent version 6.2.16* | | |
|---|---|---|
| **Mesh generation** | | |
| **Meshed volume** | **Element type** | **Number of elements** |
| Inlet volume | Tetrahedral/hybrid (0.58 spacing) | 292859 |
| Porous media | Hexagonal brick (0.58 spacing) | 225036 |
| Outlet volume | Tetrahedral/hybrid (0.58 spacing) | 401828 |
| | | |
| Total | | 919723 |
| | | |
| **Model** | | |
| Turbulence modelling | The Shear Stress Transport k-w model (SSTk-w) | |
| Multiphase model | Mixture model | |
| | | |
| **Solver** | | |
| Discretisation scheme | 2nd order up winding | |
| | | |
| **Discrete phase modelling** | | |
| | **Particle description** | **Particle model** |
| Cell seeding | Material: hepatocyte (inert particle) | Rossin Rammler |
| | | |
| **Porous modelling** | | |
| Porosity | 0.92 | |
| Flow turbulent model | Laminar | |
| | **Internal resistance** | **Viscous resistance** |
| Cell seeding/plasma (multiphase) | 2256934.82 | 3055054144.07 |
| PFOB (Multiphase) | 2085290.02 | 300413657.50 |
| | | |
| **Equivalent flow speed** | | **Unit** |
| Cell seeding | 100 | ml/min |
| Animal trial perfusion | 400 | ml/min |
| | | |
| **Material properties** | | |
| Cell seeding | Williams media/ hepatocyte cells (20% volume basis) | See Table 3 |
| Animal trial perfusion | Plasma/PFOB background solution (10% volume basis) | See Table 3 |

Table 3: Material properties list used in Fluent

| *Material properties for Radial flow BALSS BR in Fluent version 6.2.16* | | | | |
|---|---|---|---|---|
| **Property** | **Units** | **Method** | **Value(s)** | **Ref** |
| | | | | |
| **Material: williams-media (fluid)** | | | | |
| Density | kg/m3 | constant | 1025 | * |
| Viscosity | kg/m-s | constant | 0.00118 | * |
| Molecular weight | kg/kgmol | constant | 18.02 | ** |
| | | | | |
| **Material: PFOB background-solution (fluid)** | | | | |
| Density | kg/m3 | constant | 1109.37 | [6] |
| Viscosity | kg/m-s | constant | 0.012 | [6] |
| Molecular weight | g/mol | constant | 498.96 | [6] |
| | | | | |
| **Material: plasma (fluid)** | | | | |
| Density | kg/m3 | constant | 1025 | [6] |
| Cp (specific heat) | j/kg-k | constant | 3935 | [62] |
| Thermal conductivity | w/m-k | constant | 0.58 | [62] |
| Viscosity | kg/m-s | constant | 0.00118 | [63] |
| Molecular weight | kg/kgmol | constant | 18.02 | ** |
| | | | | |
| **Inert particles** | | | | |
| **Material: hepatocyte (inert particle)** | | | | |
| Density | kg/m3 | constant | 1065 | *** |
| Cp (specific heat) | j/kg-k | constant | 1000 | [64] |
| Thermal conductivity | w/m-k | constant | 0.512157 | [64] |
| Particle size | µm | constant | 20 | *See* Chapter 4.3 |
| | | | | |
| **Material: Polyurethane (Solid)** | | | | |
| Density | kg/m3 | constant | 1083.31 | **** |
| Cp (specific heat) | j/kg-k | constant | **NA** | |
| Thermal conductivity | w/m-k | constant | **NA** | |
| | | | | |
| Temperature | 37 | degC | | |
| * | Assumed close to plasma due to composition | | | |
| ** | Assumed close to water due to composition | | | |
| *** | Assumed just greater than Percoll | | | |
| **** | From the specification sheet from CH chemicals for polyurethane foam | | | |

# 4 SCANNING ELECTRON MICROSCOPE STUDY OF POLYURETHANE FOAM SCAFFOLDING

*"In the small matters trust the mind, in the large ones the heart." - Sigmund Freud (1856-1939)*

The driving reason for the Scanning Electron Microscope (SEM) study was to gain an understanding of the micro circulatory morphology of the PUF, the method of cell attachment, the area and volume cells occupy on the BALSS scaffolding and to determine how the cells group during the cell seeding process. There's a limited database referring to the study of hepatocyte cells in polyurethane scaffolding. The author did find some investigations of hollow fiber systems using Transmition Electron Microscope (TEM) and SEM [23]. And a SEM study of hepatocyte cells seeded in a loofa sponge [64].

**Short description of SEM and how it works:** SEM is an important electron-optical instrument for the investigation of bulk specimens [66]. The Electron microscope bombards the sample surface with primary electrons that lead to the formation of secondary and backscattered electrons from the sample; these electrons are then detected. They're then converted into images by the secondary electron (SE) and backscattered electron (BSE) detectors and amplified. Figure 32 shows the schematic layout of a SEM.

The thermal emission scanning electron microscope operates at accelerating voltage from 200 V to 40 kV. Its magnification ranges from 10x to 300,000x, with a resolution of 4 nm.

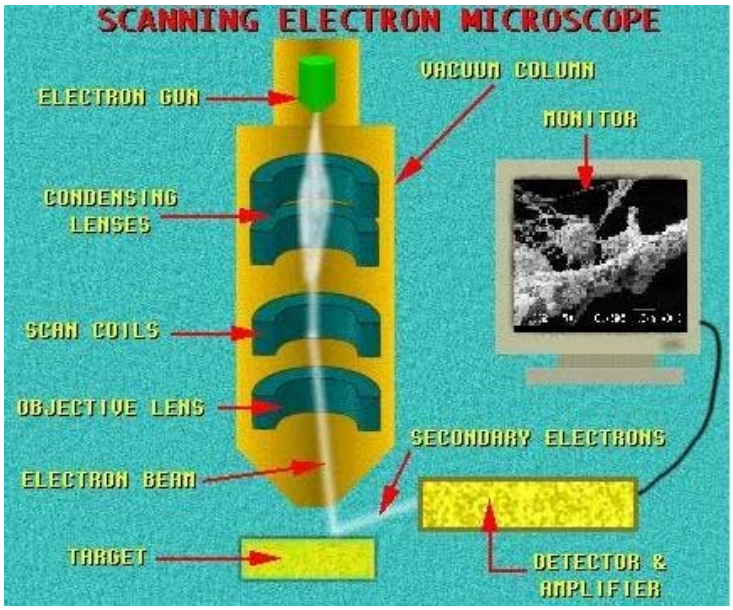


Figure 32: Schematic of SEM modified from the Museum of Science [67]

## 4.1 Description of SEM method and preparation

The SEM samples were prepared from slices of the PUF scaffolding after termination of a metabolic study. The cells were seeded as per the perfusion method described previously, with ammonia clearance evaluated over a five-day period. Slices were cut from the foam from various regions and fixated in glutaraldehyde fixation solution. The slices were cut from the foam, using a scalpel, with the positioning shown schematically in Figure 33. There were three sets of radial slices cut roughly 120° from each other. There was also a set of lateral slices cut down the length of the foam.

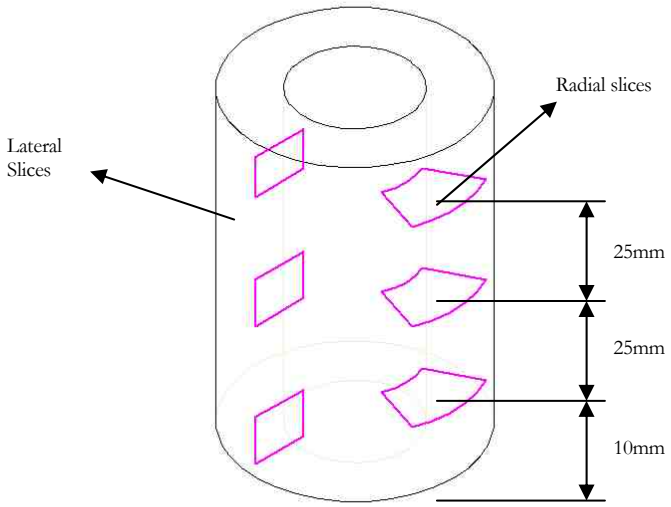


Figure 33: Schematic of slices for the SEM preparation

The samples were fixated with a 2.5% glutaraldehyde[29] solution dissolved in a 0.075M phosphate buffer with a PH of 7.4, for approximately one hour at 37°C directly after the BR was disassembled[30]. The samples were rinsed three times for 10 minutes each in a 0.075 phosphate buffer solution. The samples were then again fixated in a 0.5% aqueous osmium tetroxide solution for approximately one hour, and rinsed in distilled water. They were dehydrated in an ethanol and water solution using 30%, 50%, 70%, 90%, and three steps of 100% ethanol concentration respectively [65]. A critical point dryer, Bio-Rad E3000, Watford England, was used for final drying. And a Sputter coater[31], Polaron E5200C, Watford England, was used to make the surface conductive.

[29] The glutaraldehyde was mixed with 50% (volume basis) Williams's media and applied to the scaffolding for half an hour. Then the 2.5% glutaraldehyde solution was applied to the scaffolding for the remainder of the hour.

[30] Temperature was held at 37°C in an incubation cabinet.

[31] Gold was used to make the scaffolding and cells conductive.

The samples were viewed on a Thermal Emission Scanning Electron Microscope, JSM-840, JEOL Tokyo Japan. Noran imaging software supplied the frame grabber software.

## 4.2 Structure and topography of the foam scaffolding

The scaffolding is made from polyurethane EXFH2054 polyol[32]. It is a polyol blend, a mixture of polyol, water, tertiary amines, silicone surfactants and glycols. The catalyst is tertiary amine. The foam is considered non-hazardous according to the EC criteria [68]. It is assumed that all the catalyst is used in the reaction and for all practical purposes the foam is biologically compatible. The foam is also washed with de-mineralized water and autoclaved prior to use.

The structure and topography of the foam is shown in Figure 34. It can be assumed with relative certainty that the cells found in the scaffolding receive media flow; this is based on the seeding method used in the BR. The cells will only seed in areas of flow and were the flow stagnates to a point were the cells could become attached. In general most of the cell-like structures were found in the interior of the pours or in the pour openings.

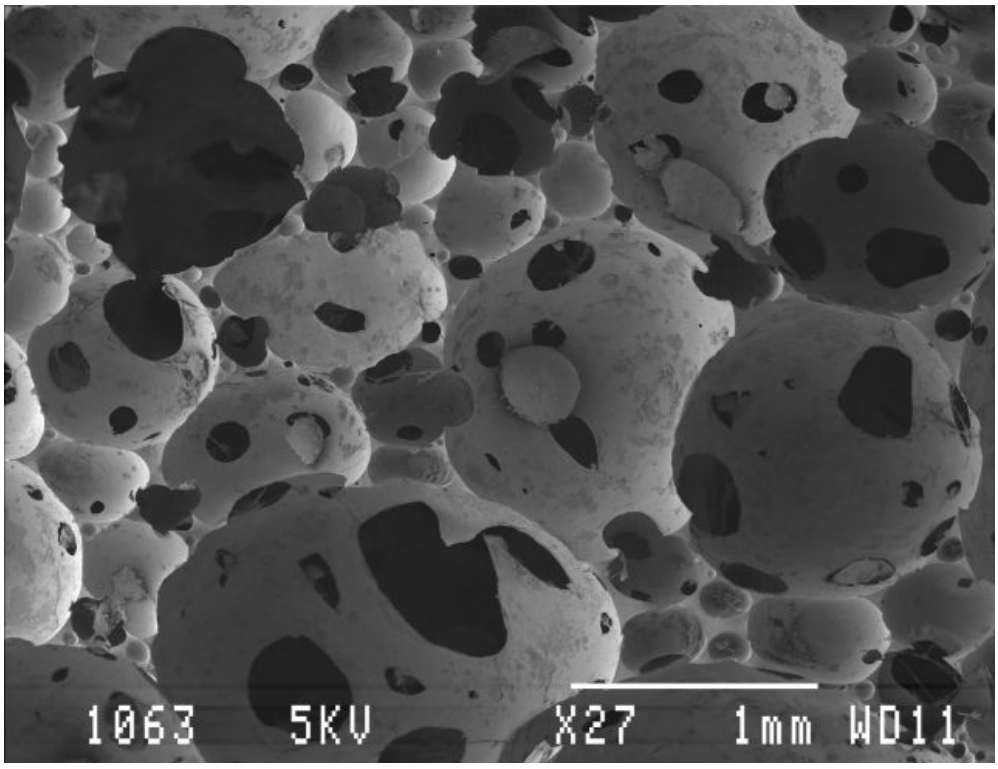


Figure 34: Structure and topography of the PUF foam showing cell spheroids in the foam

[32] Supplied by CH Chemicals (pty) ltd

## 4.3 SEM results and discussion

From the SEM a number of interesting observations were made. To use the SEM procedure as a method to count the number of cells would not result in good data. During the fixation and subsequent drying steps a number of cells became dislodged and could be seen floating in the fixation solution[33]. From visual inspection the same could be deduced due to the debris where cells were suspected to have been attached and became dislodged. Due to the shrinkage inherent to the SEM preparation process, the cell size could also not be determined with any accuracy, according to Glauert *et al* [3] shrinkage of as much as 30% is possible. It is important to note, then, that the results are purely of a quantitive nature intended to give the reader a better visual understanding of the scale and cell geometry. The cell footprint[34] could be determined based on the assumption that the cells shrink where they have the most moisture, evidence to the contrary would be cell structures that have been lifted around the edges or cell debris around the cell periphery, very few cells of this nature were observed. The footprint of the monolayer cells can be estimated, from the photos, as having a diameter between 10-30μm.

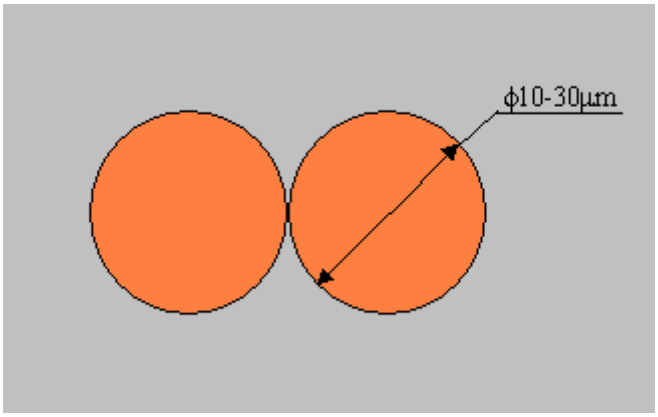


Figure 35: Projected hepatocyte area, or cell footprint observed from SEM studies

### 4.3.1 Single cells and monolayer cells

Monolayer cells were defined as a single layer of cells (relative to the scaffolding) that are in contact with each other either by direct cell-to-cell contact or via a protein like web or strand, Figure 36 and Figure 37. Monolayer cells were found in most of the areas investigated. These cells, from a diffusion point of view give the best surface to volume ratio. Unfortunately for use in classical tissue cultures the monolayer culture is unstable and the hepatocytes rapidly lose the capacity to express certain of the liver specific functions [42]. Figure 36 and Figure 37 are examples of monolayer cells with protein strands connecting neighbouring cells.

[33] This was found by the lab technician at the UP SEM labs, Mr A N Hall.

[34] The footprint, for the purpose of this study, is the projected area of the cell as viewed from the SEM.

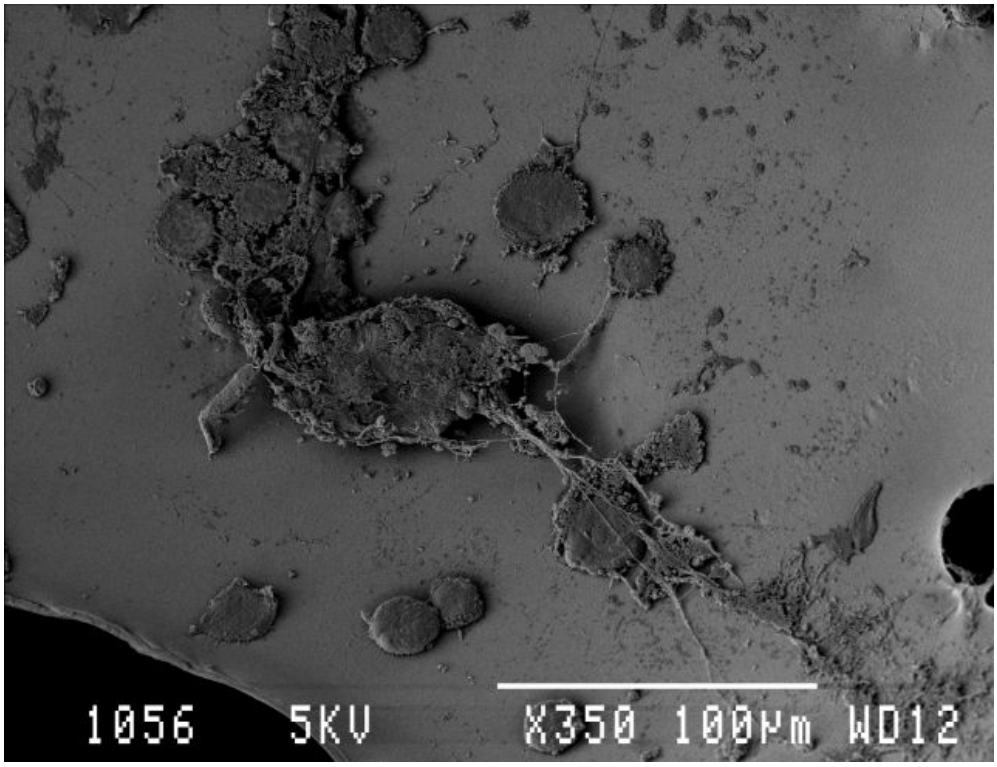


Figure 36: Monolayer cells connected by a protein like web or strand

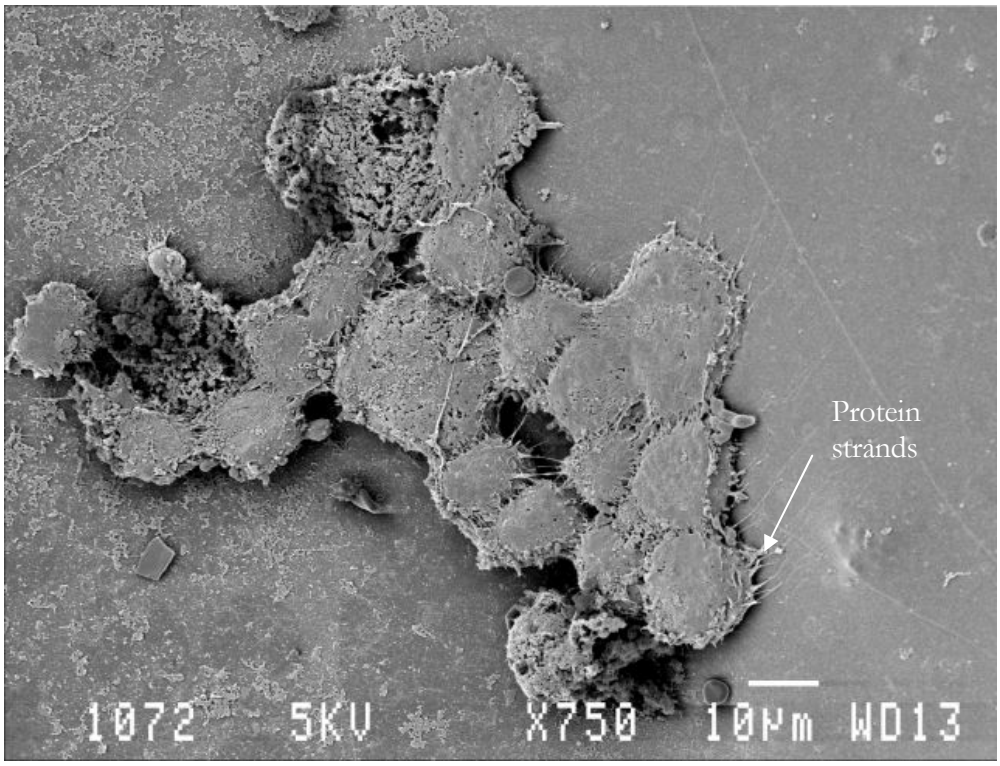


Figure 37: Monolayer cells that are in direct cell-to-cell contacct

The singular and more spherical nature of the individual cells suggests that they were single cells during suspension and they did not aggregate[35] before seeding. The fact that the protein strands are not only connected to adjacent cells but also the polyurethane scaffolding strengthens the argument for the polyurethane's biocompatibility. In a number of areas what looked like debris from single cell adhesion could be seen. An example is shown in Figure 38.

Most of the single cells had an average diameter of roughly 10μm, similar cells sizes were found by Gerlach *et al* after SEM studies of their system [23]. The debris found were typically of a spherical nature, normally smaller than the average single cells found, thus suggesting that the single cells did not for the most part flatten to the scaffolding but kept a "droplet shape".

### 4.3.2 Cell clusters (spheroids)

Cell clusters were defined as a group of cells with more than one layer relative to the scaffolding without a biological skin visible, see Figure 38. This suggesting the clusters were formed after the seeding process had begun or just prior. The cells might have aggregated just before seeding but not enough time was allowed for a skin to form, or the cells might have built on top of one another during seeding.

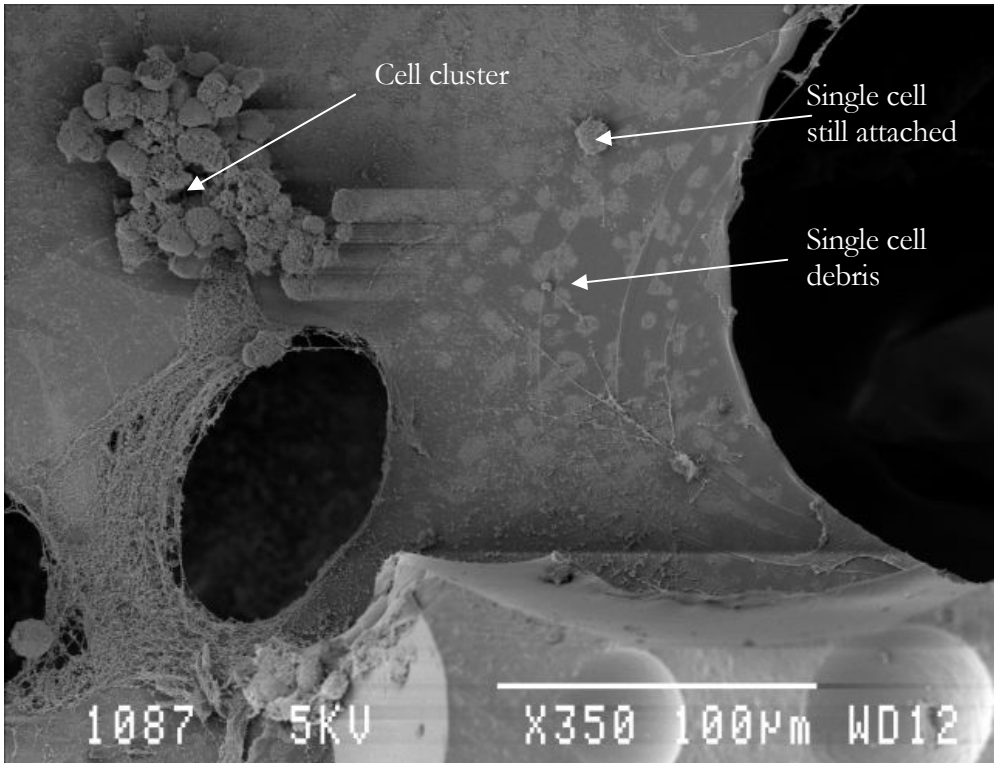


Figure 38: Hepatocyte cell cluster and evidence of single cell debris

[35] Cell aggregates discussed in 4.3.3: Cell aggregates.

This is not the optimal mass transfer configuration; however, provided the clusters remain smaller than 100µm there is little chance of cell narcosis[36] [15,44,58]. Most of the clusters observed were within the 100µm range. The close proximity of the cells in their clusters and other non-parenchymal cells may even contribute to cell viability and expression of liver function by lowering their stress levels, as reported by a number of researchers [42,46,47]. Generally hepatocyte cells in spheroid form keeps the differentiated capacity, with the DNA synthetic ability of spheroids lower in comparison to monolayers [70].

### 4.3.3 Cell aggregates

Cell clusters with a number of cells were a biological skin has given the structure a smooth spherical appearance is classified as aggregates. These aggregates, see Figure 39, differ is size and construction but for the most part are larger than the accepted largest size[37] of 100µm. These aggregates were most probably formed during the isolation process prior to seeding and have subsequently formed a biological skin. This configuration is detrimental for mass transfer with the large diffusion distances outweighing the advantages of cell-to-cell interaction. Another detrimental result of the large volumes of cells that aggregate is the blockage of pores shown in Figure 39, Figure 40 and Figure 34, which is discussed in more detail later.

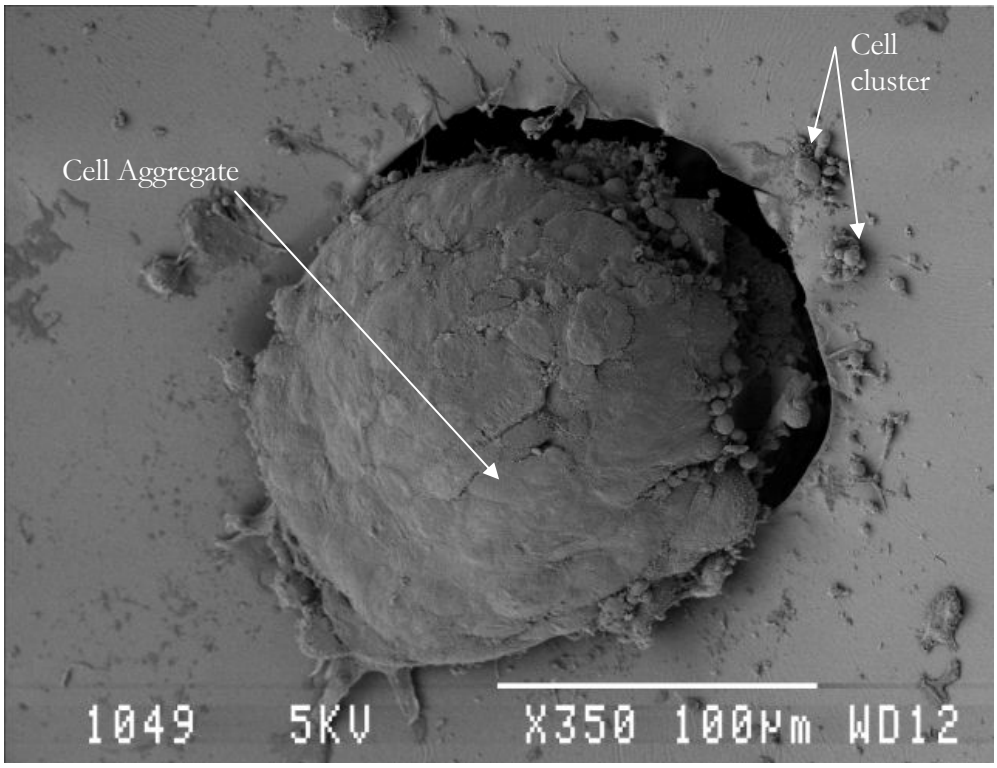


Figure 39: Comparison of cell clusters and cell aggregates

[36] References point to the hepatic microvascular system were this value was most probably derived from. It was also reported that no cells other than chondrocytes exist further than 25-100um away from a blood supply [69].

[37] See section 4.3.2: Cell clusters (spheroids)

Figure 34 gives an indication of the relative number of aggregates present in the foam scaffolding. This distribution of cells is not optimal and the large cell aggregates will most definitely result in cell narcosis.

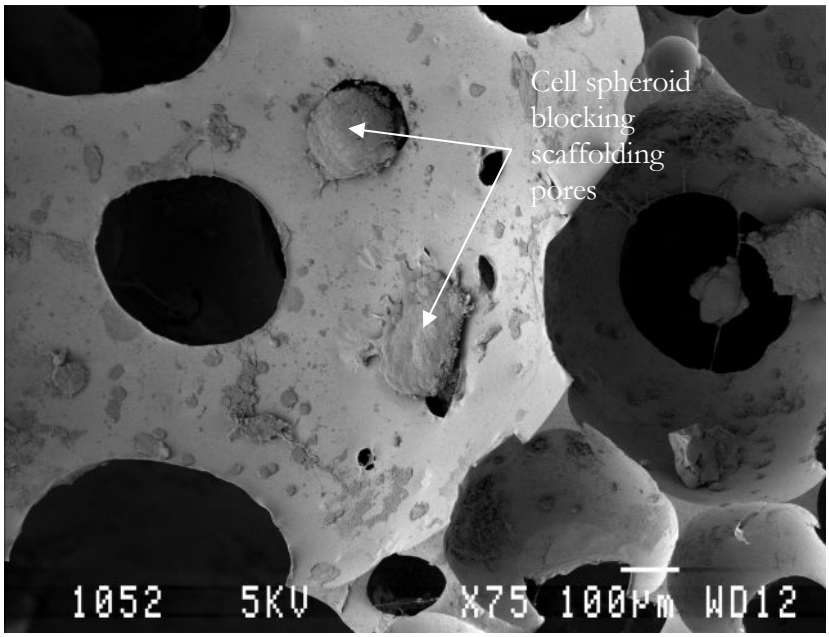


Figure 40: Cell aggregates blocking the scaffolding pore openings

## 4.4 Method of hepatocyte adhesion to the scaffolding

Cell adhesion to the scaffolding plays a role in a wide variety of biological processes, including proliferation differentiation and metastasis in animal tissue [71]. The molecules of the cell surface initialise cell adhesion to materials. They cooperate through biological recognition or non-specific mechanisms with the surface molecules to become attached to the scaffolding [71,72].

The Asialoglycoprotien receptor, which appears on the hepatocyte surface and the E-cadherin, which regulates the intracellular adhesion between hepatocytes have been studied in connection with various scaffolding materials and coating techniques [71,70]. From Figure 41 to Figure 44 these abovementioned attachment mechanisms are shown. The string like structures varies in construction and form with a number localising the cells in the flow path and others connecting the cells firmly to the scaffolding as a monolayer. It is clear that the cells were either environment driven with the flow conditions dictating the placement of the cells and their location or they were positioned at the points of maximum diffusion gradients. These two placement conditions are by no means exclusive and a combination is also probable. In a hepatocyte BR it is highly unlikely that the cells position is purely diffusion driven because hepatocytes lack the ability to migrate. **From the aforementioned statement the design of viable scaffolding is largely flow and mass transfer dependent.**

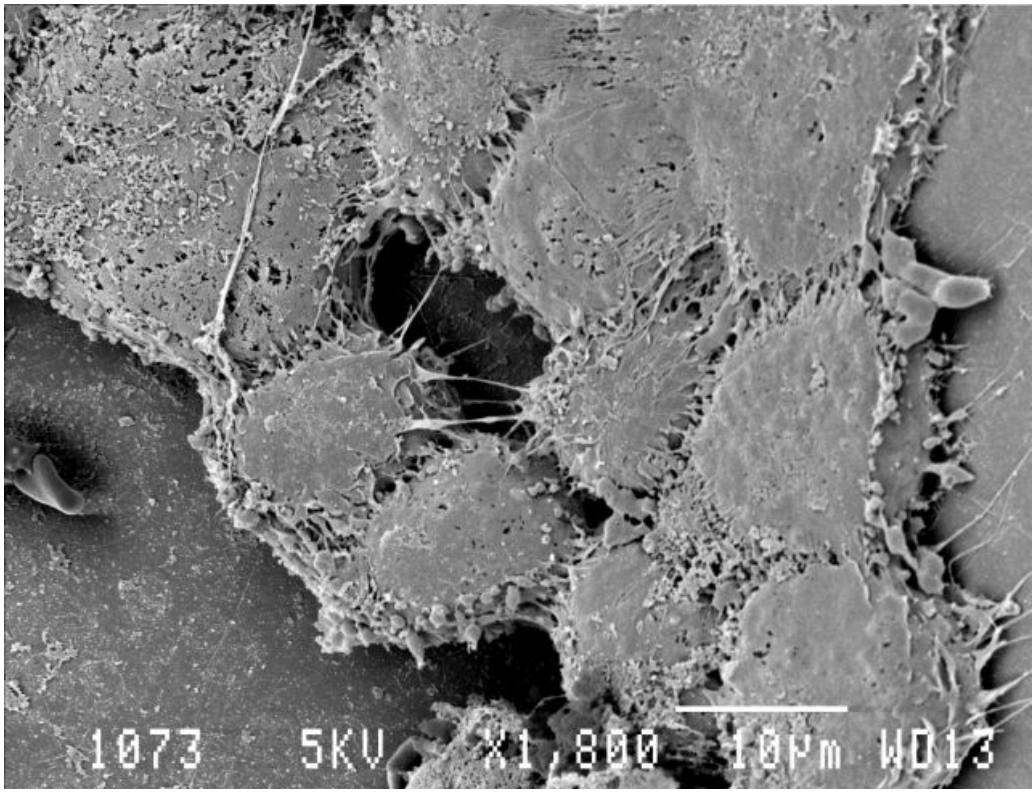


Figure 41: Hepatocyte attachment to the scaffolding showing cell-to-cell interaction with protein like strands

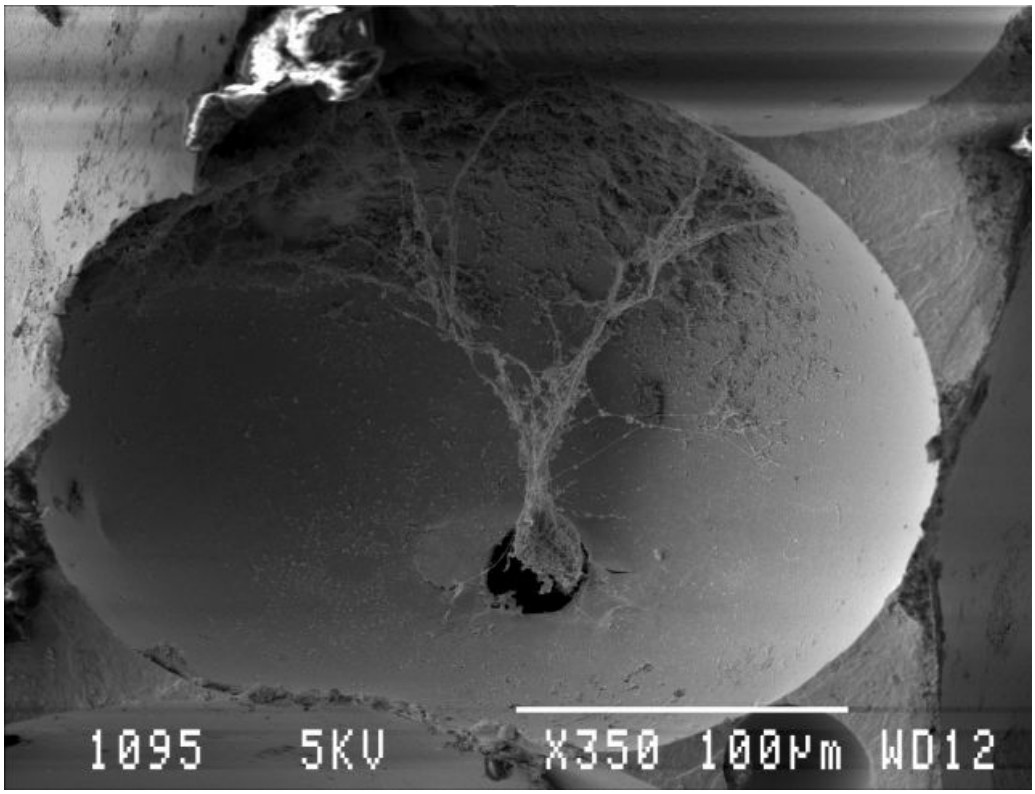


Figure 42: Hepatocyte cell attachment with cells in areas of pore openings i.e. assumed flow paths

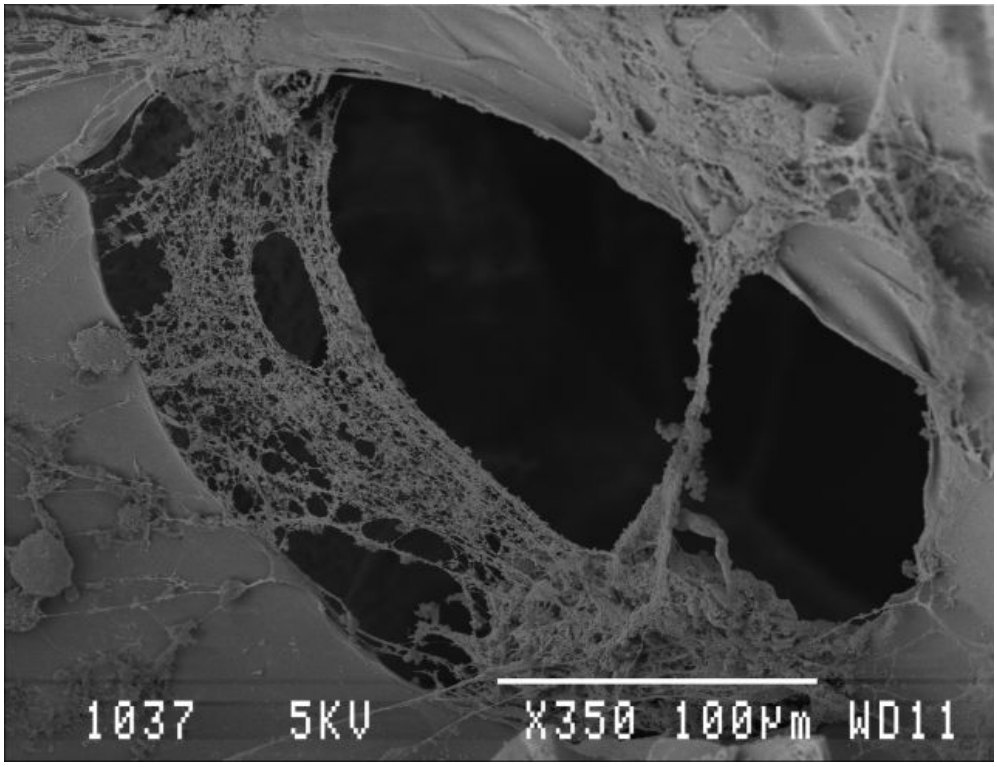


Figure 43: Protein matrix with hepatocyte cells visible on the PUF scaffolding

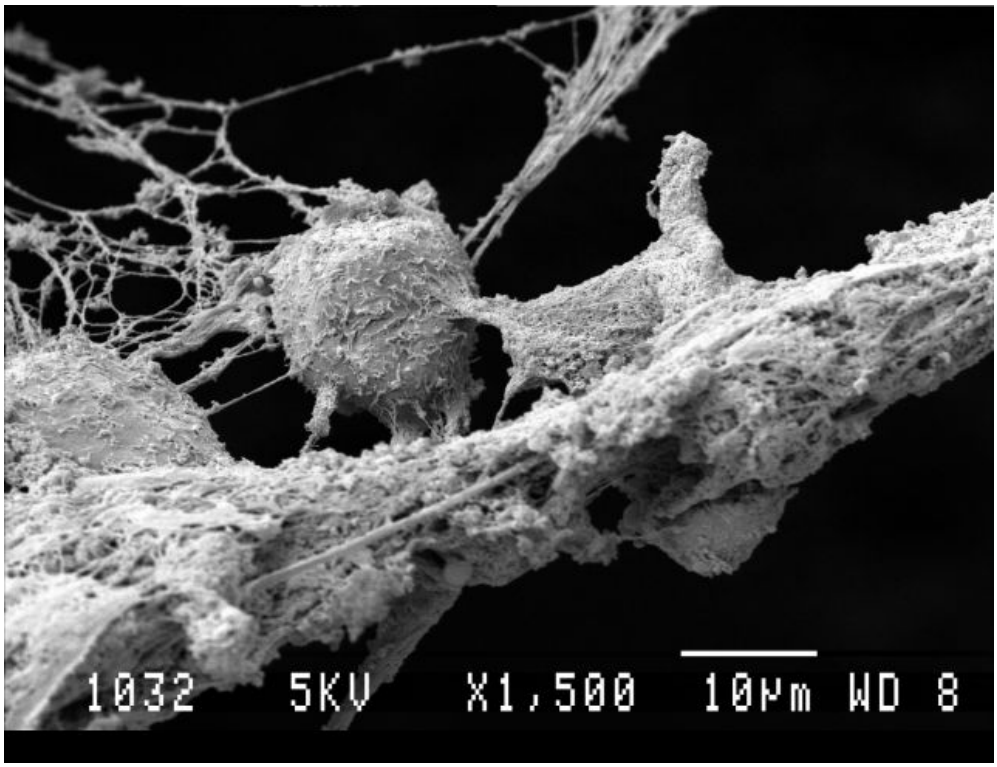


Figure 44: Protein matrix with hepatocyte cells visible in the cellular matrix

From the results presented above the cells are adhering to the PUF scaffolding, thus the polyurethane is biologically compatible and suitable for the use in a hepatocyte BR's. In a separate study (not included in this report, because it is outside the scope of this study) the cells were seeded on Polyethylene fibres (PET) and photographed using SEM in a similar method described above. The author could find no evidence of single or monolayer cells with any evidence of cell attachment.

## 4.5 Flow direction

From Figure 42 and Figure 43 it is evident that the cells prefer unidirectional flow. The probability of cellular detachment depends on the cell orientation and cell deformation with respect to the flow direction [72]. The cells orient themselves to maximise the flow conditions they were subjected to during seeding. Changing the flow direction can result in stresses on their anchorage resulting in cells breaking away from the scaffolding. With the small flow rates during seeding (100ml/min) it is unlikely turbulent flow conditions will be manifested in the radial flow BR.

## 4.6 Blocking of pores

A major concern with the present seeding configuration is the blockage of pours and the resulting filter effect of the foam, see Figure 39 and Figure 40. The blockage of the foam pores could result in stagnated flow condition downstream resulting in the narcosis of cell groups upstream. Dead end cell pours will in all likelihood not experience the cell blockage because of the small pour sizes as well as the lack of the driving pressure drop for this to occur. Essentially the blockage of the pours in any considerable degree would result also in the foam acting as a filter, with a localized increase of flow velocity in other regions.

# 5 MAGNETIC RESONANCE IMAGING (MRI) FOR THE FLOW VISUALISATION OF HEPATOCYTE CELL CULTURES

*"Not everything that can be counted counts, and not everything that counts can be counted." - Albert Einstein (1879-1955)*

As shown in Chapter 3 the characterization of flow in a BR seeded with hepatocytes is no simple task. The experimental methods for determining the flow in porous media are expensive requiring specialist equipment and expertise. These methods include amongst others visual and laser Doppler animetery methods [73]. Visual and laser Doppler animetry methods are only effective in clear or opaque media, where in the medical fields this is not commonly the case. If this were to be overcome the scale at which the flow needs to be investigated becomes a problem. For a spheroid diameter of 100μm it makes sense to determine the flow conditions at a smaller scale. The author however was unable to locate apparatus in South Africa with a spatial resolution of smaller than 500μm.

The use of intrusive measuring apparatus for example Pito tubes and hot wires, would not only disturb the flow, but to determine localized flow conditions in a scale relative to the cells makes these techniques unsuitable [74].

Numerically modeling the flow conditions allows the designer to visualize flow related phenomena i.e. flow rates, pressure drops, particle tracking etc. and affords the opportunity to optimize the geometric design of BR's. Due to the constraints of flow visualisation currently encountered in cell cultures a novel approach was adopted to visualise the seeding of the hepatocyte cells and localised flow through the BR scaffolding. In doing this the outcomes that the simulation techniques where unable to address, can be answered. These include the flow patterns in the scaffolding as well as the location of cell masses and possibly preferential seeding mechanisms.

**Short description of MRI and how it works:** Magnetic Resonance Imaging (MRI)[38] is based on the absorption of energy in the radio frequency range of the electromagnetic spectrum. Essentially MRI works on the specific properties of the hydrogen atom [75]. The hydrogen atom has a unique property called spin, which can be thought as a small magnetic field, causing the nucleus (of the hydrogen atom) to produce a MRI signal. Unfortunately the large wavelength typical of the radio frequency range limits the MRI in resolution. This is circumvented by measuring the spatial variation, in phase and frequency, from energy that is absorbed and emitted by the imaged object. In other words the change or gradient is measured instead of the specific frequency.

[38] The correct acronym for MRI is in fact NMRI, which stands for Nuclear Magnetic Resonance Imaging. The Nuclear was dropped in the 70's as a result of the negative connotations.

Previously Wolfe *et al* [15] used MRI studies to determine the flow conditions in a multi-coaxial hollow fiber bioreactor, the axial flow conditions along the fiber was measured and compared to experimental measurement of axial flow using common pressure drop techniques. The radial flow conditions could not be determined due to the large signal to noise ratio. This was typically due to the small local velocities.

Although there are a number of research groups currently busy with BAL systems, there is very little consensus on the optimal perfusion and seeding flow rate of the different BR's. Table 4 shows different groups and their various seeding and perfusion rates as well as an average local velocity for their specific BR. Table 4 shows clearly the poor consistency of flow rates used by researchers in the BAL field, with flow rates in the localised regions of the cells ranging from 0.01 to 1.55cms$^{-1}$, this is effectively two and a half orders of magnitude inconsistency.

Groups that are busy with a membrane type BR was excluded from the Table 4 because cells are not in direct contact with the perfusion media. The local velocity was based on the volumetric flow rate divided by the specific wetted cross sectional area, perpendicular to the flow direction, in the bioreactor. If the local velocities were given they were quoted.

The MRI study could show insight into the flow patterns as well as the channelling of the flow inside the scaffolding for different flow rates.

Table 4: Comparison of flow rates of different BAL systems or metabolic BR's

| Comparison of flow rates of different BAL systems or metabolic BR | | | | | | | | |
|---|---|---|---|---|---|---|---|---|
| **Discription of BR configuration** | **Flow rate (ml/min)** | **Cross sectional area (m)** | **Local velocity (cm/s)** | **Cell types** | **Number of cells** | **Direct media-cell contact or microporous membrane** | **BR Volume (ml)** | **Reference** |
| Flat plate BR | 0.06 | 2.88E-06 | 0.03 | Lewis rats | 2*10^6 | Media direct | 215.63 | [76] |
| Module of multi-capillary polyurethane foam | 400 | 2.12E-03 | 0.31 | Dog and porcine | 3*10^9 | Plasma direct | 382 | [24] |
| Flat plate BR | 0.6 | 2.50E-06 | 0.40 | Rat Hepatocytes | 2.5*10^4 | Media direct | 187.5 | [77] |
| Flat plate BR | 0.3 | 2.50E-06 | 0.20 | Rat Hepatocytes | 2.5*10^4 | Media direct | 187.5 | [77] |
| Hollow fiber module, matrix attached hepatocytes | 200 | 2.12E-04 | 1.57 | Porcine | 5*10^9 | Plasma direct | Not reported | [77] |
| Cellulose nitrate/cellulose acetate hollow fiber BR | 300 | 3.98E-04 | 1.26 | Porcine | 7.5*10^9 | Hollow fibre | 177 | [78] |
| Polyethersulphone hollow fiber BR | 300 | 9.51E-04 | 0.53 | Porcine | 7.5*10^9 | Hollow fibre | 195 | [78] |
| Polyethersulphone radial flowr BR | 300 | 4.10E-02 | 0.01 | Porcine | 15*10^9 | Media direct | 185 | [78] |
| Flat plate BR | 10 | 6.99E-05 | 0.24 | Porcine | 13.9*10^6 | Plasma direct | 6 | [79] |
| Multicapillary polyurethane foam pached bed BR | 400 | 2.12E-03 | 0.31 | Dog | Not reported | Plasma direct | 294 | [79] |
| | | | | | | | | |
| *BALSS UP-CSIR BR* | *400* | | *0.039* | | | | | |
| *Optimized BALSS UP-CSIR BR* | *100* | | *0.010* | | | | | |
| | | | | | | | | |
| **Velocity range in sinusoid** | | | **0.003-0.03 cm/s** | | | | | |

## 5.1 MRI experimental methodology

The effect of flow speed on cell seeding including local positioning and cell grouping characteristics were an expected outcome of the MRI experiments. By incorporating this technology it was hoped the flow regime and flow patterns would have been recognized in the scaffolding filling the gaps of the CFD simulations.

### 5.1.1 Design choice of MRI BR configuration

When designing the test set-up for flow visualisation using MRI the following needs to be considered:

1. Ease of sterilization, to avoid possible contamination.
2. Uniform flow through the scaffolding, design constraint for all foam BR's.
3. Minimum medium volume for cell marking, minimizing the dilution effects.
4. Minimum BR surface area, to prevent cells seeding on materials other than the scaffolding.
5. BR must be translucent and non magnetic for MRI.
6. Channeling of flow other than through the scaffolding must be minimized.

In order to satisfy the requirements of the experimental procedure a radial or axial flow BR might be used. A comparison between an axial flow (an example is shown in Figure 47) and a radial flow BR (an example is shown in Figure 7) was done to determine which configuration would best suite the experimental method, and desired experimental flexibility. The flow velocity in the radial BR is not uniform so a weighted average was calculated[39]. The mass weighted average calculated in the simulations would give better results, but the author used the analytical method of calculating the flow velocities to compare the results with those of other researchers in the field. Equation 51 is reproduced below for convenience.

$$V_{avg} = \frac{A_i V_i + A_o V_o}{A_i + A_o}$$

The average velocity in an axial flow BR is considerably easier to calculate. This is based on the assumptions of no channeling and uniform flow distribution. The average velocity in the axial flow BR is given in Equation 15.

[39] See Appendix C: : Calculation of analytical velocity for the BALSS radial flow BR For detailed description

$$V_{Axial} = \frac{\dot{Q}}{\frac{\pi}{4} d^{2}}$$

Equation 15

With these two equations the designer can gain a better understanding of the velocity in the BR's and decide which option to use for specific test setups and experiments. From Equation 51and Equation 15, an increase in volumetric flow rate in the radial flow BR results in a small local velocity change, however, increasing the flow in the axial flow BR results in a large local velocity change. This is due to the area of the axial flow BR being dependent on the diameter squared were as the area of an axial flow BR is dependent on just the diameter. Figure 45 illustrates this concept.

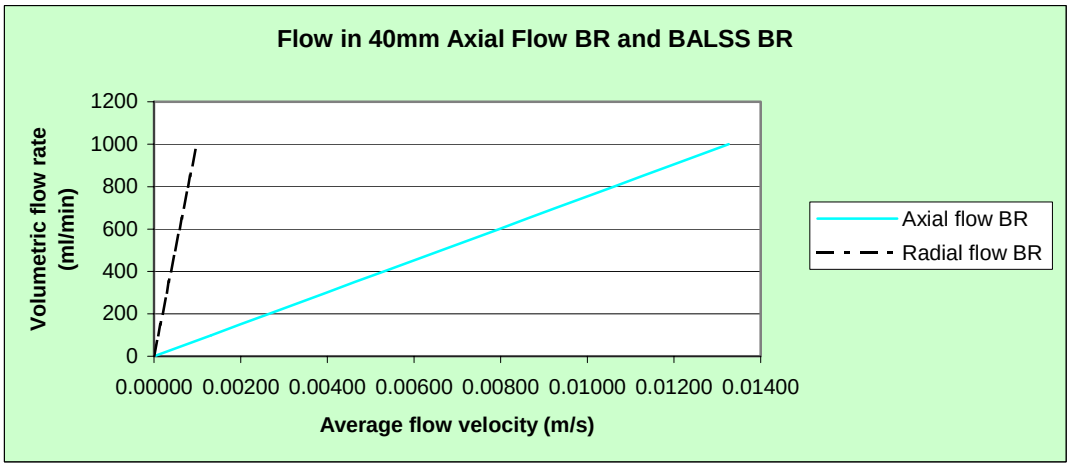


Figure 45: Flow comparison of axial and radial flow BR

Based on the before mentioned analysis an axial flow BR was chosen over the radial flow BR for the MRI study for better flow control and testing range. The design of such an axial flow BR is presented in Figure 46 and Figure 47. In designing the axial flow BR not all the design considerations given previously could be met. For example the use of diffusers to guide the flow to be more uniform conflicted with consideration 3. As a rule of thumb to prevent flow separation an optimal diffusion rate with an included angle of 7deg is recommended [80]. This results in an increasing of the BR's internal volume. Baffle plates were considered as an alternative, this would; result in an increased surface area.

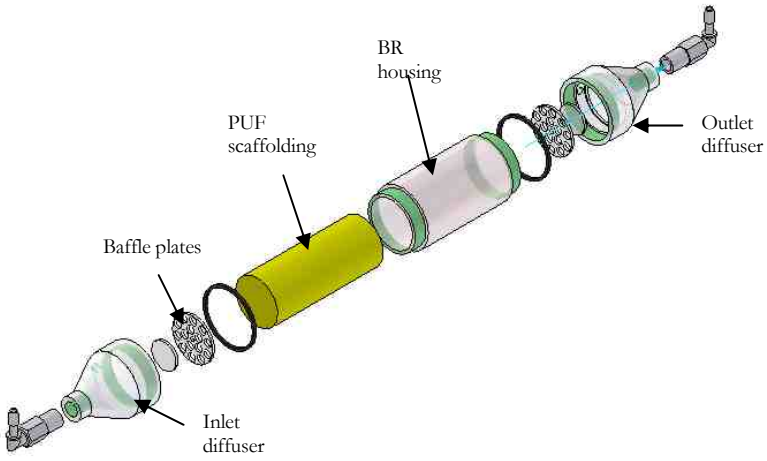


Figure 46: Exploded view of the axial flow BR used for the MRI experiments

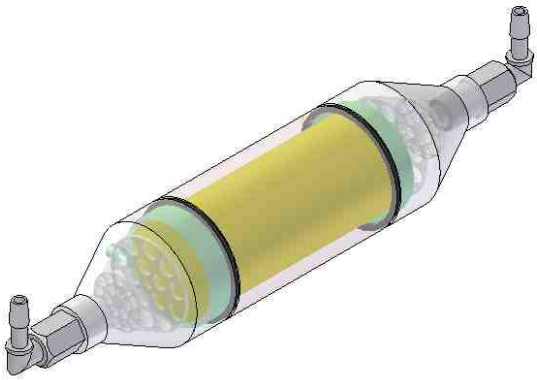

Figure 47: Assembly of the axial flow BR used for the MRI experiments

To interpret the visualised flow results in the axial flow BR a CFD model was constructed. The results form this model will act as qualitative comparator to the flow results generated by the MRI scan. The point of departure for the MRI flow study was that the results would give

1. A better understanding of the flow inside the porous scaffolding, previously modelled as a momentum source term in the CDF simulations (Chapter 3).

2. Show what effect the flow will have on the cell seeding by inspecting the seeding patterns and positions within the scaffolding.

3. and serve as a validation of the CFD porous modelling results of the scaffolding material.

In order to correctly analyse the flow phenomena in the axial flow BR, a CFD model of the axial flow BR was created with various aspects simulated. These include different baffle plate configurations and effects of gravity on the test setup. A volumetric flow rate of 100ml/min was evaluated by making use of the K-ω turbulent model. The outcomes of the simulations served as a qualitive indicator of the various inlet configurations.

Figure 48 shows that the additions of baffle plates makes the flow more uniform limiting jetting effects of a single undisturbed inlet, Figure 48(a). Figure 48(b) shows an initial baffle plate configuration with the schematic in the middle of the figure. The result shows good flow distribution with the non-symmetric flow effects due to the turbulence model. To machine this configuration would be time consuming and the structural integrity would be questionable, thus another configuration was opted for. The final simulation shows an excellent compromise between the relative flow speeds and manufacturing practicalities. The configuration in Figure 48(c) was chosen for the experimental setup.

The BR used to encapsulate the foam scaffolding was machined out of polycarbonate rod. Polycarbonate has the necessary thermal resistance needed to autoclave the BR for sterilization[40] and the necessary resistance for gamma radiation sterilization[41], if it was decided to change sterilization procedure. Polycarbonate is also a non-ferrous material allowing it to be used in MRI and NM (Nuclear medicine) imaging techniques.

The inclusion of a manometer allowed the measurement of pressure drop over the scaffolding, with the placement of the manometer just after the diffuser section allowed for different test sections to be tested.

[40] Polycarbonate, extruded has a Vicat softening point of 147-150°C [81] this was experimentally tested at 120°C in an autoclave, showing the material didn't soften.

[41] Polycarbonate can withstand an excess of 500Kgy in ambient air [82].

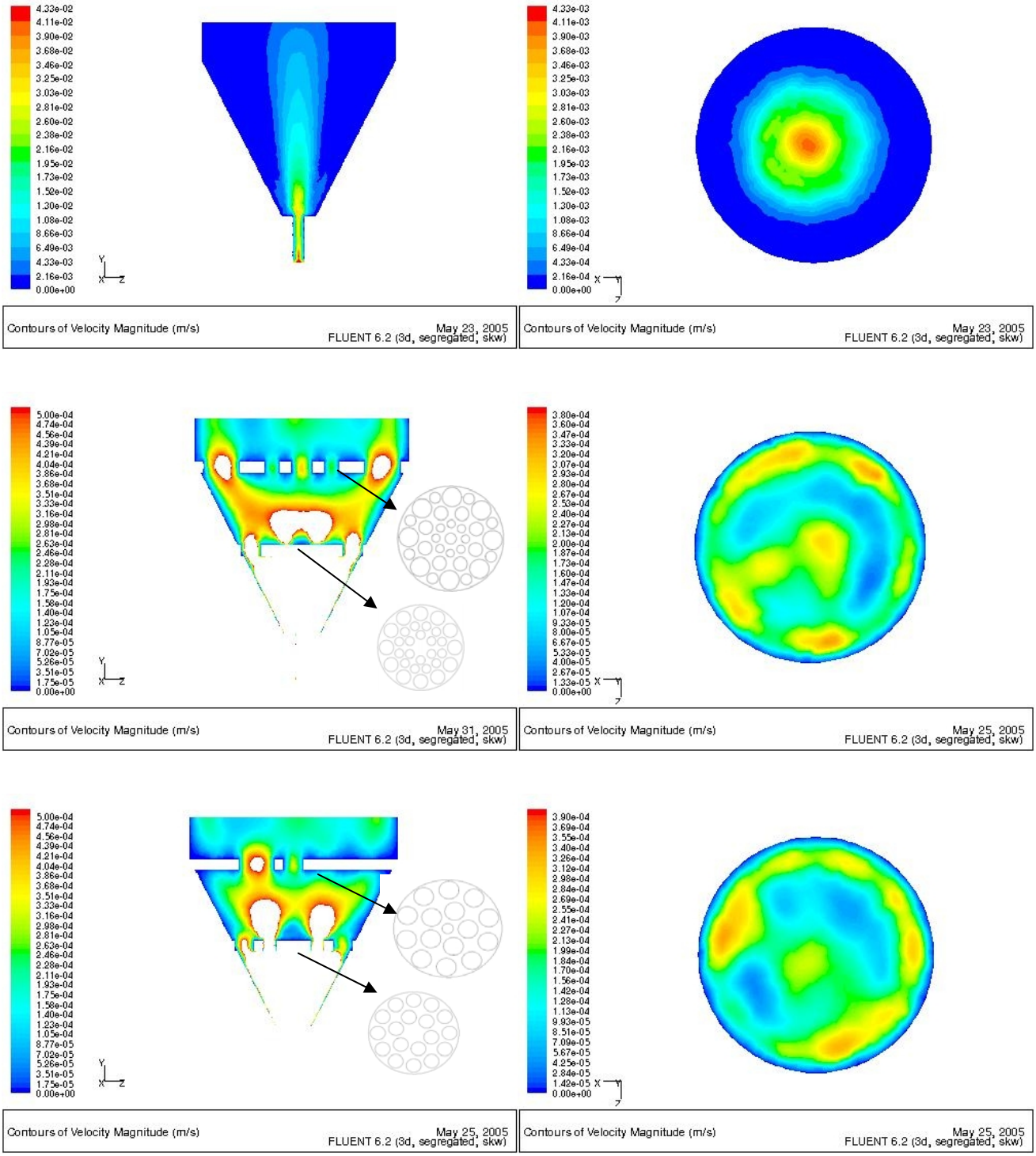


Figure 48: CFD modelling of the axial flow BR with a) no baffle plates, b) initial baffle plate configuration, c) final baffle plate configuration.

The inclusion of a manometer allowed the porous scaffolding to be characterised in the CFD model and a first order velocity calculation to be completed. Elbow connectors were used to connect the diffuser at the inlet and outlet; this prevented kinks in the tubing that would be the result of poor BR positioning.

### 5.1.2 Modeling effects of gravity on the MRI BR

In experimentally determining the effect of flow on the preferential seeding of the cells, a concerted effort was made to eliminate all other variables. The effects of gravity were modeled in Fluent using a laminar porous model with post processing via discrete phase modeling. The number of mesh cells used were in the order of 150 000.

Figure 49-Figure 51 shows the effects of gravity on released particles in the flow. The particles were modeled as spheroids with a density of 1065kg/m$^3$ and a diameter of 20µm. Based on this it was decided to orientate the BR in the vertical position as shown in Figure 52. It was decided to have the inlet at the top to minimise cells becoming trapped in the volume surrounding the baffle plates.

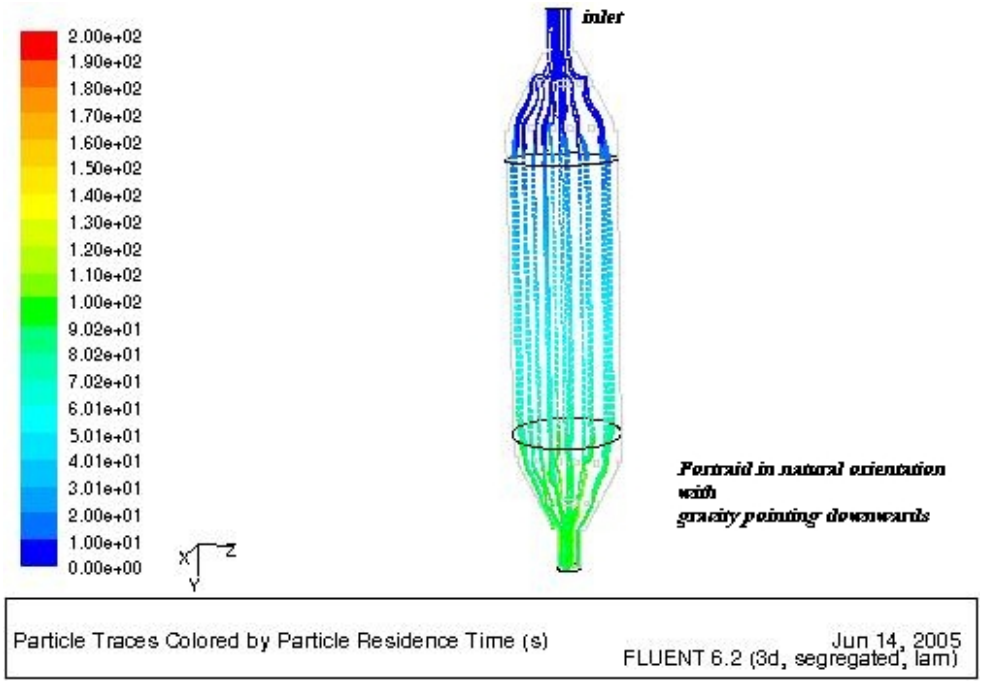


Figure 49: Simulated flow through the MRI BR to determine the optimal orientation; simulated vertical orientation

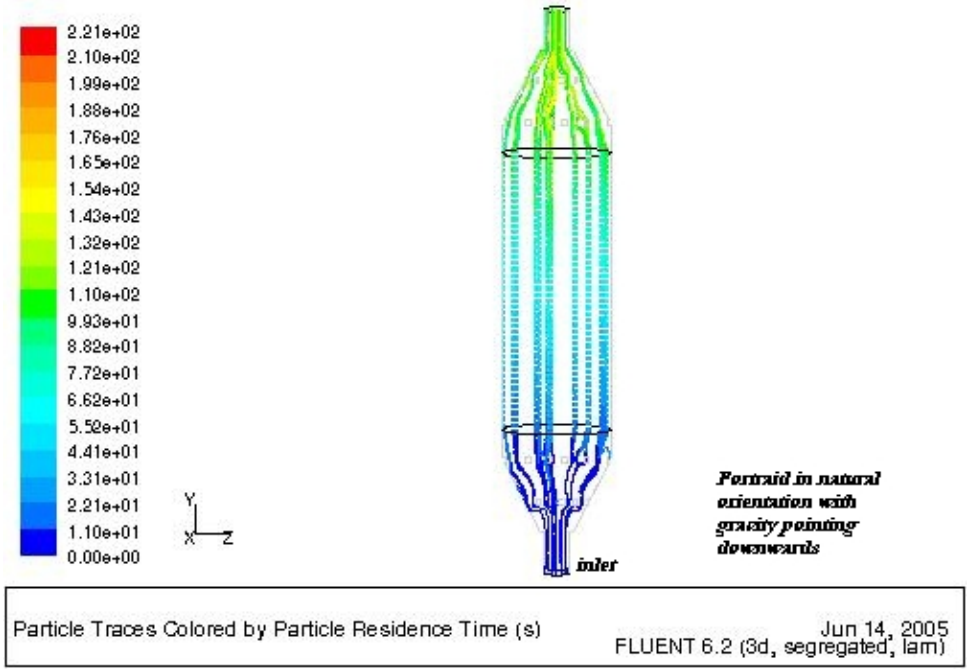


Figure 50: Simulated flow through the MRI BR to determine the optimal orientation; simulated vertical orientation-inverted

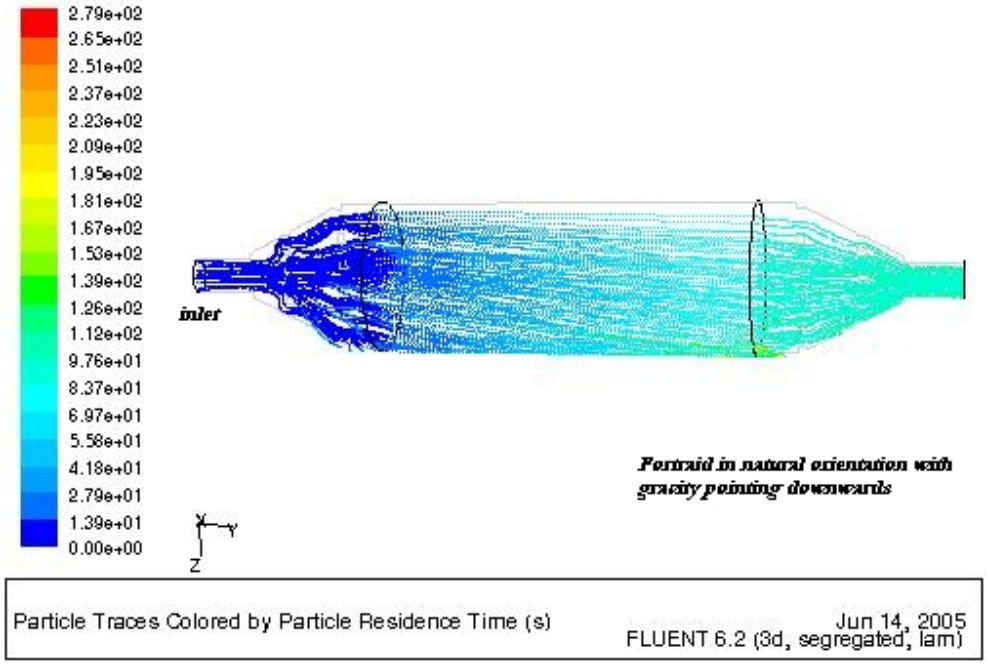


Figure 51: Simulated flow through the MRI BR to determine the optimal orientation; simulated horizontal orientation

## 5.2 MRI materials and methods

To determine the flow patterns in the scaffolding, Multihance® (paramagnetic contrast agent used in diagnostic MRI) supplied by BRACCO was used as the MRI contrasting agent. The experimental setup is shown in Figure 53. The BR, described above, has a volume of 180ml; the reservoirs used each have a volume of 575ml respectively and the perfusion lines and BR combined have a volume of 390ml. The reservoirs, custom made from Pyrex, have a double wall construction with a water jacket for temperature regulation. They have a media inlet and outlet, a gas inlet and outlet to atmosphere through a 0.2µm filter (Midisart®2000 supplied by Sartorius), and a port to inject the contrast/hepatocyte solution in a sterile fashion. The perfusion and manometer lines are silicone lines with an ID=0.125inch and thickness of 0.0625inch (supplied by Cole Parmer). The gas mixture, consisting of a 5.01% $CO_2$, 35.29% N and the remainder $O_2$, is supplied to the reservoir via stone bubblers. All gas mixtures were supplied by AFROX®(BOC special products). The gas bubblers served not only to provide oxygen transfer but also to mix the reservoirs maintaining a uniform temperature. The temperature of the water bath (Labcon (Model CPE50) supplied by laboratory marketing services cc.) was regulated at 47deg. The large temperature difference was as a result of the temperature loss from the BR to the reservoirs.

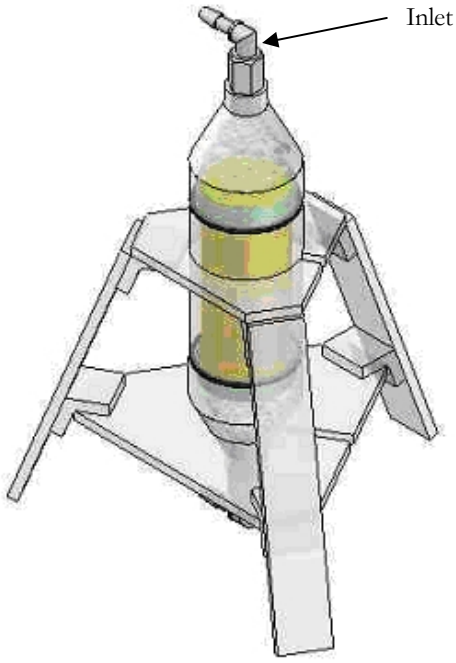


Figure 52: Orientation of BR in MRI machine

## 5.3 MRI experimental set-up, layout and procedures

A graphical representation of the experimental setup is shown in Figure 53, with the BR, reservoir perfusion and manometer lines autoclaved prior to experimental set-up. The cells were isolated using the method described previously and 1ml of contrast agent was added to the cells in 500ml suspension and left for 10min. The media was then spun off and re-suspended in new media, 500ml. The setup was primed with media from the media reservoir with hepatocyte/contrast isolated, valves 2 & 1 closed (see Figure 53). The hepatocyte solution was injected via the injection port of the reservoir, and then with valves 2 & 3 closed they were allowed to seed into the BR while the remaining media in the lines returned to the media reservoir. This was done to measure the real time seeding of the hepatocyte cells into the scaffolding, as well as the flow paths of the media during the seeding step. After a predetermined volume the hepatocyte pulse is returned to the hepatocyte reservoir, valves 4 & 1 closed. The seeded hepatocytes are flushed with media, valves 1 & 2 closed, and finally another seeding step was perfused continuously, valve 4 & 3 closed.

After the continuous seeding step the BR was scanned to determine where the cells were situated in the scaffolding.

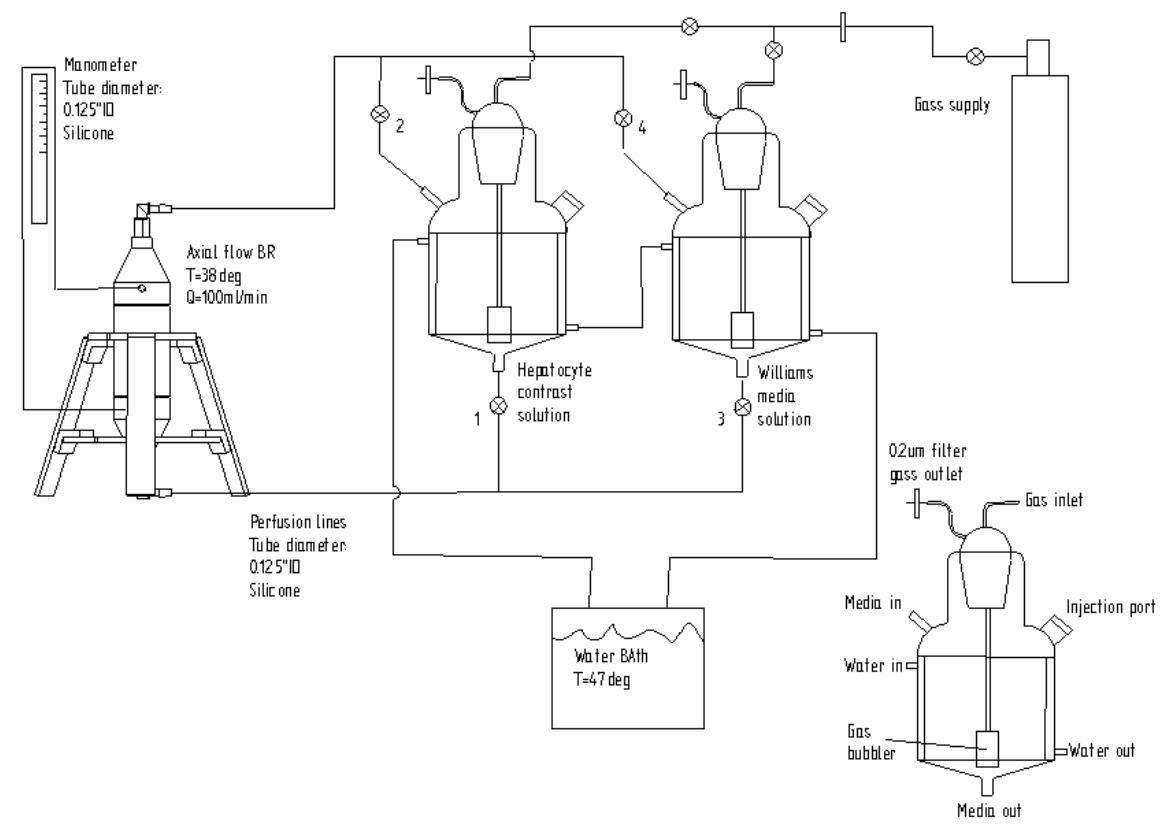


Figure 53: Schematic for MRI flow and preferential cell seeding experiments

## 5.4 MRI experimental results and discussion

### 5.4.1 MRI flow verification with de-mineralized water and contrast media

An experiment was done with only contrast and demineralised water perfused through the BR, to determine the flow paths through the BR and imaging quality. The experimental method and set-up is identical to that described above with the exception that the labelled hepatocyte suspension introduced in the reservoir was replaced by a mixture of de-mineralized water and contrast medium.

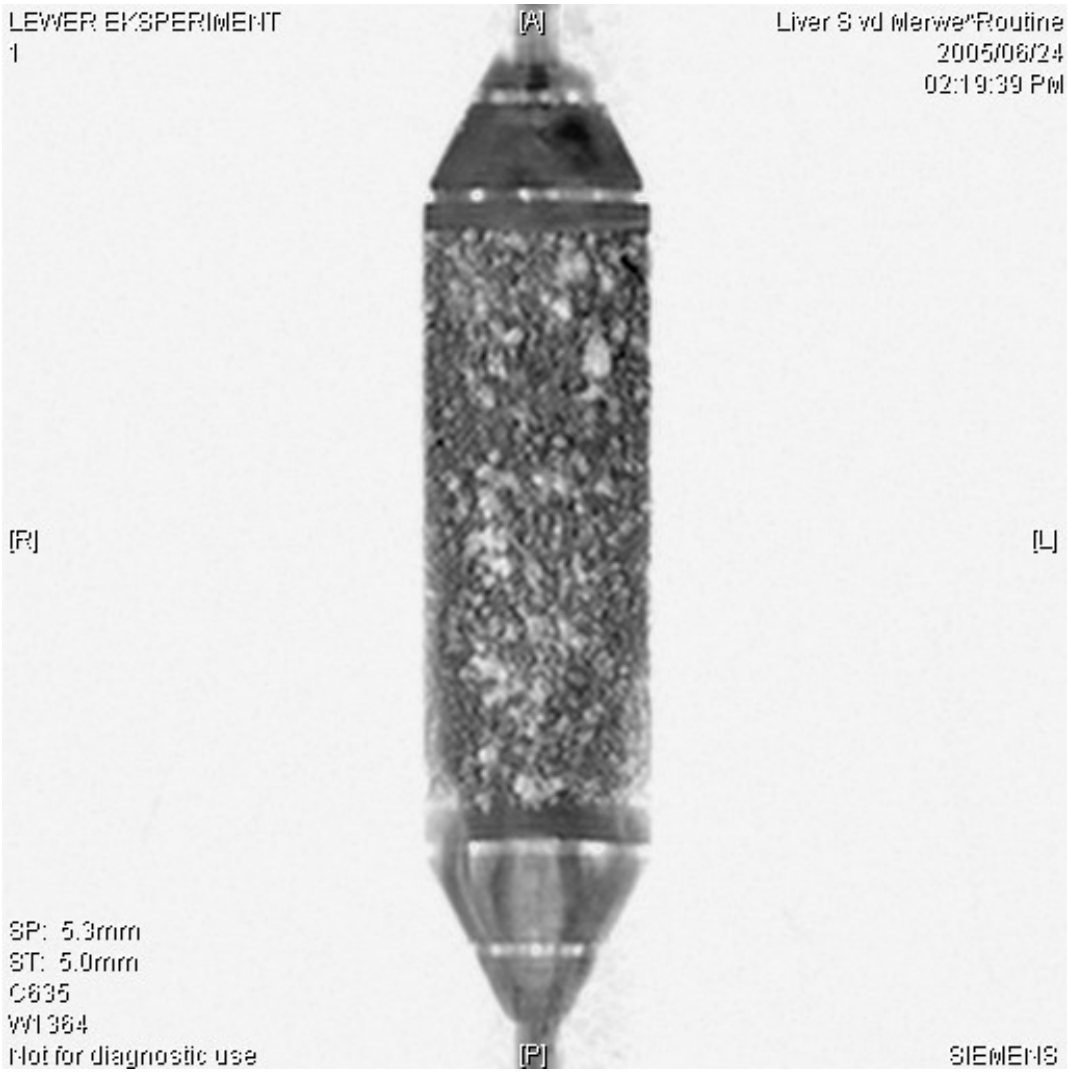


Figure 54: MRI image of axial flow BR with contrast and demineralised water

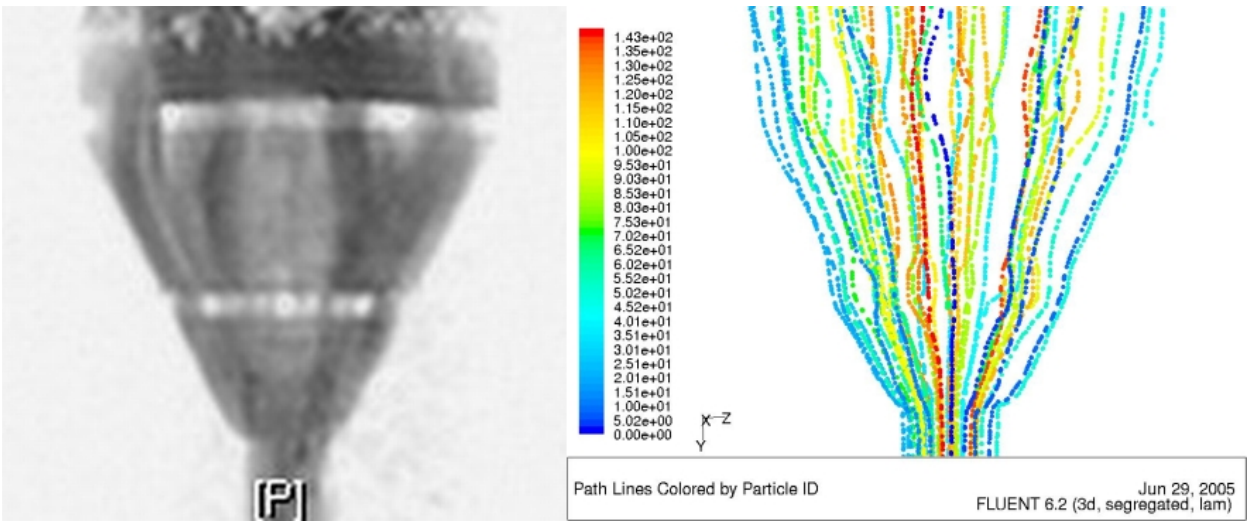


Figure 55: Comparison of a CFD simulation and MRI experimental results for the outlet flow conditions

Figure 54 shows the infusion of the contrast mixture through the BR and beginning to exit at the bottom. From Figure 54 it is clear the contrast passes uniformly through the foam with the baffle plates diffusing the flow efficiently. The MRI and simulated flow paths are presented for comparison in Figure 55, with particle tracks following similar paths compared to the MRI study. From these results it was clear that the flow could be visualised in the scaffolding by means of a MRI technique.

### 5.4.2 MRI flow verification with hepatocyte/contrast

Although the first experiment with contrast media and demineralised water gave good flow visualisation the uptake of contrast media in the cells were not sufficient to visualise the final position of the cell masses or the preferential seeding that was envisaged from the onset of the design of the experiment. On close scrutiny of the method it was determined that the lack of Kupffer cells in the cell culture might contribute to the less than optimal contrast uptake. The Kupffer cells take up the contrast agent by means of a phagocytic uptake process where they encapsulate the contrast. In the isolation procedure the Kupffer cells are removed from the cell culture mixture.

The hepatocyte cells do take up the contrasting agent to a certain degree according to the pharmacological classification because it is secreted in the bile ducts [83]. The lack of uptake could also be explained due to the stressed nature the cells due to the isolation procedure. Figure 56-Figure 58 shows the experimental set-up. The reader should note that the nature of the instrumentation used to complete the study limited the use of any ferrous metals in the MRI room. The use of pumps etc needed to be outside the venue with lines to the polycarbonate BR. This resulted in large temperature differences between the BR and reservoirs.

Figure 56: MRI experimental set-up showing numerous experimental components made from ferrous materials

Figure 56 shows the instrumentation that could not be used in the MRI room; the only non-ferrous material that entered the room was the BR and silicone tubing shown to the left of Figure 56 and Figure 57.

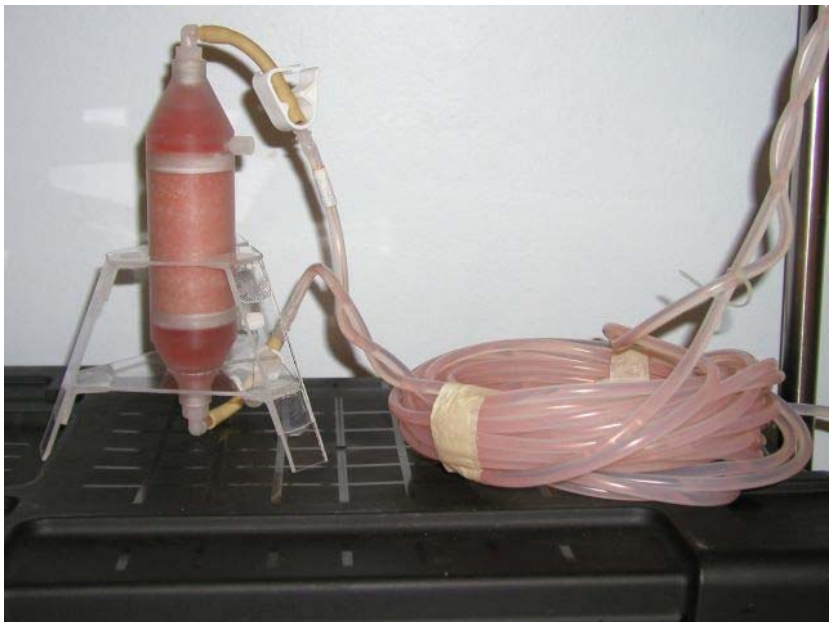

Figure 57: Non ferrous BR and silicone tubing allowing safe operation in the MRI facility

The BR in the MRI scanner shown in the upright position is shown in Figure 58.

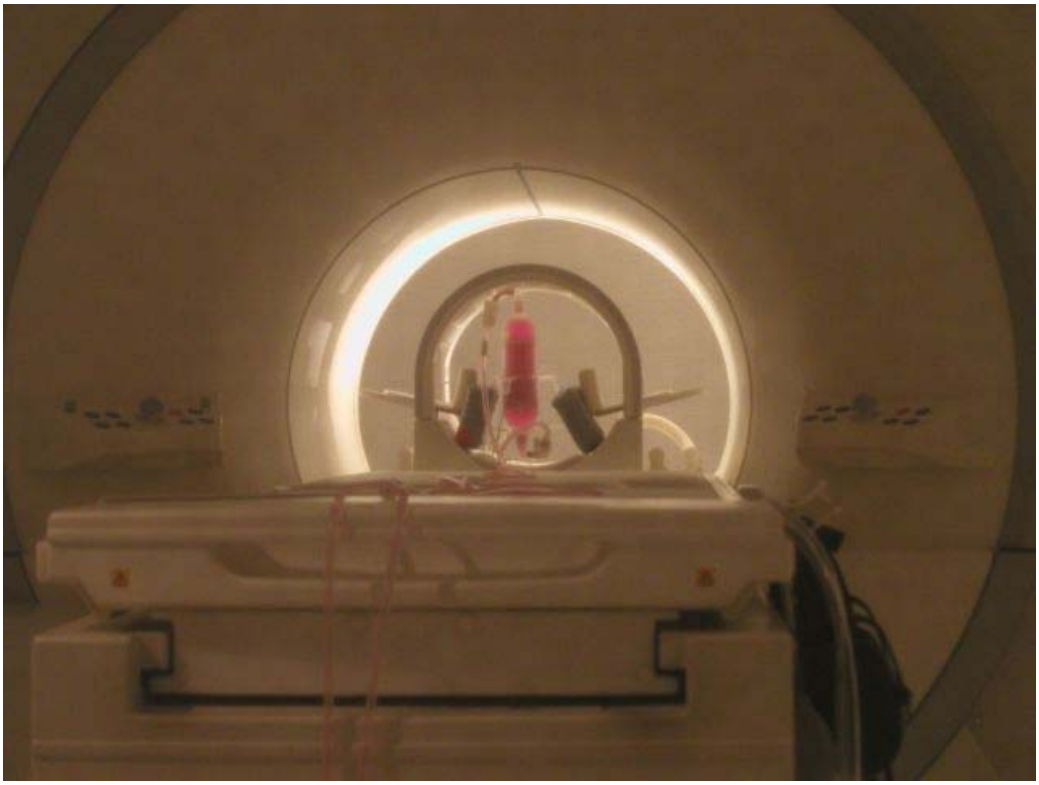

Figure 58: The BR in the MRI room in the simulated upright position

Notwithstanding the lack of clear preferential cell seeding data, a number of valuable observations were made. Figure 59 shows clear flow channelling in the foam at different depths or slices through the foam. These photos were taken using an arterial imaging technique typically used to measure arterial flow in the brain. No contrasting agent is required and depends on the flux of the flow.

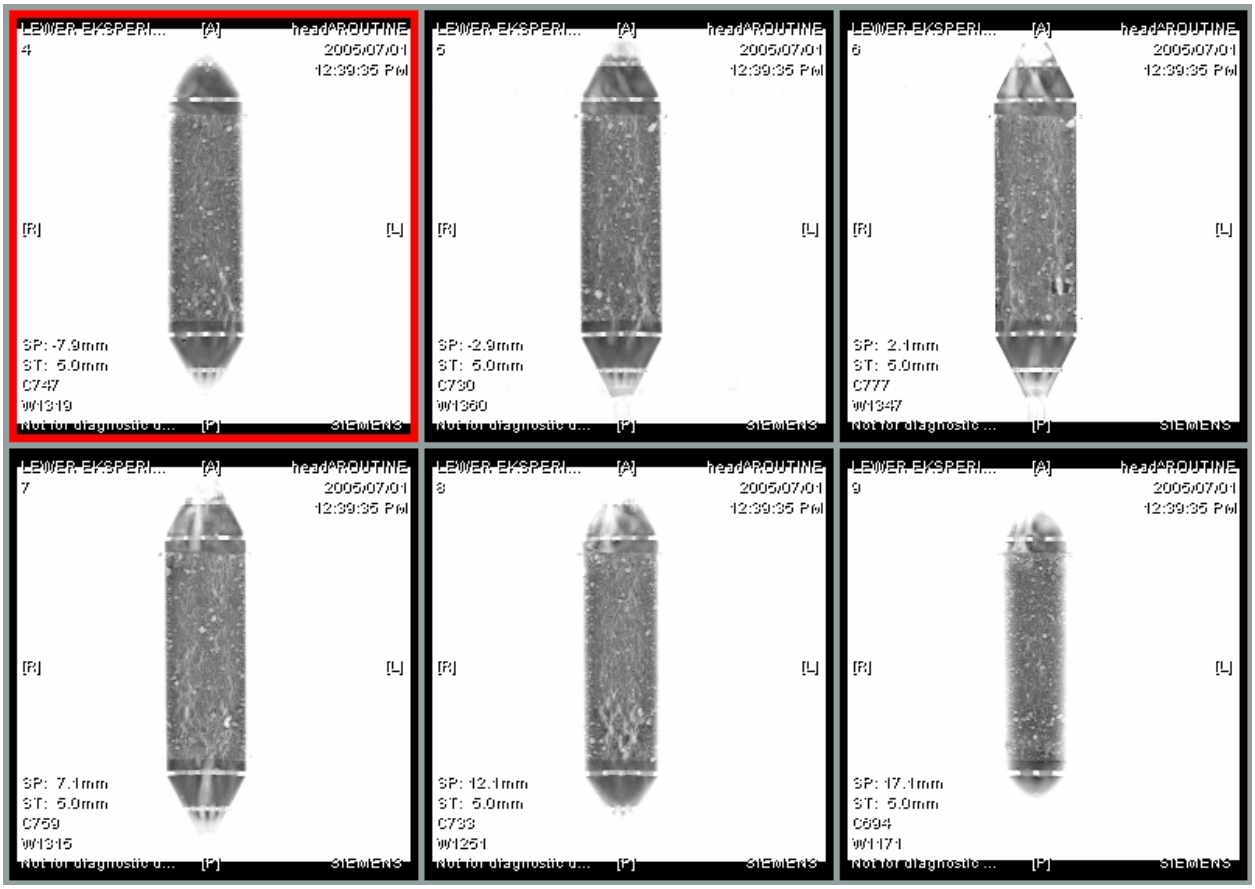


Figure 59: MRI imaging of axial slices

A major concern during the experiment was the effect of entrapped air in the foam scaffolding, this was minimised to a large degree by wetting the foam before autoclaving it. The best way to minimise the entrapped air was to fill the BR from the bottom displacing the air from the bottom[42]. Notwithstanding air still became entrapped in the scaffolding. Figure 31 and Figure 59 shows how the foam is channelled around foam discontinuities and air bubbles. This decreases the effective BR scaffolding volume and effectively increases the flow in localised areas.

To determine the local position of the air bubbles and to verify the fact that there was entrapped air in the foam scaffolding a computer axial tomography (CAT) scan[43] was done. Figure 60 shows entrapped air as white spheres with the media the surrounding grey areas. This occurred due to the inadvertent inverting of the BR to minimise air bubbles entrapped in the lines.

[42] The same effect can be demonstrated with a sponge, if water is placed on the top, it forms a dome and doesn't penetrate the foam, if you dip the foam into water the air is displaced from the bottom.

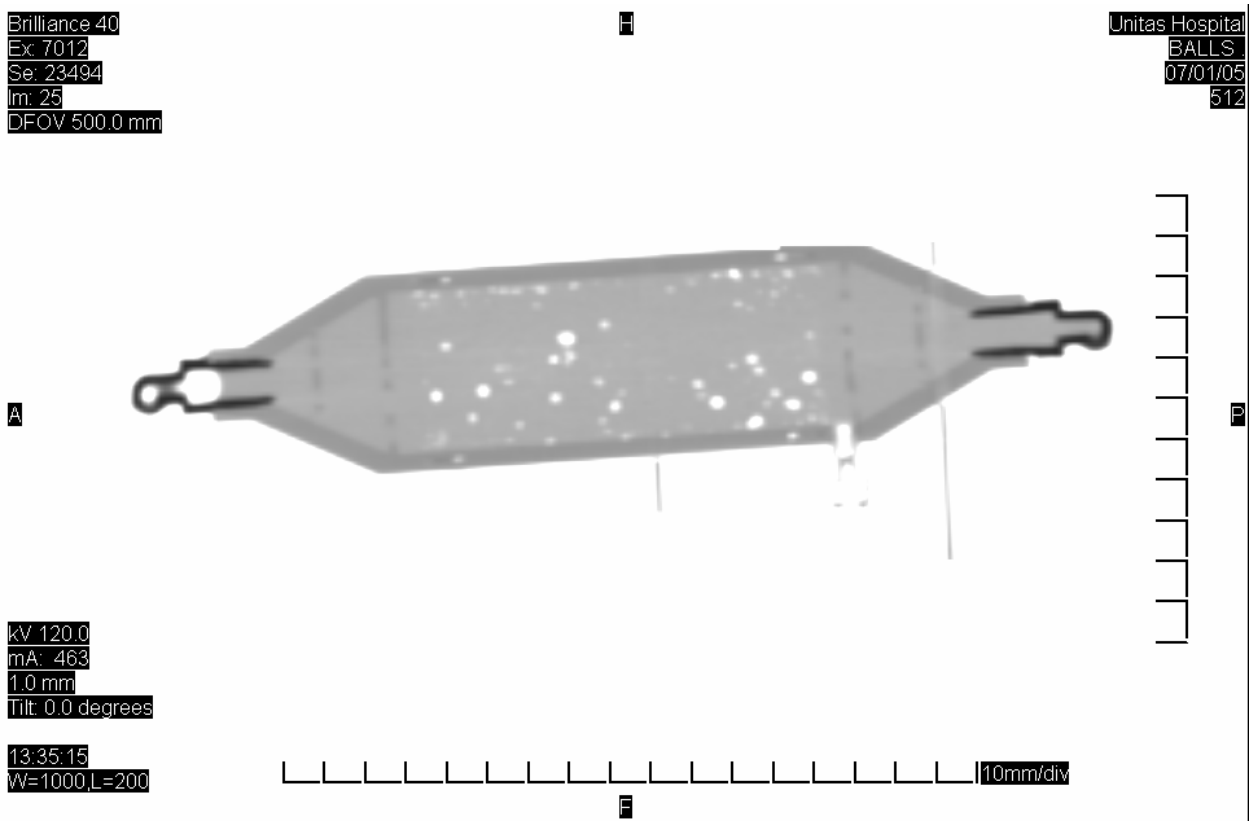


Figure 60: Cat scans done at Unitas Hospital, Pretoria, South Africa. Entrapped air shows up as white spheres

### 5.4.3 MRI BR differential pressure drop determination

Following the experiment, pressure drop experiments were done to determine the pressure drop over the foam test section. A simple manometer was used, filled with media were the pressure is related to the height difference as described by Equation 16 and schematically shown in Figure 61, the derivation of which is given in any good undergraduate fluid dynamics textbook [84]. The BR was orientated in the manner depicted in Figure 61 to eliminate the static height difference that would result in a static pressure difference between the inlet and outlet.

$$P_b - P_a = (\rho_2 - \rho_1) g (L - h)$$

Equation 16

[43] Seimens Brilliance 40, Unitas hospital.

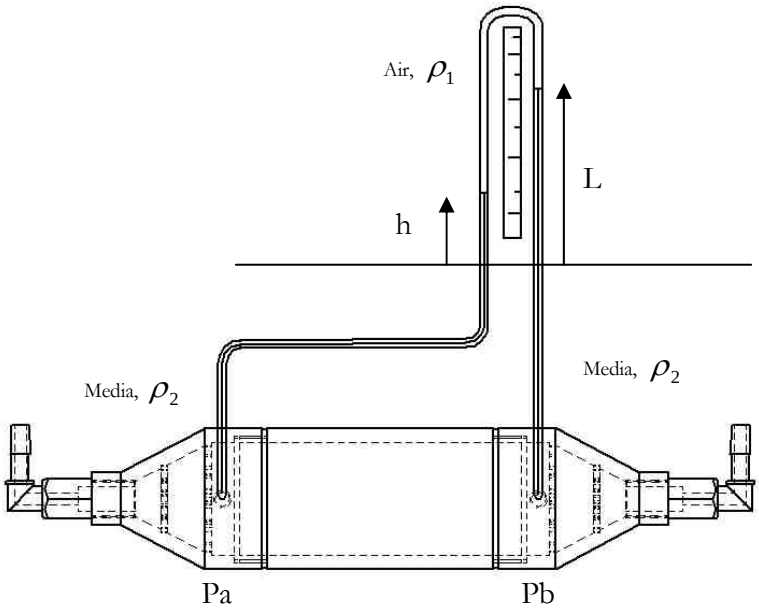


Figure 61: Manometer schematic used for MRI BR pressure drop calculations

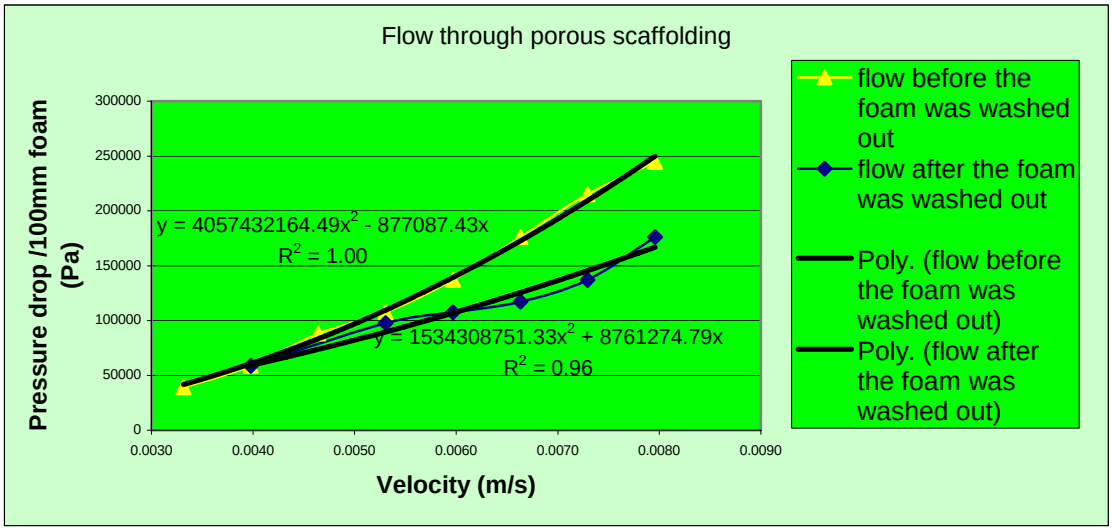


Figure 62: Results of the manometer pressure drop experiments over the MRI BR

The pressure drop was measured for varying flow rates. The BR was then stripped and washed out and the experiment was repeated. The curves in Figure 62 were obtained. There is clearly a blockage effect due to the cells, or entrapped air causing an increase in the pressure drop over the scaffolding. Weather or not the localised increase in

the pressure drop adversely effects the cells remains to be seen and another experimental set-up needs to be developed to test this effect on the cells. These tests were outside the scope of this investigation.

## 5.5 Outcomes of MRI/pressure drop experiment and recommendations

From the MRI experiments there was conclusive evidence to show localized channeling in the foam scaffolding. A contributor to this was entrapped air in the scaffolding, which can be minimized by carefully displacing the air upwards and by pre-wetting the foam. This would decrease the localized channeling in the foam.

The contrast uptake during seeding is not sufficient for seeding visualization.

There is a blockage of the foam resulting in a pressure drop over the foam.

# 6 MAXIMUM PRESSURE DROP AND SHEAR ALLOWED ON HEPATOCYTE MONOLAYER CELLS

*"Every really new idea looks crazy at first." - Alfred North Whitehead (1861-1947)*

The lack of definitive shear and pressure calculations and experimentation on cell cultures, especially hepatocyte cells, was the driving factor to determine the maximum allowable flow conditions and flow induced shear stresses on hepaocyte cell cultures. This is important for understanding of cells in scaffoldings especially in BALS related systems and the effect the flow has on these cell structures [72]. Research based on normal-orientated detachment forces is not well suited for studies with mammalian cells [85]. Thus there is a need to determine the maximum flow induced shear stress hepatocyte cells are able to endure in a tangent orientated perfused system. To accomplish this the cell cultures need to be subjected to varying flow rates, where the shear can be calculated from first principles. This posed certain design constraints on an experimental system as a whole. The flow related shear data can be used in conjunction with flow simulations to determine if the BR's perfusion conditions are within the limits of cellular function.

At the time of this study it was impractical to experimentally determine the shear stress directly in the porous media because shear rates are determined from the flow conditions. Because of this researches are forced to use experimental set-ups where flow conditions and therefore shear can be easily solved. The analytical solution for flat plate flow is readily available and is widely accepted as accurate. The radial flow between circular plates from the inner to outer diameter is another example of flow where the analytical solution can be determined. Ledezma *et al* used this flow configuration as a flat plate radial flow BR with heights varying between $10\mu m<H<100\mu m$ by means of spacers. Numerical methods were used to solve shear and velocity with analytical solutions as control; oxygen concentrations were also solved numerically using typical diffusion gradients. The pressure drop used in their calculations were assumed with the results showing numerically an increase in oxygen concentration as the Reynolds number increased, but they found that the channel height had a negligible effect on the oxygen transfer to the cells [50]. Tilles *et al* studied bioreactor channel heights ranging between 85 and 500µm, with flow rates ranging between 0.06 - 4.18ml/min. The study involved cell viability with an oxygenation membrane and without. Cells where the oxygenation membrane was included showed considerable better viability and function [76]. No comment was made regarding the oxygen transfer as a function of channel height. Unfortunately the author found no literature describing shear induced detachment kinetics for hepatocyte cells. There has been work on other cell lines (D. discoideum amebas) concentrating on nonconfluent monolayers or single cells by Décave *et al* where the shear was

regulated using a radial flow chamber with calibrated spacers between the flow plates. The reported accuracy of the gap was 20µm for a 200µm gap. The resulting data showed a exponential cell detachment for the applied shear flow [86]. Goldstein *et al* measured the detachment kinematics of murine 3T3 fibroblasts using a fracture analysis method, which relates the area of cells that became detached with the minimum shear that resulted in cell breakaway. This was fitted to a normal distribution, in varying forms. The height over the cells was 200µm with no accuracy given [85].

Peel *et al* studied the effects of shear on stoma cells. The confluence of the cells was varied and the related kinematics of the cells were determined based on the methods described by Goldstein *et al*. The group used a radial flow BR with a channel height of 140µm with polycarbonate spacers. Unfortunately no accuracy was given, which is a concern because the author found evidence that in machining polycarbonate the material does not keep its shape especially in an aqueous environment and at that small profile [87]. The group also found an exponential result describing the cell breakaway with regard to the maximum flow induced shear stress [72].

In order to evaluate the flow induced shear stress and other flow related phenomena that would affect hepatocyte cell detachment from the scaffolding, an experimental set-up was designed where maximum shear, local velocity and flow rates for hepatocyte breakaway could be determined. The BR had to be flexible in the sense that different shear rates and flow conditions could be tested uniformly, with other effects i.e. third body shear etc. minimised. Because of the difficulty of determining viability during dynamic testing it was assumed that if the cells were attached their potential to be viable was large compared to the cells that became detached. This assumption is especially valid during seeding, because cells that do not remain in the BR will not be inserted in the BALSS system and will be left in the isolation system.

## 6.1 Design considerations for hepatocyte cell breakaway experiments

From the onset the following constraints were imposed on the design.

- Varying flow speed and shear.
- Visual inspection of cells.
- Uniform flow conditions.
- Adequate temperature regulation.

- True flow speed measurements instead of commonly used flow average[44].

- Multiple flow speeds and multiple tests done as well as verification on the same cell cultures to ensure similar experimental conditions.

## 6.2 Radial flat plate BR for hepatocyte cell breakaway experiments

To fulfil the design requirements as well as a number of practical considerations when testing, a flat plate radial flow BR was developed. This consists in principle of two circular disks with cells seeded on one of the disks. The disk on which the cells are seeded are made of glass to allow for the visual inspection of the cells during various perfusion conditions. Flow is perfused between the disks in a radial fashion. By varying the cross sectional area of the flow different flow velocities could be induced over the cells. This ensures the cells tested can be subjected to different flow speeds and flow conditions that are commonly solved for using simple analytical methods.

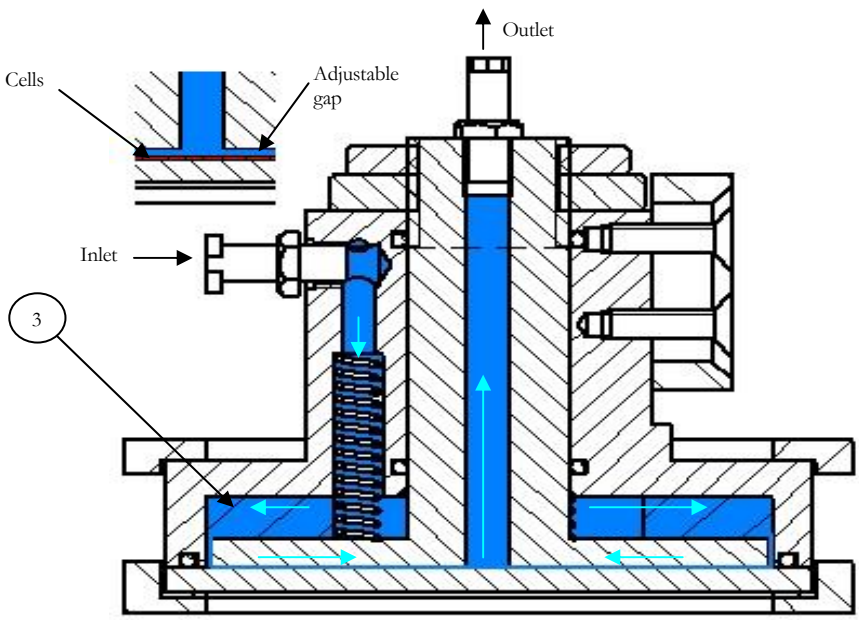


Figure 63: Radial flat plate BR for hepatocyte cell breakaway experiments, sectioned view

It also has the advantage that when testing a certain overall flow speed different local flow velocities can be observed at different radial locations. Practically this means that multiple experiments can be done on consistent cell groups by varying the overall flow speed.

[44] Discussed in more detail in 6.4: Flow speed calculations as a function of channel height.

The radial flow BR is shown in Figure 63 with the filled regions indicating the wetted areas of the BR. The flow will enter at the inlet and move from the largest radial section (slowest flow speed) to the outlet, which has the smallest radial section (fastest flow speed and highest shear). In certain experiments the flow speed can be reversed.

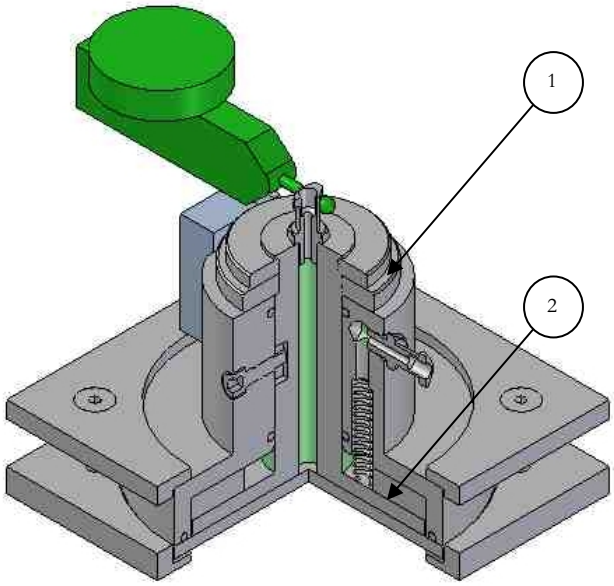


Figure 64: Radial flat plate BR for hepatocyte cell breakaway experiments, isometric-partially sectioned view

The cells were viewed during perfusion using an inverted light microscope; the configuration of which allows light to pass through the specimen into the microscope aperture. In manufacturing the BR materials had to be considered carefully, certain plastics could not be used due to their hydrophilic nature and inability to conserve their shape after machining. Thus an opaque or clear BR was impractical. Stainless steel is impractical due to its unfortunate cold welding properties, when applied as a sliding bearing. The clearances would cause welding at the tolerances specified[45]. Finally aluminum was chosen as the BR construction material for its ease of manufacture and good creep resistance. Unfortunately aluminum is not very biocompatible; therefore the BR can only be used for short intervals before the material effects render the cell environment unsuitable.

The adjusting plate (Figure 64, no2 directly over the glass slide) needed to be polished to allow the BR to be viewed by dark field illumination with the light microscope. Using a custom made light fitting mounted to the microscope,

[45] The tolerance specified for the clearance between the BR chamber and the adjusting plate was H7(g6) which amounts to a clearance between 41-7μm on diameter.

light was shone from behind the aperture and reflected off the adjusting plate back through the cells (seeded on the glass slide) into the aperture. The light source is shown schematically in Figure 65.

The BR was assembled prior to polishing to ensure the plate and glass-mounting surface was congruent. After machining the surface was measured using a machinist gauge with a surface flatness of <5µm obtained. To determine the gap height a machinist gauge was mounted to the top of the flat plate BR. It was zeroed when the adjusting plate and glass slide were in contact, then by turning the adjusting screws, Figure 64 detail 1, the correct channel height was read of the gauge. By adjusting the channel height in this fashion an accurate height could be determined and adjusted as necessary. The channel height could be varied between 20µm and 500µm. The height difference changed the cross sectional area of the flow thus changing the flow speed and related shear rates.

Detail 3, in Figure 63, is a flow diffusor to minimize channeling over the test section. This is based on the assumption there would be a uniform pressure in the top section by the inlet. The flow restriction is achieved by including a foam cylinder to disperse the flow. The inlet volume at the top of the adjusting plate is also relatively large compared to the testing flow volume so uniform dispersion can be assumed. It also serves to remove any debris or other pollutants that might influence the experiment, by colliding with the cells that are still attached.

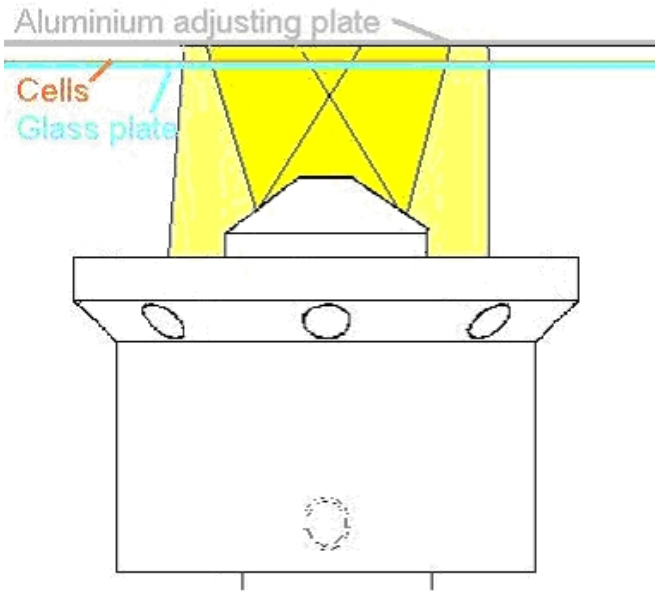


Figure 65: Schematic of light source for dark field illumination used in the flat plate shear BR experiments

## 6.3 Hepatocyte cell breakaway, experimental method and operation

The cells were seeded in culture on the glass slide[46]. The cells (isolated primary porcine hepatocytes) were grown in a petri dish, using common cell culture techniques, until the cells were confluent resulting in a monolayer of cells over the entire surface of the glass slide. The BR was then preheated in the incubator and inverted while placing the glass slide in position. The BR was assembled and the cells subjected to different flow speeds. A digital pump was used with the priming volume for the system equal to 100ml. William's media was used as priming solution. The experimental setup is presented in Figure 66 and Figure 67.

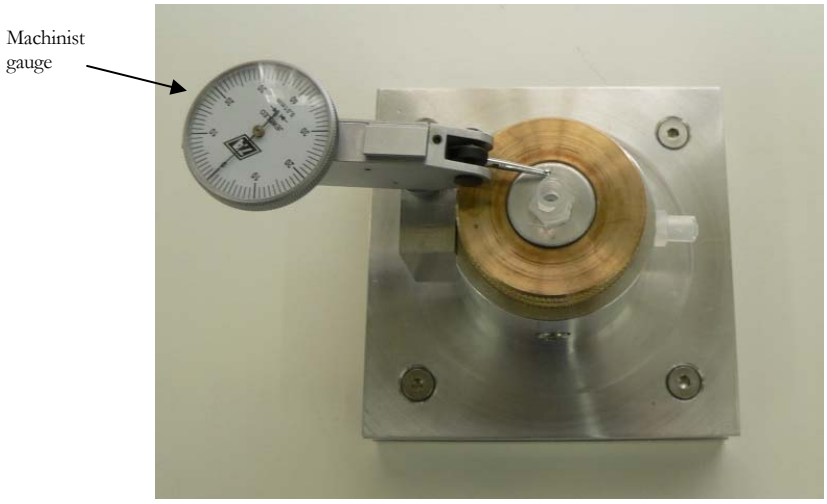


Figure 66: Radial flow flat plate BR used to determine hepatocyte cell breakaway, showing machinist gauge used for channel height calibration

## 6.4 Flow speed calculations as a function of channel height

The localised flow speed was calculated using a simple mass balance assuming constant density, Equation 17. The derivation of which is given in Appendix C. The flow rate was varied from 40ml/min to 1000ml/min at 100ml/min intervals for approximately 60s.

$$V_r = \frac{\dot{Q}}{\pi d_r h}$$

Equation 17

[46] The glass was washed in alcohol and autoclaved. It was not etched.

Where the nomenclature is as previously described.

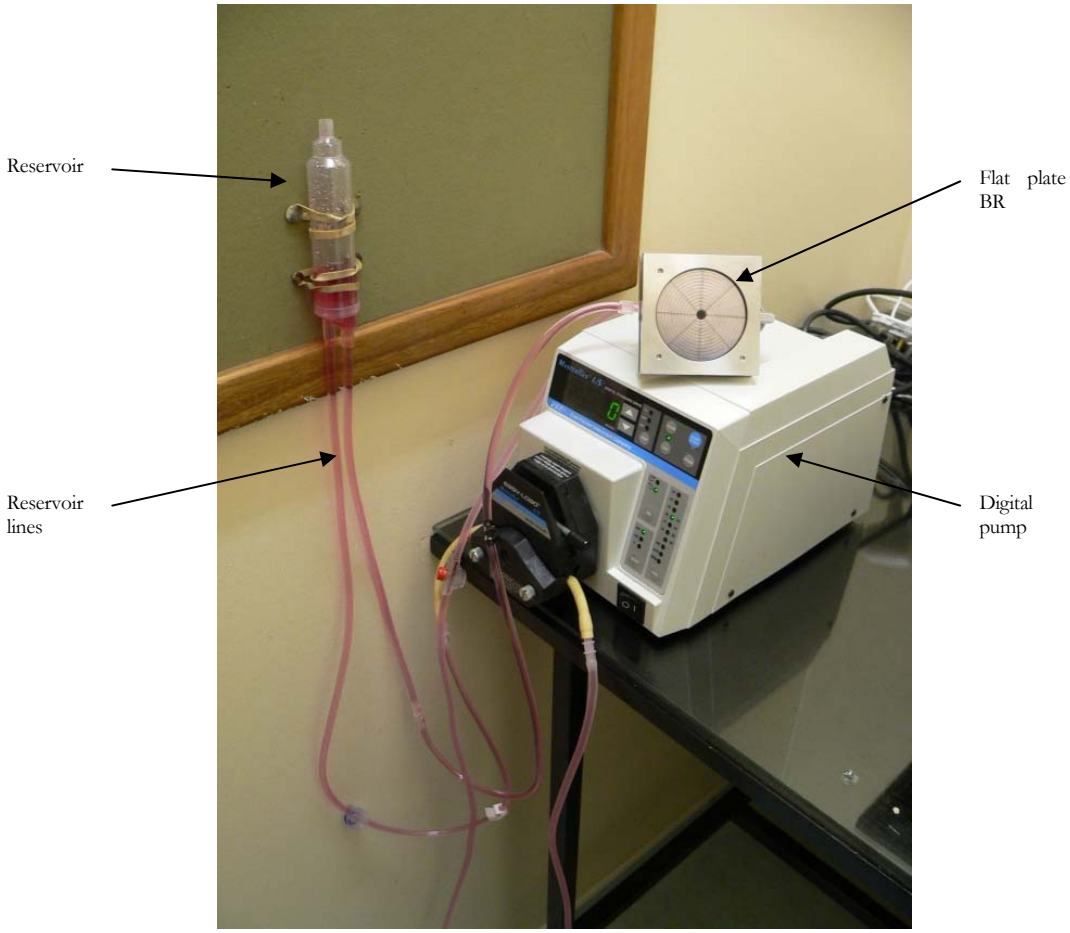


Figure 67: Hepatocyte cell breakaway experimental set-up

From Equation 17, the localized flow speed is inversely proportional to channel height and radial location, thus the gap height determines the localized flow over the cells with the smaller heights resulting in larger flow speeds, higher shear and larger pressure drops over the test section.

The height of the gap is accurately determined by means of a micrometer. The small testing height to obtain the necessary shear imposes strict machining tolerances with the machining being for the most part the main manufacturing constraint. It is important to note that Equation 17 gives the flow as an average of the true velocity profile, shown as the solid line in Figure 68, with the zero slip constraint being ignored.

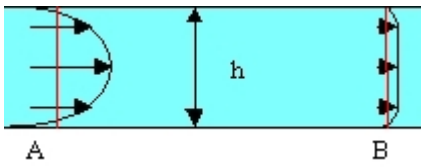


Figure 68: Velocity profiles for flat plate flow

Figure 68, shows an example of developing flow at point A and a fully developed flow at point B, it is clear that the aforementioned assumption becomes more valid as the flow becomes more developed. By decreasing the height of the channel even more to the magnitude of the cells, Figure 69, the cell height compared to the velocity profile thickness makes Equation 17 less of an assumed average. This was the argument for the considerable effort in designing the BR to adjust height in the order of magnitude comparable to the cell monolayer height. The small channel height also allowed large shear forces for low volumetric flow rates[47].

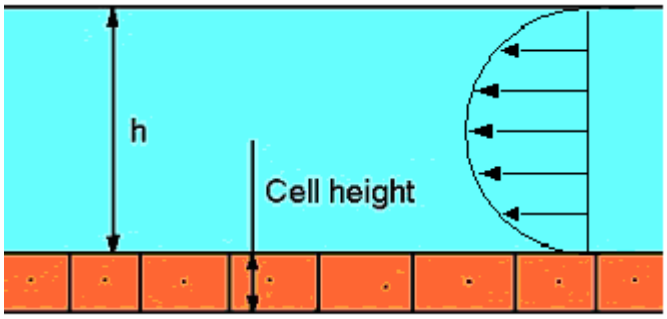


Figure 69: Cell height to channel height ratio

The Reynolds number was calculated from Equation 18.

$$\mathrm{Re}_h = \frac{\rho V_r h}{\mu}$$

Equation 18

Where $r$ is the radial position of localized velocity and $h$ is the channel height and other nomenclature is as previously described. Substituting Equation 17 into Equation 18 the Reynolds number in terms of the channel height can be

[47] From inspection of Equation 22 the shear is inversely proportional to the square of the channel height, where the channel height is very small.

determined. Note that the system configuration in terms of the Reynolds number is dependant on the density, viscosity, specific radial position of measuring and the flow rate.

$$\mathrm{Re}_h = \frac{\rho \dot{Q}}{\pi d_r \mu}$$

Equation 19

This is similar to the Reynolds number reported by Goldstein *et al* [85]. The Reynolds number remained in the laminar flow range for the channel heights investigated with the Reynolds number typically 500, were laminar flow is normally defined when Re is below 2000 [53].

## 6.5 Shear calculations as a function of channel height

If the inertial effects of the flow can be neglected (Stokes creeping flow), a common assumption used by researches using radial flow flat plate BR's, then the shear can be determined using equation Equation 22 [50,86]. Provided the radial position is larger than the RHS of Equation 20 this assumption is valid.

$$r > \left( \frac{2\left|\dot{Q}\right| h}{7\pi\upsilon} \right)^{0.5}$$

Equation 20

Where the nomenclature is as described elsewhere and $\upsilon$ is the kinematic viscosity given by Equation 21.

$$\nu = \frac{\mu}{\rho}$$

Equation 21

The shear at the wall or in the case of the radial flow BR the shear on the cells is given by Equation 22 [50,86].

$$\tau_w = \frac{3\mu\dot{Q}}{\pi h^2 r}$$

Equation 22

To compensate for the inertial effects near the centre of the BR a correction term was added as described by Goldstein *et al.* [85] This solution was obtained by applying a 3-term power series expansion in reciprocal radial position, resulting in a 1st order correction given by Equation 23.

$$\tau_w = \frac{3\mu\dot{Q}}{\pi h^2 r} - \frac{3\rho\dot{Q}^2}{70\pi^2 h r^3}$$

Equation 23

From inspection of Equation 20 if the correction factor was neglected the minimum radius for accurate results would increase with the channel height and flow rate.

The results of a shear calculation, using Equation 23, at a channel height of 80µm are shown in Figure 70.

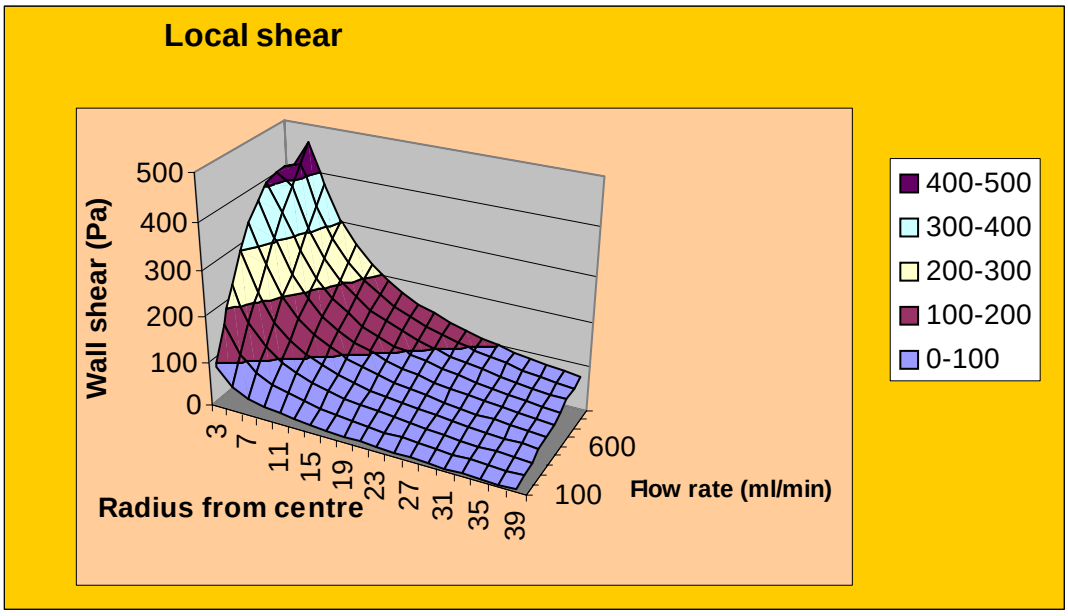


Figure 70: Local shear using Stokes flow in the radial flow flat plate BR, with a channel height of 80µm, from Equation 23

In the experimental set-up the flow rates are determined using mass conservation and the shear rates are calculated accordingly. For a gap height of 80um, using Figure 70, the researcher can read off the shear rates for specified flow rates at a specific BR position.

## 6.6 Hepatocyte breakaway: experimental results and discussion

### 6.6.1 Flow conditions for hepatocyte cell breakaway

The cell detachment was determined by measuring the distance from the center of the BR to the lowest shear point were the cells began to detach. The method used to interpret the data differs from the analysis used by previous researches in that the area of detached cells was not measured. Instead the initial point at which the cells become detached was measured. Figure 71 shows various breakaway points for a flow rate of 1000ml/min at a channel height of 80μm.

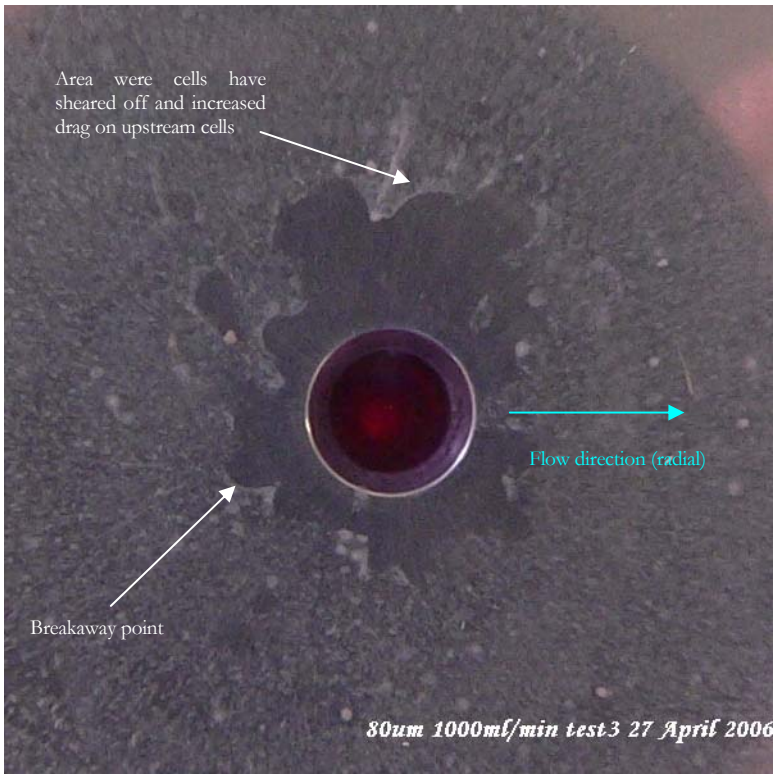


Figure 71: Example of cell shear and fold-over

Each initial point where the cells break away has a specific shear determined by Equation 23 and shown in Figure 70. These points were grouped for individual experimental flow rates with the furthest point from the BR center being

the minimum shear point. The number of breakaway points was counted for this minimum shear and testing flow rate. This was done because the author found the cells that become detached first tend to peel the remaining cells downstream as they shear off. This is not a shear phenomenon but more of a drag effect.[48]

Figure 72 shows a typical cell detachment pattern for different flow rates. The distance to each breakaway point was measured and scaled with the inlet diameter. This needed to be done because the data processing was done from pictures taken of the experiment. The data presented in Figure 73 shows the number of detachment points as a function of the minimum applied shear for a specified flow rate.

[48] See section 6.6.2: Mechanism for hepatocyte cell breakaway

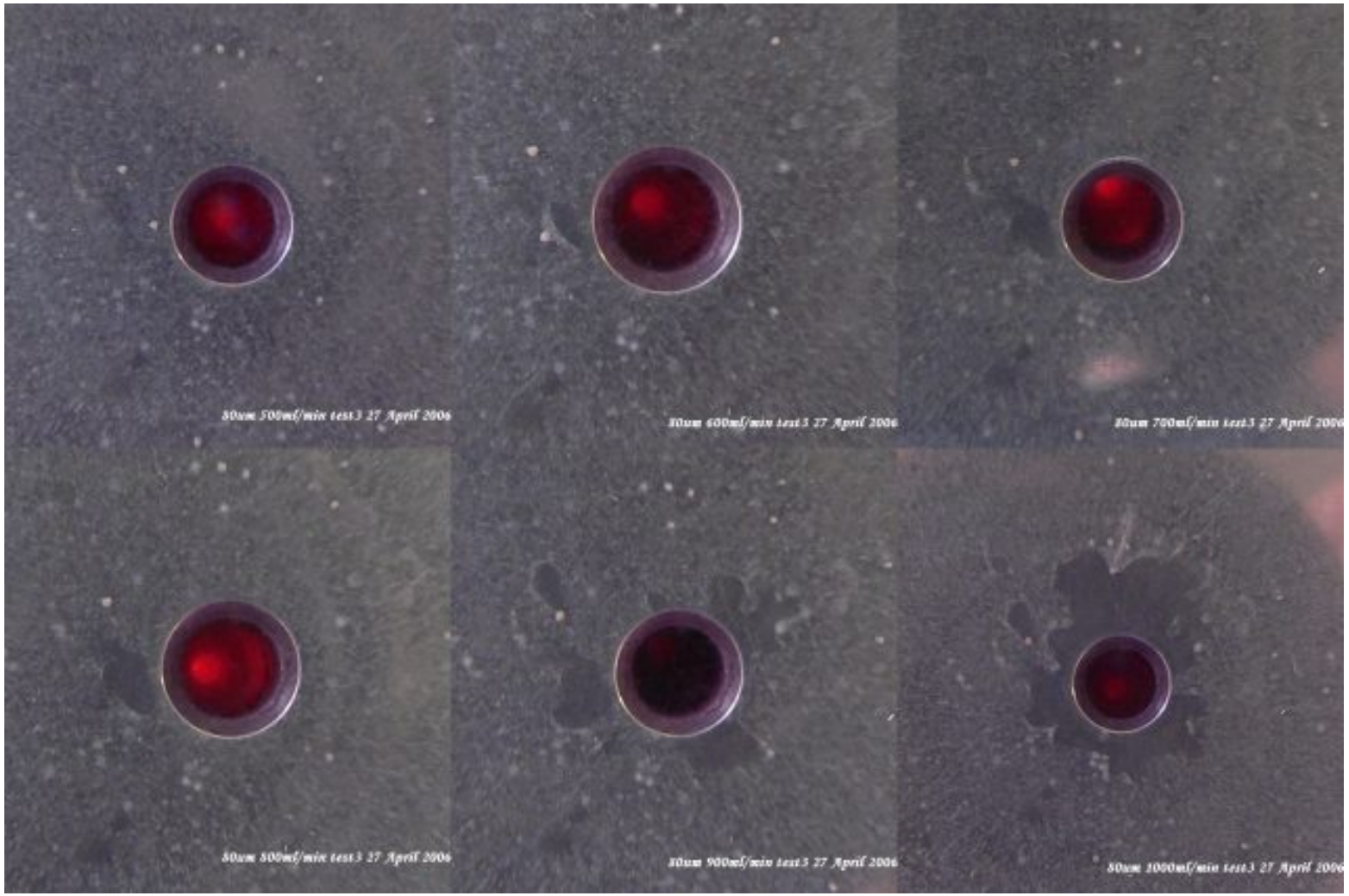


Figure 72: Test results for 500-1000ml/min flow rates and gap height of 80µm

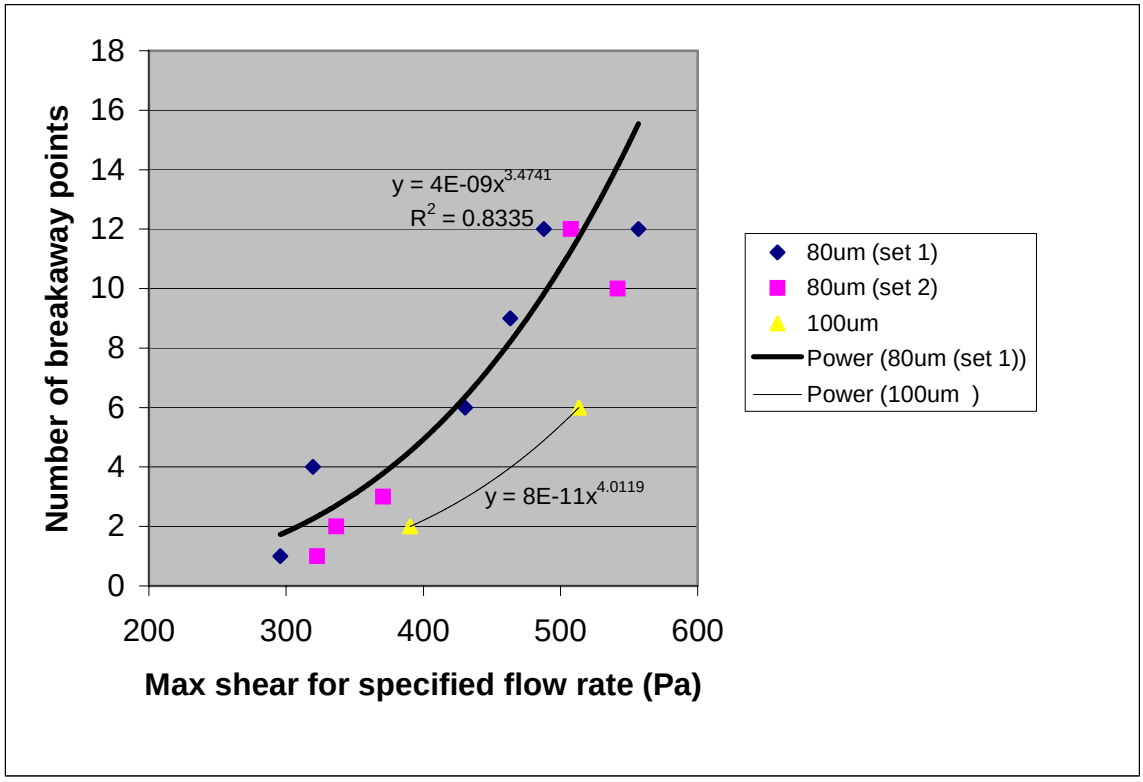


Figure 73: Minimal allowable shear for the number of breakaway points, related to shear

The data presented, in Figure 73, is for 80 and 100µm gap with the flow rates measured depending on the channel height for different shear rates. It shows that as the flow rate increases the maximum shear rate increases as well as the number of cell detachments. Only 2 points were plotted for 100µm because the flow rate for the applied shear was large with cell detachment only observed at 900ml/min. Tests were done for 20,50,60µm but the results show that the cells tend to fold over and tear off more as a result of drag effects than that of shear forces. At the smaller gap heights the flow rate was in the region of 400ml/min for large regions of cellular detachment.. A concern with the lower gaps is the inherent pulsing of the peristaltic pump with the peaks having a higher shear than the reported average. To model the effects of this would be extremely difficult and beyond the scope of this investigation. The fold over was also seen in the presented data, see Figure 71, but the effects were small compared to the flow shear effects. Figure 71 also shows the points used to determine the minimum shear that the cells began to shear off.

From Figure 73 at a gap height of 80µm the maximum shear is 500Pa. From Figure 71 which corresponds to this test the reader can see that a substantial amount of cells have been sheared off. With the results displayed, shear rates above 300Pa is not advisable in any scaffolding. The specific flow rates related to this shear needs to be determined

using Equation 23. For the foam scaffolding used in the BALSS a pore size of 80µm can be roughly related to the 80µm test height. For a maximum shear of 300Pa the corresponding maximum flow velocity is 8m/s, which is exceptionally fast. With the simulated mass weighted flow rate at the exit conditions of the scaffolding equal to 0.000759m/s (see section 3.14), the optimized BR is well within the limits of cell breakaway.

### 6.6.2 Mechanism for hepatocyte cell breakaway

The method of cell breakaway is not clearly understood. De´ cave´ *et al* postulated that the cell bonds break progressively with time, decreasing the contact surface area between the cells and the substrate resulting in greater forces on the cell structures for the same applied stress [86]. What was observed in this study is that the cell-cell bonds are much larger than the cell-substrate bonds. The cells tended to shear off in layers with confluent cells removing the neighbour cells as they become dislodged. Figure 74 shows the monolayer that had folded and removed the neighbouring cells. Singular cells with bonds to the glass stronger than that to surrounding cells remained and can be seen to the left of the figure. The reader can also see the fold of the monolayer. This fold acts like a parachute increasing the drag forces on the cells.

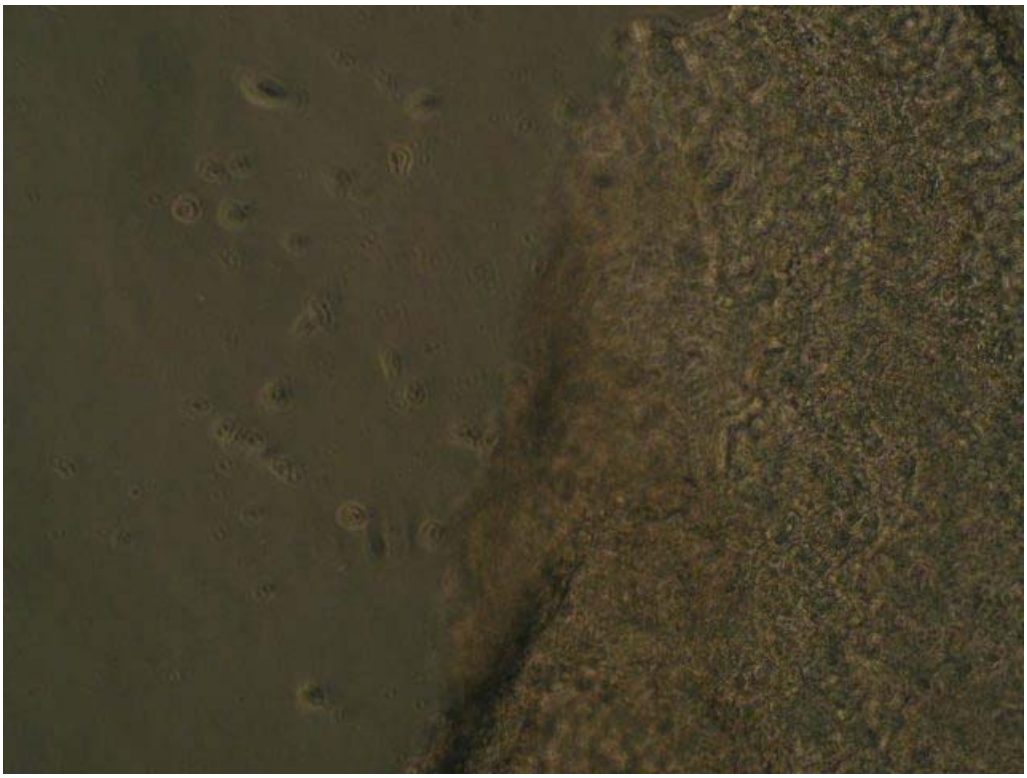

Figure 74: Monolayer of cells folded over increasing drag forces on the hepatocyte cells, viewed at 10X magnification

Another concern was the effect of bubbles on the detachment of cells, Figure 75. It was found that bubbles become trapped behind the shearing cells and significantly increased the drag area. This increases the forces on the cells and they could become detached at lower shear forces. This was investigated dynamically under the microscope using dark field illumination with the light source discussed previously.

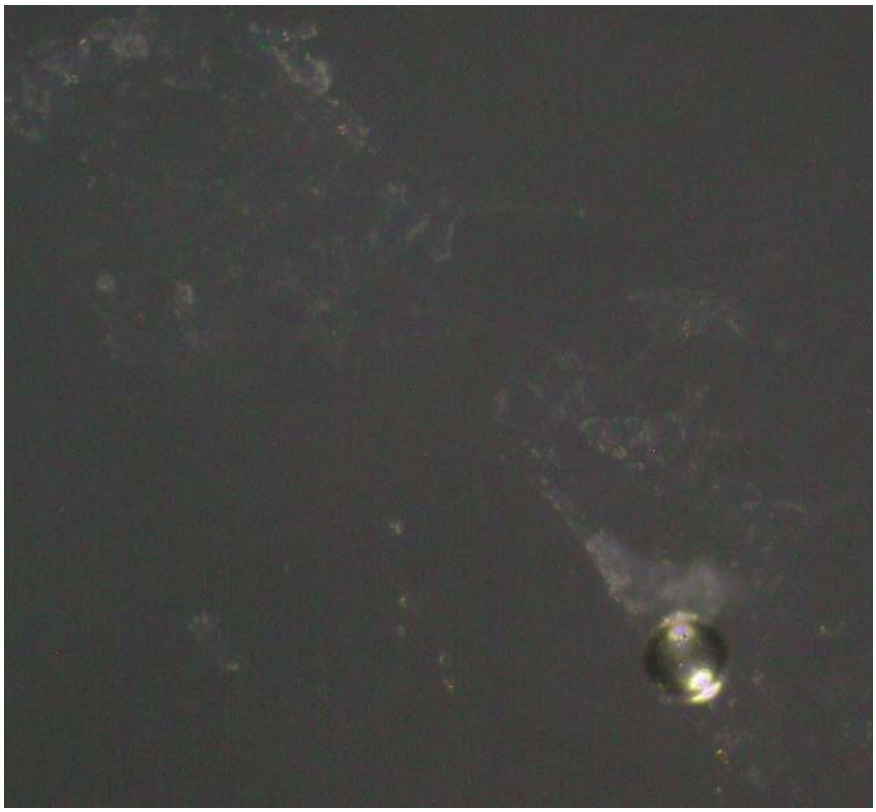

Figure 75: Dynamic drag effects of a bubble on monolayer cell detachment

# 7 CONCLUSION: OPTIMAL CONDITIONS IN A BR FOR THE SUCCESFUL CULTURING OF HEPATOCYTE AND CO-CULTURED CELLS

*"Life is the art of drawing sufficient conclusions from insufficient premises." - Samuel Butler (1612-1680)*

## 7.1 Concluding hepatocyte BR design considerations

The addition of biological components in any design adds constraints and complexity to the system. These constraints are for the increased viability of the biological component. Sub optimal BR design will result is cell death and lowered cell viability which dictate the cellular metabolic activity. The addition of hepatocytes into the three dimensional biological scaffolding used by the BALS system necessitates the following:

- Adequate temperature regulation.
- Adequate mass transfer for cell nutrients and oxygenation as well as the removal of toxins, the metabolites and bile products.
- Regulation of $CO_2$, which inherently influences the PH of the system media. $CO_2$ dissociates forming bicarbonate and hydrogen ions [6].
- Optimal flow speed; if the flow is too fast the shear becomes detrimental to the cells, if it is too slow then this could result in inadequate mass transfer.
- Dead spots in the BR resulting in large volumes that are not efficiently utilized by the perfusion loop as well as cells in those regions dieing due to oxygen and nutrient starvation.
- The scaffolding must be wetted completely, removing the chance of gas pockets, which would effectively be a dead spot in the BR.
- Cell seeding must be uniform within the scaffolding.
- Flow must be homogeneous within the scaffolding.

- The formation of cell clusters must be promoted to the point were mass transfer to the innermost cells impede their function.
- Regulated porosity and surface areas, closely related to pore size-influencing flow conditions.
- Large numbers of hepatocytes, requiring large surface area for cell adhesion [76].
- Small BR volume to prevent patients becoming hemodynamically unstable and to minimize distance between cells encouraging cell-cell interaction.
- Immune protection for the patient as well as the hepatocytes in the BR [6].

## 7.2 Surface characterization

Hepatocyte cells are by nature anchorage dependent. From previous investigations[49], describing the mechanism for cell attachment, we know the cells are more viable in a three-dimensional structure where cell-to-cell interaction is promoted. The cells use a protein-like string to attach themselves to the scaffolding and to each other. In design of the scaffolding the surface chemistry and biocompatibility needs to be considered. The scaffolding needs to have the following characteristics:

- Must be hydrophilic, minimizing non-wetted surface area and entrapped bubbles.
- Large surface area to volume ratio.
- Non-toxic and biocompatible with hepatocyte cells.
- The surface topography must be predominantly concave.

### 7.2.1 Cell number and surface area required

There is a general consensus that for adequate liver supports approximately[50] 20% of a liver mass is required for survival, this relates to approximately $20\times10^{10}$cells in an average human [11,17,58,59,60]. To determine the surface required the designer could calculate the maximum and minimum surface area for the specific BR. In the design of

[49] *See* 4.4: Method of hepatocyte adhesion to the scaffolding.

[50] Derived from partial hepatectomy studies where 10-30% of a healthy liver mass is needed for survival [11,17].

the BALSS optimal BR a weighted value for monolayer and speroid conditions was assumed based on the groups findings[51].

## 7.3 BR scaffolding

In any tissue engineering, or organ cultures, the cells need a 3d scaffolding to form a 3d structure. In the absence of scaffolding the cells tend to randomly migrate to form 2d layers of cells [69]. 3D scaffolding also has numerous flow advantages including relatively uniform flow distribution and inherent diffusion of nutrients and oxygen as a result of the flow.

For a scaffolding to be effective the following is required [69]:

1. Interconnecting pours of appropriate scale to favor tissue integration.
2. The scaffolding material must be made of a biocompatible material i.e. a substance that has no detrimental effect to the differentiation and viability of the cells in question and promotes cell to cell interaction as well as cell growth.
3. The surface chemistry should promote favorable differentiation and proliferation.
4. The surface should not induce any adverse response.
5. Surface chemistry to favor cellular attachment[52].

### 7.3.1 Pore size and porosity

The minimum pore size would be the maximum allowable spheroid diameter to prevent the pores from blocking[53]. Porosity can be defined as in Equation 24.

$$p = \frac{V_{void}}{V_{total}}$$

Equation 24

[51] See 3.14: Modelling of the optimized BR.

[52]This can be achieved by coating the scaffolding with Collagen. It has the major advantage of providing a favourable surface for cellular attachment and major protein constituent of the extra cellular matrix recognised by cells [69].

[53] See 4.6 Blocking of pores.

Were the void volume is the sum of all the open pore volume. For an optimal BR the porosity should be as close to unity as possible, but the material used and the pore size specified limits this. Practically the expansion of the polyurethane foam limits the porosity to between $0.9<p<0.94$. A number of researchers have indicated that cells in a cluster or spheroid have higher function and viability in comparison to monoculture cells. This is attributed to the lower stress levels of the cells when they are in close proximity with other cells. This however has an upper limit; if the spheroid becomes too large the inner cells are starved for the necessary nutrients and oxygen[54].

### 7.3.2 Dead spots

Dead spots must be limited in any BR design. They result in unused volume making metabolic measurements difficult due to dilution effects. Cells in dead spots die due to lack of oxygen and nutrients, which is detrimental, to the BR as a whole. Dead spots in the form of entrapped gas result in flow dispersion, accelerating the flow in unwanted areas. CFD modeling of the BR geometries and flow conditions has proven to be a useful tool in locating dead spots in the BR.

## 7.4 Pressure drops, surface shear and local flow velocity

Pressure drop, shear stress and velocity are closely related and mathematically linked[55]. An increase in one will result in an increase of the other two. This influences the cells due to the forces accompanying the flow conditions. Increased forces strain the cells, decreasing viability, and functionality. Shear stresses can cause damage to the membranes of cells and can cause a loss of viability [49,50]. Hepatocyte cells in a healthy liver do not see direct shear on them thus in the same respect to the examples given, high flow rates should be minimized in a hepatic BR. For an 80µm channel height (see section 6.6.1) a maximum shear of 300Pa (8m/s) would result is cell breakaway, for 100µm channel height the maximum shear increases to approximately 400Pa. These are excessive flow rates are impractical in hepatocyte BR's. The author recommends keeping the flow rate in hepatic BR's to an order of magnitude to that found in the sinusoids.

## 7.5 Hepatocyte cell seeding technique

The direction of flow during the seeding of the cells could possibly influence their viability especially if the perfusion direction is different to that of seeding. This is evident from the SEM investigation were the cells had oriented themselves to the flow. A change in the flow direction could dislodge them or result in different mass transfer gradients, starving the cells of nutrients and oxygen.

[54] See 4.3.2 Cell clusters (spheroids).

[55] See 6.5: Shear calculations as a function of channel height.

When a large number of cells are seeded the risk of cell narcosis is increased due to lower oxygen concentration per cell mass. This was found by Chen *et al* when the oxygen model did not support their measured values [64]. The answer to this would be faster flow rates, higher oxygen concentrations or introduction of an oxygen carrier (i.e. red blood cell substitute like PFOB).

## 7.6 Metabolic design considerations

### 7.6.1 Oxygen metabolism and nutrient metabolism

Hepatocyte cells need nutrients and due to their high metabolic rates they require large amounts of oxygen. The liver consumes as much as 22-30% of the oxygen used by the body [58].

One of the unsolved problems in a BAL system is the removal of bile salts [88]. This was not addressed and was outside the scope of this study but in future developments this needs to be investigated.

In summery a concise table for the design and optimisation of BR's used specifically in the BAL realm can be generated. Table 5[56] can be used for future BALSS developments, and in principle the fundamentals of BR design can be used for any BR used to support cell cultures.

[56] Table 5 can be found at the end of the chapter on pg 101.

Table 5: Design specifications summarized

| Design specifications for optimal BR | | | | | |
|---|---|---|---|---|---|
| **BALSS configuration dependent** | | | | | |
| | Design range | Min | Max | Ref | Notes |
| **Flow** | | | | | |
| Flow direction | Unidirectional | NA | NA | See section 4.5 Flow direction | |
| Shear | Nutrient transfer/ BR dependant | NA | 300Pa (80µm ) | See section 6.6.1 Flow conditions for hepatocyte cell breakaway | Pressure drop and shear dependant on flow. BR must be designed for minimum shear supporting adequate mass transfer |
| | | | | | |
| **Functional requirements** | | | | | |
| BR volume | As small as possible | Related to scaffolding used where specific BR volume depends on the minimum allowable surface area for cell cultures. See section 3.13 Design refinement and optimisation | | | |
| Immune barrier pore size | 50-150kDa | | | [17] | This allows most toxins and transport proteins like albumin to pass through while preventing immunoglobulins, complements, viruses and cells to pass through |
| Number of cells | 20*10^10 | 10*10^9 | Liver isolation dependant | [11,17,58,59,60] | Derived from partial hepatectomy studies where 20% of a healthy liver mass is needed for survival |
| Temperature °C | 38°C* | 37°C* | 42 °C** | NA | *Specific to core temperature of animal wherefrom hepatocytes were isolated. ** Human soft tissues can withstand approximately 42-43°C [89]. |
| | | | | | |
| **Metabolic indices** | | | | | |
| Cell cluster/aggregate size (µm) | 40-100µm | NA | 100µm | See section 4.3.2 Cell clusters | Generally accepted that aggregates larger than 100µm result in cell narcosis of the middle cells. |
| Oxygen consumption [nmol/s/10^6 cells] | | 0.31 | 0.9 | [90] | The minimum oxygen consumption is the reported steady state values. |
| | | | | | |
| **Scaffolding** | **Foam scaffolding dependent** | | | | |
| Pore size (µm) | Lower limit constrained by maximum spheroid size with the upper limit constrained by the surface area requirements. | | | See section 7.3 BR scaffolding | Open cell and interconnected geometry essential |
| Porosity | 0.9-0.94 | 0.9 | 1 | See section 7.3 BR scaffolding | Quoted values are practical expansion limits for polyurethane foam, expanded at the University of Pretoria. |
| Surface area (m^2) | 66.9 | 12.56 | 62.8 | See section 7.3 BR scaffolding | |
| Scaffolding volume (L) | 0.1 | 0.02 | 0.09 | See section 7.3 BR scaffolding | Design range based on BALSS group research/ optimised BR designed accordingly. |

# 8 RECOMMENDATIONS

*"The person who has no opinion will seldom be wrong." - Unknown*

## 8.1 Recommended generic procedure for designing a BAL BR

This chapter aims to present a generic design methodology for the design of a BR for implementation in a BAL. The methodology, presented graphically in Figure 76, aims to focus the designers attention to various design aspects and considerations during the design process.

### 8.1.1 Scope of problem

In the author's opinion the lack of consistency with the choice of data presentation, as well as different BR's and perfusion system flow rates; inhibit useful interpretation of data from researchers in the field. An example of which is the flow rate necessary for the perfusion of hepatocyte cells. The reported localized flow rates vary considerably with the volumetric flow rates being more consistent[57], it is however important to note that the localized flow rate over the cells differ considerably with the flow rates in the perfusion loop. Table 4[58] shows the difference in the calculated flow rates, of some of the more recent reported data.

### 8.1.2 Methodology for the design and implementation of a BAL BR

A proposed design methodology, presented in Figure 76, is expanded upon in more detail below. From the onset the designer should realize that the further down the design phases you move the more constrained you become, and the more costly design changes are. Each design phase should be evaluated after the completion of the phase with the designer stepping back and deciding how to continue or which steps need to be redone. The design loop is inherently an iterative process with multiple solutions to a specific problem; the most economical and efficient design will inevitably benefit future BAL systems.

[57] With up scaled clinical systems varying between 400-600ml/min, see Table 4

[58] Table 4 can be found at the end of the Chapter 5 on pg 62.

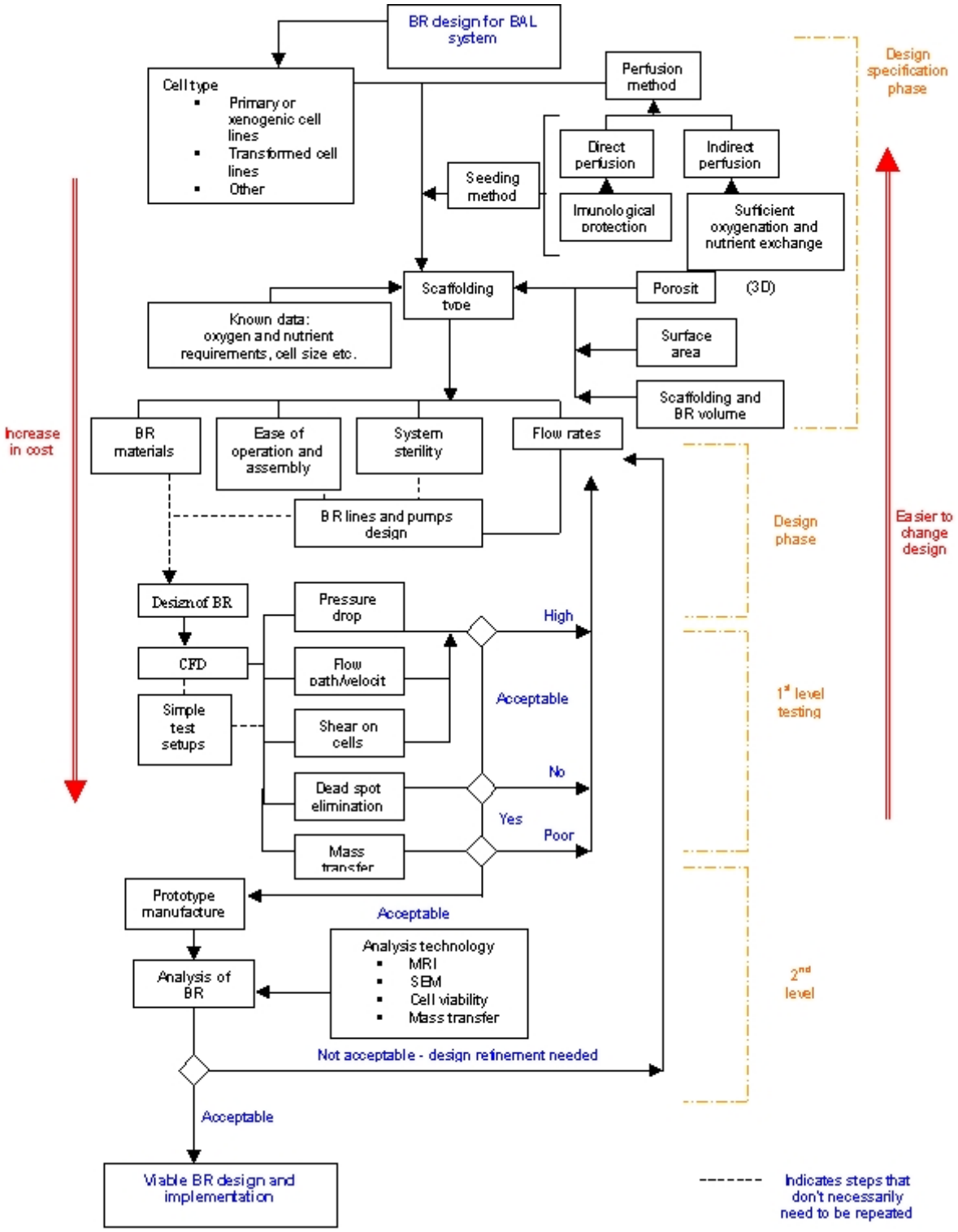


Figure 76: Flow diagram for BR Design

### 8.1.3 Design specification phase

In the Design specifications phase the researcher needs to make a number of decisions, which constrain certain aspects of the later design. For example if the researcher chooses porcine hepatocytes for seeding then the temperature of the BR is constrained to 38°C, and certain immunological constraints are imposed. For the specific choice of scaffolding the question of continual cell viability over time needs to be verified and the limitations identified. The final product architecture and clinical application poses questions of practicality for the BR when used in the medical field, i.e. will the cells be cryo-preserved or continuously harvested and would it be possible to cryo-preserved the BR as a modular unit after the hepatocytes have been seeded?

The seeding method used may also add designs constraints other than the BR design to the system. The method cells are introduced into the BR needs to be defined and the subsystems designed. This includes the tubing used, methods to minimize infections etc.

A simple design tool is to first determine what is known in the BAL field. A simple table, Table 5[59], illustrates that the designer has known data that he can work with in making design specific decisions.

Caution should be practiced when using other researchers data. Care should be taken in comparing the data sets with equivalent data sets of other researchers, i.e. when comparing a certain metabolic consumption rate, the cell type, number of cells, surface area, scaffolding type etc. should be equivalent or alternatively the data sets should be normalized for comparison.

Once the said design constraints are decided on, the design and simulation of the BR can be done. From this point on the choice of the design tool used i.e. CFD, prototype construction etc. depends on the cost as well as the time involved in the specific testing phase.

### 8.1.4 Design phase

The design phase is simply the design of the BR incorporating the above steps or the re/design from knowledge obtained by a lower step, depending at which stage of the design process you are in. At this point, other than the known knowledge directly related to the BR itself, the designer has to take the complete system including the perfusion lines and sterility of the system into account. Will the BR be at the adequate temperature and will the pressure drop over the lines have detrimental effect to the BR itself. High pressures should be minimized in any medical device at any point of the system especially with silicone tubes, because as they expand the tubes release from their fittings, or alternatively under negative pressure collapse, which could lead to disastrous results. The material of

[59] Table 5 can be found on pg 101.

the BR should be consistent with other design constraints i.e. if the whole BR is cryo-preserved the material needs to take the subzero temperatures, if the BR needs to be autoclaved then the extreme opposite is needed.

Special emphasis on the system sterility especially in terms of operator handling needs to be considered. Although the final connectors might only be added at a later stage their incorporation should be envisaged at early stages of the design. Researchers have gone as far as to say that sub optimal BR design might be the cause of hepatocyte's not surviving in certain locations of the BR [23].

### 8.1.5 1st level testing phase

In the 1st level-testing phase the main concepts of the design are tested for. The designer should have reviewed the relevant data previously published and verified it to minimise the cost of more tests and simulations. The BR can be designed and simulated using the solid modelling and CFD programs. As the geometry and flow conditions increase in complexity so does the computational effort and cost of the simulation.

All CFD programs currently available use numerical simulation of the flow, thus the flow domain needs to be modelled with a mesh, essentially a number of discrete points each solved individually in terms of the surrounding points and boundary conditions. Each time the design geometry is changed the model needs to be reconstructed and solved.

If the designer opts for 3d scaffolding there are porous modelling tools available that model the pressure drop as a function of flow rate, but unless data is available on the specific scaffolding used, simple pressure/velocity tests need to be conducted. It is important to note that these porous modelling tools model the flow and essentially dampens the momentum in the governing equations to get the measured pressure drop. The scaffolding is not modelled physically only the effect thereof. At the time of this investigation there was no porous modelling tools that could effectively model the scaffolding directly, with unlikely development of such models in the foreseeable future.

Other than porous modelling, CFD has the capability to model the pressure drop within the BR, the flow path of the fluid and particle trajectories for hepatocyte seeding in the BR. The use of CFD, in the design of BR's in general, is of great importance as a tool to optimise BR geometries.

### 8.1.6 2nd level testing

By the 2nd level of testing a physical BR needs to have been constructed. Not necessarily identical to the final BR but essentially the materials used and the flow geometry must be consistent with the final design. At this stage testing the metabolic function as well as the integration into the system is essential. Various methods to determine the validity of the CFD simulations can be adopted including MRI and metabolic trials.

SEM is an important tool in the arsenal of the bio-design engineer. Using SEM, the designer can determine to what extent the cells are clustering and if there is any pore blockage.

In this phase the following needs to be determined for the specific BR design

1. Is the flow rate/ shear stress within the cellular limit?
2. Is the pressure drop within the cellular limit?
3. Have BR dead spots been eliminated?
4. Is there sufficient mass transfer and toxin removal?
5. Are the cells viable after an extended metabolic trial?
6. Are the cells blocking the specific scaffolding?
7. Are the cell clusters within the limitations of mass transfer?
8. Are their imunological problems with the BR?
9. Will the volume of the BR/system make a patient hemodynamically unstable?

If any of the above questions have a negative reply the designer should consider a redesign or modification to the system.

With these tools and considerations, in theory, a designer has the arsenal to design, build and optimise a BAL BR.

# REFERENCES

1. Anderson, D.M. Novac, P.D. Keith, J. and Elliott, M.A. 2003. *Dorland's Illustrated Medical Dictionary* (30th edition). Philadelphia: Saunders.

2. Smith, W.F. *Principles of Materials Science and Engineering* (3rd Edition). 1996. McGraw Hill: United States of America.

3. Glauert, A.M. and Lewis, P.R. *Biological Specimen Preparation for Transmition Electron Microscope* (volume 17). 1998. Great Britain university press: Cambridge UK.

4. Chapter by: McCuskey, R.S. edited by: Arias, I.M. Boyer, J.L. Fausto, N. Jakoby, W.B. Schachter, D.A. and Shafritz, D.A. *The Hepatic Microvascular System*. 1994. *The Liver Biology and Pathology* (3rd edition).

5. Chapter by: Bear, J Edited by: De Wiest. *Flow Through Porous Media*. 1969. Academic press: United Kingdom, London.

6. Moolman, F.S. 2002. *Oxygen Carriers for a Novel Bio-Artificial Liver Support System*. PhD-Thesis. Pretoria: University of Pretoria.

7. Howard, J & Worman, M.D. 1999. *The Liver Disorders Sourcebook*. Lowell house: Chicago.

8. Donini, A. Baccarani, U. Risaliti, A. Sanna, A. Degrassi, A. and Bresadola, F. In vitro Functional Assessment of a Porcine Hepatocytes Based Bioartificial Liver. 2001. *Transplant Proceedings*, 33:3477-3479.

9. Desille, M. Frémond, B. Mallédant, S. Seguin, P. Bouix, A. Lebreton, Y. Desbois, J. Campion, J.P. and Clément, B. Improvement of the Neurological Status of Pigs With Acute Liver Failure by Hepatocytes Immobilized in Alginate Gel Beads Inoculated in an Extracorporeal Bioartificial Liver. 2001. *Transplantation Proceedings*, 33:1932-1934.

10. Unknown. 2003. *The First Liver Transplant*. http://www.transweb.org/qa/asktw/answers /answers9505/ Firstlivertransplant.html (12 September 2005).

11. Nyberg, S.L. and Misra, S.P. Hepatocyte Liver Assist Systems- a Clinical Update. 1998. *Mayo Clin Proc,* 73:765-771.

12. Fey, V.R. Rivin, U.I. 2004. *Guided Technology Evolution (TRIZ Technology Forecasting).* www.triz-journal.com/(10 March 2004).

13. Rani, H.P. Sheu, T.W.H. Chang, T.M. Liang, P.C. Numerical Investigation of non-Newtonian Microcirculatory Blood Flow in Hepatic Lobule. *Journal of Biomechanics* (Article in press).

14. Beath, S.V. Hepatic Function and Physiology in the Newborn. 2003. *Seminars in Neonatology,* 8:337-346.

15. Wolfe, S.P. Hsu, E. Reid, L.M. Macdonald, J.M. A Novel Multi-Coaxial Hollow Fibre Bioreactor for Adherent Cell Types. Part 1: Hydrodynamic Studies. 2001. *Biotechnology and Bioengineering*, 77(1): 83-90.

16. Sauer, I.M. and Gerlach, J.C. Thoughts and Progress: Modular extracorporeal Liver Support. 2002. *Artificial Organs*, 26(8): 703-733.

17. Jalan, R. Sen, S. Williams, R. Prospects for Extracorporeal Liver Supprt. 2004. *Gut*, 53: 890-898.

18. Sauer, I.M. Steffen, I. Kehr, D.C. Schwartlander, R. Hwang, Y.J. Pascher, A. Gerlach, J.C. and Neuhaus, P. In vitro Comparison of the molecular Absorbant Recirculation System (MARS) and Single-Pass Albumin Dialysis (SPAD). 2004. *Hepatology,* 39:1408-1414.

19. Demetriou, A.A. Brown, R.S. Busuttil, R.W. Fair, J. McGuire, B.M. Rosenthal, P. Schulte, J. Esch, A. Lerut, J. Nyberg, S. Salizzoni, M. Fagan, E.A. De Hemptinne, B. Broelsch, C.E. Muraca, M. Salmeron, J.M. Rabkin, J.M. Metselaar, H.J. Pratt, D. De La Mata, M. McChesney, L.P. Everson, G.T. Lavin, P.T. Stevens, A.C. Pitkin, Z. and Solomon, B.A. Prospective, Randomized, Multicenter, Controlled Trial of a Bioartificial Liver in Treating Acute Liver Failure. 2004. *Annals of Surgery,* 239:660-670.

20. Unknown. 2005. http://www.arbios.com/technologyhepatassist.html (27 September 2005).

21. Unknown. 2005. http://hugroup.cems.umn.edu/Research/bal/BAL.html (27 September 2005).

22. Patzer, J.F. Mazariegos, G.V. Lopez, R.C. Pre-clinical Evaluation of the Excorp Medical, Inc, Bioartificial Liver Support System. 2002. *J Am Coll Surg*, 195(3): 299-310.

23. Gerlach, J.C. Schnoy, N. Encke, J. Smith, M.D. Müller, C. and Neuhaus, P. Improved Hepatocyte In Vitro Maintenance in a Culture Model With Woven Multicompartment Capillary Systems: Electron Microscope Studies. 1995. *Hepatology,* 22:546-552.

24. Kaneko, M. Fukuda, J. Ijima, H. Nakazawa, K. Gion, T. Shimada, M. Shirabe, K. Takenaka, K. Sugimachi, K. Funatsu, K. Development of a Hybrid Artificial Liver Support System Using Spheroid Culture and Application to Warm Ischemic Liver Failure in Dog and Pig as a Preclinical Test. 1998. *Material Science and Engineering*, 6:245-248.

25. Gion, T. Shimada, M. Shirabe, K. Nakazawa, K. Ijima, H. Matsushita, T. Funatsu, K. and Sugimachi, K. Evaluation of a Hybrid Artificial Liver Using A Polyurethane Foam Packed-Bed Culture System in Dogs. 1999. *Journal of Surgical Research*, 82:131-136.

26. Flendrig, L.M. Te Velde, A.A. and Chamuleau, R.A.F.M. Semipermeable Hollow Fiber Membranes in Hepatocyte Bioreactors: A Perquisite for a Successful Bioartificial Liver? 1997. *Artificial Organs*, 21(11): 1177-1181.

27. Flendrig, L.M. La Soe, J.W. Jörning, G.G.A. Steenbeek, A. Karlsen, O.T. Boveé, W.M.M.J. Ladiges, N.C.J.J. Te Velde, A.A. and Chamuleau, R.A.F.M. In Vitro Evaluation of a Novel Bioreactor Based on an Integral Oxeygenator and a Spirally Wound Non-woven Polyester Matrix for Hepatocyte Culture as Small Aggregates. 1997. *Journal of Hepatology*, 26:1379-1392.

28. Van de Kerkhove, M.P. Di Florio, E. Scuderi, V. Mancini, A. Belli, A. Brac, A. Dauri, M. Tisone, G. Di Nicuolo, G. Amoroso, P. Spadari, A. Lombardi, G. Hoekstra, R. Calise, F. Chamuleau, R.A.F.M. Phase I Clinical Trial with the AMC- Bioartificial Liver. 2003. http://www.PubMed/Abstract (12 March 2004).

29. Unknown. 2005. http://www.teraklin.com/index-eng.html (27 September 2005).

30. Unknown. 2005. http://www.aegis.com/news/ads/1994/AD941806.html (27 September 2005).

31. Unknown. 2005. http://www.hemocleanse.com/TechnologiesLLC/index.html (27 September 2005).

32. Unknown. 2005. http://www.fresenius.de/5/pdf/prometheus.pdf (27 September 2005).

33. Unknown. 2005. http://www.biotec-systems.at/en/prometheus.html (27 September 2005).

34. Unknown. 2005. http://www.excorp.com/excorp/.html (27 September 2005).

35. Unknown. 2005. http://www.charite.de/avt/research/sauer/projects/mels_lab/mels_mainframe.html (27 September 2005).

36. Qian, Y. LanJuan, L. JianRong, H. Jun, L. HongCui, C. SuZhen, F. Xia, Y. ShuHong, Y. Study of Severe Hepatitis Treated with a Hybrid Artificial Liver Support System. 2003. *Int J Artif Organs*, 26: 507 – 513.

37. Unknown. 2005. http://www.vitaltherapies.com/pdf/VTIFactSheet.pdf (27 September 2005).

38. Unknown. 2005. http://www.vitaltherapies.com/ (27 September 2005).

39. Unknown. 2005. http://www.xs4all.nl/~reitsma/wwwarticle1.html (27 September 2005).

40. Unknown. 2005. http://www.multicelltech.com/technology/xenogenics.htm (27 September 2005).

41. Unknown. 2005. http://www.cellbiotechltd.com/ (27 September 2005).

42. Chen, Z. Ding, Y. Xu, Q and Yu, D. Bioartificial Liver Inoculated with Porcine Hepatocyte Spheroids for Treatment of Canine Acute Liver Failure Model. 2003. *Artificial organs*, 27(7): 613-622.

43. Yin, C. Chia, S.M. Quek, C.H. Yu, H. Zhuo, R. Leong, K.W. and Mao, H.Q. Microcapsules with Improved Mechanical Stability for Hepatocyte Culture. 2003. *Biomaterials*, 24: 1771-1780.

44. McClelland, R.E. MacDonald, J.M. and Coger, R.N. Modeling O2 Transport within Engineering Hepatic Devices. 2002. *Biotechnology and Bioengineering*, 82(1): 12-27.

45. Nieuwoudt, M. Kunnike, R. Smuts, M. Becker, J. Stegmann, G.F. Van der Walt, C. Neser, J. Van der Merwe, S. Standardization Criteria for an Ischemic Surgical Model of Acute Hepatic Failure in the Pig. (*Article in press*).

46. Riordan, S.M. Skouteris, G.G. and. Williams, R. Metabolic activity and Clinical Efficiency of Animal and Human Hepatocytes in Bioartificial Support Systems for Acute Liver failure. 1998. *The International Journal of Artificial Organs*, 21(6): 312-318.

47. Prof. Saltzman, W.M. and Prof. Leong, K. Enhancement of Cell Function in Culture by Controlled Aggregation Under Microgravity Conditions. 2005. http://peer1nasaprs.com/ (25 July 2005).

48. Nieuwoudt, M. Kreft, E. Olivier, B. Malfield, S. Vosloo, J.F. Stegmann, F. Kunneke, R. Van Wyk , A.J. Van der Merwe, S. A Large Scale Automated Method for Hepatocyte Isolation: Effects on Proliferation in Culture. 2005. *Cell Transplantation,* (Article in press).

49. Curran, S.J. and Black, R.A. Quantitave Experimental Study of Shear Stresses and Mixing in Progressive Flow Regimes within Annular-Flow Bioreactors. 2004. *Chemical Engineering Science*, 59: 5859-5868.

50. Ledezma, G.A. Folch, A. Bhatia, S.N. Balis, U.J. Yarmush, M.L. and Toner, M. Numerical Model of Fluid Flow and Oxygen Transport in a Radial Flow Microchannel Containing Hepatocytes. 1998. *Journal of Biomechanical Engineering* (Unknown).

51. McClelland, R.E. and Coger, R.N. Predictive Model of Enhanced O2 Transport within Bioartificial Liver Devices. 2001. *Bioengineering Conference*, BED (50): 547-548.

52. Unknown. Version 6.2.16. http://Fluent. Inc/gambit2.2.30/help/html/users_guide/ spec_quality_type (22 September 2005).

53. White, F.M. 1991.*Viscous Fluid Flow* (2nd edition). Singapore: McGraw Hill.

54. Unknown. Version 6.2.16. http://help/users guide/chapter 11.2.9 The Shear Stress Transport k-ω model.htm. (22 September 2005).

55. Unknown. Version 6.2.16. http://Fluent.Inc\fluent6.19\help\users guide\chapter 6 Porous Media Conditions.htm. (4 October 2005).

56. Unknown. Version 6.2.16. http://Fluent.Inc\fluent6.19\help\users guide\ 8.13.1 The Effect of Numerical Round off on Pressure Calculation in Low-Mach-Number Flow.htm. (4 October 2005).

57. Kreamer, B.L. Staecker, J.L. Sawada, N. Sattler, G.L. Hsia, M.T. and Pitot, H.C. Use of a Low-Speed, Iso-Density Percoll Centrifugation Method to Increase the Viability of Isolated Rat Hepatocyte Preparations. 1986. *In Vitro cell DEV Biol Apr*; 22(4): 201-211.

58. McClelland, R.E. and Coger, R.N. Use of Micropathways to Improve Oxygen Transport in a Hepatic System. 2000. *Transactions of ASME*, 122:268-273.

59. Van de Kerkhove, M.P. Hoekstra, R. Chamuleau, R.A.F.M. and Van Gulik, T.M. Clinical Application of Bioartificial Liver Support Systems. 2004. *Annals of Surgery*, 240(2): 216-230.

60. Park, J.K. and Lee, D.H. Bioartificial Liver Systems: Current Status and Future Perspective. 2005. *Journal of Bioscience and Bioengineering*, 99(4): 311-319.

61. Carté, M. (CH Chemicals - EDV) Personal communications with Ronné, L. 07 April 2004.

62. Victor, S.A. and Shah, V.L. Steady State Heat Transfer to Blood Flowing In the Entrance Region of a Tube. 1974. *Journal of Heat and Mass Transfer*, 19: 171-783.

63. Hay, P.D. Veitch, A.R. and Gaylor, J.D.S. Oxygen Transfer in a Convection-Enhanced Hollow Fiber Bioartificial Liver. 2001. *Artificial Organs*, 25(2): 119-130.

64. Chen, J.P. and Lin, T.C. Loofa Sponge as a Scaffold for Culture of Rat Hepatocytes. 2005. *Biotechnol*, 21(1): 315-319.

65. Coetzee, J. Van der Merwe, C.F. and Hall, A.N. 2000. *Brief Notes on Some Standard Procedures for the Preparation of Biological Materials for Microscopy*. Laboratory for Microscopy and Microanalysis: University of Pretoria, SA.

66. Reimer, L. 1984. *Transmission Electron Microscopy*. Springer-Verlag Berlin: Heidelberg.

67. Unknown. 2005. Modified from: http://www.mos.org/sln/sem/seminfo.htm. (12 July 2005).

68. Carté, M. (CH Chemicals - EDV). Polyurethane Specification Sheet FH2054. Serial number: 212054. 16 January 2002.

69. Sachlos, E. and Czernuszka, J.T. Making Tissue Engineering Scaffolds Work. Review on the Application of Solid Freeform Fabrication Technology to the Production of Tissue Engineering Scaffolds. 2003. *European cells and Materials*, 5: 29-40.

70. Akaike, T. Control of Cell Recognition and Attachment of Hepatocytes by Glycopolymers. 2001. *European Cells and Materials* 2(1): 19.

71. Kim, S.H. Kim, J.H. and Akaike, T. Temporal and Spatial Control of Cell-Glycopolymer Surface Integration; Regulation of Hepatocyte Cell Signalling by Glycopolymer. 2001. *European Cells and Materials*, 2(1): Page 52-53.

72. Peel, M.M. and Dimilla, P.A. Effect of Cell–Cell Interactions on the Observable Strength of Adhesion of Sheets of Cells. 1999. *Annals of Biomedical Engineering*, 27: 236–246.

73. Drain L.E. *The Laser Doppler Technique*. 1980. John Wiley and Sons: Great Britain, Norwich.

74. Hayward, A.T.J. *Flowmeters- A Basic Guide and Source Book for Users*. 1979. The MacMillan Press LTD: London.

75. Hornak, J.P. 2005. *The Basics of MRI*. http://www.cis.rit.edu/htbooks/mri. (19 December 2005).

76. Tilles, A.W. Baskaran, H. Roy, P. Yarmush, M.L. Toner, M. Effects of Oxygen and Flow on the Viability and Function of Rat Hepatocytes Co cultured in a Microchannel Flat Plate Bioreactor. 2000. *Biotechnology and Bioengineering*, 73(5): 379-389.

77. Roy, P. Washizu, J. Tilles, A.W. Yarmush, M.L. and Toner, M. Effect of Flow on the Detoxification Function of Rat Hepatocytes in a Bioartificial Liver Reactor. 2001. *Cell Transplantation*, 10: 609-614.

78. Morsiani, E. Galavotti, D. Puviani, A.C. Valieri, L. Brogli, M. Tosatti, S. Pazzi, P. and Azzena, G. Radial Flow Bioreactor Outperforms Hollow-Fiber Modules as a Perfusing Culture System for Primary Porcine Hepatocytes. 2000. *Transplant Proceedings*, 32:2715-2718.

79. Shito, M. Tilles, A.W. Tompkins, R.G. Yarmush, M.L. and Toner, M. Efficacy of an Extracorporeal Flat-Plate Bioartificial Liver in Treating Fulminate Hepatic Failure. 2002. *Journal of Surgical Research*, 111:53-62.

80. Dixon, S.L. 1998. *Fluid Mechanics and Thermodynamics of Turbo machinery* (4th edition). Butterworth-Heinmann: United States of America.

81. Unknown. 2005. http://www.matweb.com. (01 June 2005).

82. Hemmerich, K.J. Polymer Materials Selection for Radiation-Sterilized Products. 2000. *Medical Device & Diagnostic Industry Magazine*: MDDI archive Feb 00.

83. Multihance, Pharmacological classification sheet. 2002. *Bracco*. Registration number: 35/28/0086.

84. White, F.M. *Fluid mechanics* (4th edition). 1999. Singapore: MacGraw Hill.

85. Goldstein, A.S. and DiMilla, P.A. Application of Fluid Mechanic and Kinetic Models to Characterize Mammalian Cell Detachment in a Radial-Flow Chamber. 1996. *Biotechnol Bioeng*, 55: 616-629.

86. De´ Cave´, E. Garrivier, Bre´ chet, D.Y. Fourcade, B. and Bruckert, F. Shear Flow-Induced Detachment Kinetics of Dictyostelium Discoideum Cells from Solid Substrate. 2002. *Biophysical journal*, 82: 2383-2395.

87. Brand, J. (University of Pretoria, SA, Machining department). 2005. Personal communications with Ronné, L. 5 June 2005.

88. Chamuleau, R.A.F.M. Artificial liver support in the Third Millennium. 2003. *Artificial cells, Blood substitutes and biotechnology*, 31(2): 117-126.

89. Bergmanna, G. Graichena, F. Rohlmanna, A. Verdonschotb, N. van Lentheb, G.H. Frictional Heating of Total Hip Implants. Part 2: Finite Element Study. 2001. *Journal of Biomechanics*, 34: 429–435.

90. Balis, U.J. Behnia, K. Dwarakanath, B. Bhatia, S.N. Sullivan, S.J. Yarmush, M.L. and Toner, M. 1999. Oxygen Consumption Characteristics of Porcine Hepatocytes. *Metabolic Engineering*, 1:49-62.

91. Unknown. Version 6.2.16. http:\\help\users guide\chapter 11.5 The standard and Shear Stress Transport k-ω model.htm. (23 September 2005).

# APPENDIX

## Appendix A : Number of patients on the organ donor waiting list (liver) in the USA

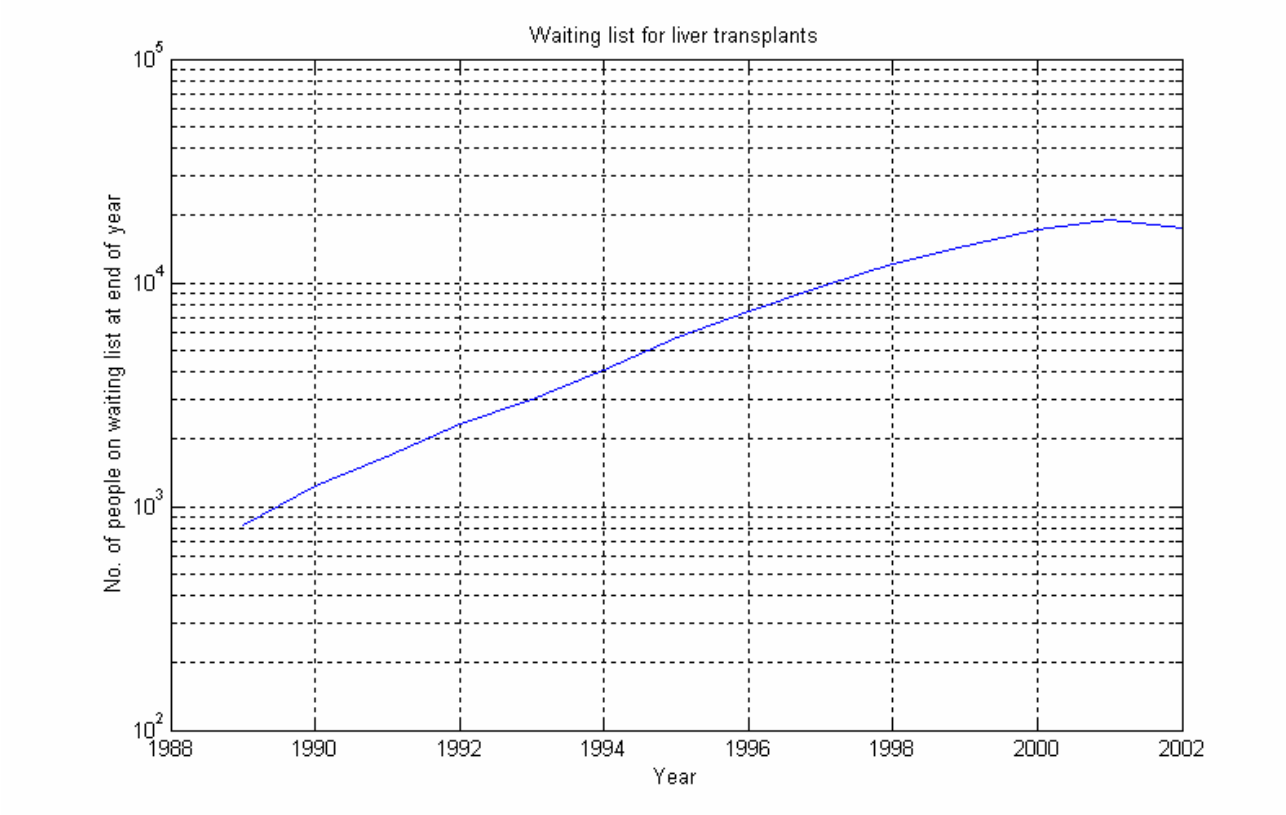


Figure A.1: Waiting list for liver patients, per year in the USA

The waiting list from 1988-2000 shows an exponential increase in the number of people waiting for a liver. Upon speculation the following can be attributed to the increase:

- Procedure more widely available with an increase in the success rate
- Increase in awareness of the procedure

The data presented was obtained from Mrs. DM Tripp from the United Network of Organ Sharing.

## Appendix B : The shear stress transport k-ω model (SSTk-ω)[60]

The k-ω model as well as the SST modification both solve for turbulent generation (k) and turbulent dissipation (ω) from the transport equations given in Equation 25. The model is described using Einstein summation convention for convenience. Where $u_i = (u_1, u_2, u_3)$ and repeated subscripts imply summation i.e. $u_i u_i = u_1^2 + u_2^2 + u_3^2$ [53]. The difference between the two models is the manner in which the wall region and free stream is blended as well as the definition of the turbulent viscosity were the SST model accounts for the transport effects of the principle shear stresses.

$$\frac{\partial}{\partial t}(\rho k) + \frac{\partial}{\partial x_i}(\rho k u_i) = \frac{\partial}{\partial x_j}\left(\Gamma_k \frac{\partial k}{\partial x_j}\right) + \tilde{G}_k - Y_k + S_k$$

$$\frac{\partial}{\partial t}(\rho \omega) + \frac{\partial}{\partial x_i}(\rho \omega u_i) = \frac{\partial}{\partial x_j}\left(\Gamma_\omega \frac{\partial \omega}{\partial x_j}\right) + G_\omega - Y_\omega + D_\omega + S_\varpi$$

Equation 25

Where $\tilde{G}_k$ is the generation of turbulence kinetic energy due to mean velocity gradients, calculated from Equation 26.

$$\tilde{G}_k = \min(G_k, \beta^* k\omega)$$

$$G_k = -\rho \overline{u_i u_j} \frac{\partial u_j}{\partial x_i}$$

Equation 26

$\beta^*$ is calculated from Equation 27.

[60] Modified by Luke Ronné.Fluent.Inc\fluent6.2.16\help\users guide\chapter 11.5 The standard and Shear Stress Transport k-ω model.htm. 23 September 2005

$$\beta^* = \beta_i^*\left[1+1.5F(M_t)\right]$$

$$\beta_i^* = 0.09\left(\frac{4/15+\left(\mathrm{Re}_t/8\right)^4}{1+\left(\mathrm{Re}_t/8\right)^4}\right)$$

Equation 27

With $F(M_t)$ a compressibility function given by Equation 28.

$$F(M_t)=\begin{cases}0 & M_t \le 0.25\\ M_t{}^2-0.0625 & M_t > 0.25\end{cases}$$

$$M_t=\frac{2k}{a^2}$$

$$a=\sqrt{\gamma RT}$$

Equation 28

And $\mathrm{Re}_t$ is calculated from Equation 29.

$$\mathrm{Re}_t=\frac{\rho k}{\mu\omega}$$

Equation 29

$G_\omega$ is the generation of the specific dissipation rate (ω) given by Equation 30.

$$G_\omega=\alpha\frac{\omega}{k}G_k$$

Equation 30

$\alpha$ can be calculated from Equation 31-Equation 32.

$$\alpha = \frac{\alpha_\infty}{\alpha^*}\left(\frac{\frac{1}{9}+\mathrm{Re}_t/2.95}{1+\mathrm{Re}_t/2.95}\right)$$

Equation 31

$$\alpha^* = 1\left(\frac{\frac{3}{125}+\mathrm{Re}_t/6}{1+\mathrm{Re}_t/6}\right)$$

Equation 32

$\alpha_\infty$ differs from the standard k-ω model (were it was a constant) and is given by Equation 33-Equation 34.

$$\alpha_\infty = F_1\alpha_{\infty,1} + (1-F_1)\alpha_{\infty,2}$$

Equation 33

$$\alpha_{\infty,(1,2)} = \frac{\beta_{i,(1,2)}}{0.09} - \frac{0.14^2}{\sigma_{\omega,(1,2)}\sqrt{0.09}}$$

Equation 34

Where F1 is a blending function and is given by Equation 35-Equation 36, and $\beta_{i,1} = 0.075$ $\beta_{i,2} = 0.0828$.

$$F_1 = \tanh\left(\Phi_1^4\right)$$

Equation 35

$$\Phi_1 = \min\left[\max\left(\frac{\sqrt{k}}{0.09\omega y}, \frac{500\mu}{\rho y^2 \omega}\right), \frac{4\rho k}{\sigma_{\omega,2} D_\omega^+ y^2}\right]$$

Equation 36

Where $D_\omega^+$ is the positive portion of the cross diffusion term Equation 37 and y is the distance to the next surface.

$$D_\omega^+ = \max\left[\frac{2\rho}{\sigma_{\omega,2}\omega}\frac{\partial k}{\partial x_j}\frac{\partial \omega}{\partial x_j}, 10^{-10}\right]$$

Equation 37

And $\sigma_{\omega,k}$ is the turbulent Prandalt numbers for k or ω. The turbulent Prandtl numbers are given in Equation 38 and are also blended from the wall to free stream by means of the blending function $F_1$ shown in Equation 35.

$$\sigma_{k,\omega} = \frac{1}{F_1 / \sigma_{(k,\omega),1} + (1 - F_1) / \sigma_{(k,\omega),2}}$$

Equation 38

$Y_k$ represents the dissipation of turbulent kinetic energy and is defined by Equation 39.

$$Y_k = \rho\beta^* k\omega$$

Equation 39

$Y_\omega$, Equation 40, represents the dissipation of ω.

$$Y_\omega = \rho\beta\omega^2$$

Equation 40

Were $\beta$ is defined by Equation 41.

$$\beta = \beta_i \left[1 + 20\frac{5}{6}\beta_i^* F(M_t)\right]$$
$$\beta_i = F_1\beta_{i,1} + (1 - F_1)\beta_{i,2}$$

Equation 41

And $\beta_i^*$ is as in Equation 27. The effective diffusivity, $\Gamma_{k,\omega}$, is given by Equation 42.

$$\Gamma_{k,\omega} = \mu + \frac{\mu_t}{\sigma_{k,\omega}}$$

Equation 42

The turbulent viscosity, $\mu_t$, is given by Equation 43.

$$\mu_t = \frac{\rho k}{\omega}\frac{1}{\max\left(\frac{1}{\alpha^*}, \frac{SF_2}{a_1\omega}\right)}$$

Equation 43

S is the strain rate magnitude, $F_2$ is a blending function given by Equation 44-Equation 45.

$$F_2 = \tanh\left(\Phi_2^2\right)$$

Equation 44

$$\Phi_2 = \max\left[2\frac{\sqrt{k}}{0.09\omega y}, \frac{500\mu}{\rho y^2 \omega}\right]$$

Equation 45

The cross diffusion term, which is a result of the blending of the k-ω model and the k-ε model, is given in Equation 46.

$$D_\omega = 2(1-F_1)\rho\sigma_{\omega,2}\frac{1}{\omega}\frac{\partial k}{\partial x_j}\frac{\partial \omega}{\partial x_j}$$

Equation 46

$S_{k,\omega}$ are user defined source terms. An example of which would be the method of modeling the porous region described in section 3.3.2.2.

## Appendix C : Calculation of analytical velocity for the BALSS radial flow BR

Using the conservation of mass with the control volume around the BR, assuming no heat loss/gain or mass conversion.

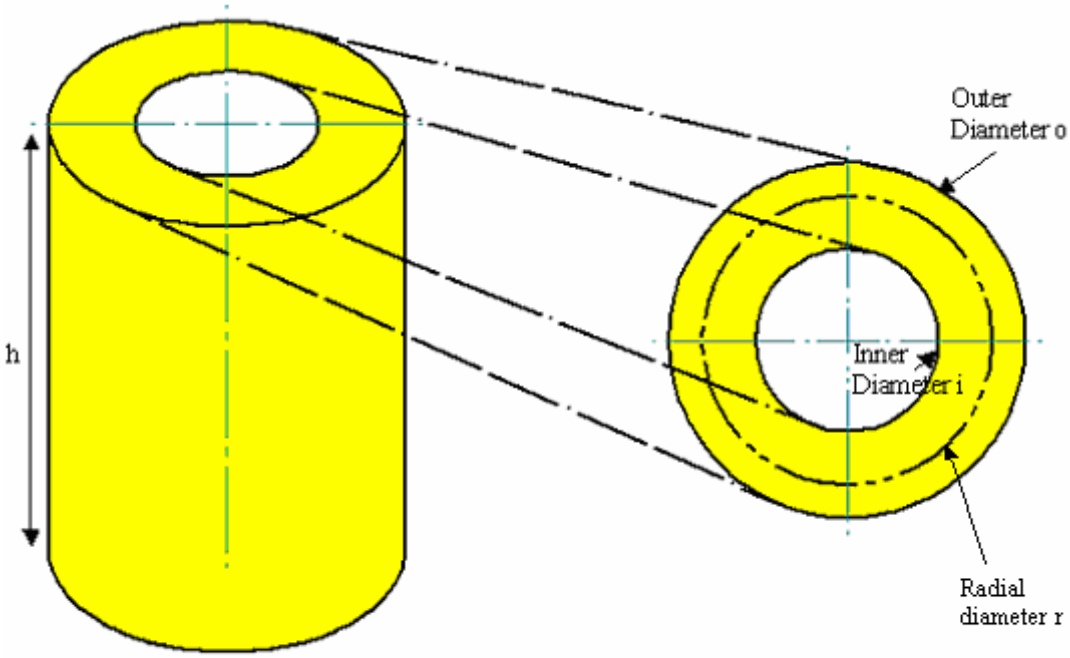


Figure 77: Schematic of porous scaffolding used in the BALSS radial flow BR

$$\sum \dot{M}_{in} = \sum \dot{M}_{r}$$
$$(\rho AV)_{in} = (\rho AV)_{r}$$

Equation 47

Assuming constant density.

$$(AV)_{in} = (AV)_r$$

Equation 48

Relating the volumetric flow a velocity.

$$\dot{Q} = A_r V_r$$
$$A_r = \pi d_r h_r$$

Equation 49

Substituting Equation 49 into Equation 48 and rearranging.

$$V_r = \frac{\dot{Q}}{\pi d_r h_r}$$

Equation 50

The weighted average velocity, is the staggered line in Figure 77, and is defined by Equation 51.

$$V_{avg}\left(\frac{A_i + A_o}{2}\right) = \frac{A_i V_i + A_o V_o}{2}$$
$$V_{avg} = \frac{A_i V_i + A_o V_o}{A_i + A_o}$$

Equation 51

# INDEX